INFLUENCE INDICES FOR RAINFALL-INDUCED

SHALLOW SLOPE FAILURES IN VIEW OF

WARNING SYSTEM IMPLEMENTATION

Somjai   Yubonchit

A Thesis Submitted in Partial Fulfillment of the Requirements for the

Degree of Doctor of Philosophy in Civil Engineering

Suranaree University of Technology

Academic Year 2016

ดัชนีผลกระทบต่อการวิบัติของลาดดินตื้นเนื่องจากน้ำฝน
เพื่อการพัฒนาระบบเตือนภัย

นายสมใจ   ยุบลชิต

สมใจ ยุบลชิต : ดัชนีผลกระทบต่อการวิบัติของลาดดินตื้นเนื่องจากน้ำฝนเพื่อการพัฒนาระบบ
เตือนภัย (INFLUENCE INDICES FOR RAINFALL-INDUCED SHALLOW SLOPE
FAILURES IN VIEW OF WARNING SYSTEM IMPLEMENTATION) อาจารย์ที่ปรึกษา :
รองศาสตราจารย์ ดร. อวิรุทธิ์ ชินกุลกิจนิวัฒน์, 185 หน้า.

วิทยานิพนธ์นี้ประกอบด้วยสองส่วน ในส่วนแรกนำเสนอผลการทดสอบในห้องปฏิบัติการ
ร่วมกับการวิเคราะห์เสถียรภาพบนหลักการลาดดินอนันต์เพื่อบูรณาการความเข้าใจพื้นฐานเกี่ยวกับดิน
โคลนถล่มแบบตื้นและเป็นแนวทางในการพัฒนาระบบเตือนภัยเบื้องต้นผ่านการติดตั้งเครื่องมือวัด
สำหรับผลการทดสอบเพื่อศึกษาอิทธิพลของความเข้มฝน ความชันลาดดิน และช่วงเวลาระหว่างพายุ
(Inter-storm periods) ต่อการตอบสนองเชิงอุทกวิทยาในลาดดินตื้น พบว่า การตอบสนองทางอุทกวิทยา
ภายใต้ฝนสามารถแบ่งได้เป็น 2 ช่วง ได้แก่ การตอบสนองต่อช่วงการซึม (Infiltration phase) และช่วง
การอิ่มตัว (Saturation phase) ในช่วงการซึม ปริมาณความชื้นสูงสุดในดินจะพบเมื่อผิวหน้าเปียก
(Wetting front) ที่ถูกขับเคลื่อนด้วยฝนเคลื่อนที่ผ่านมวลดิน ซึ่งเรียกปริมาณความชื้นสูงสุดนี้ว่าความชื้น
หลังผิวหน้าเปียก (Water content behind wetting front, θ_{wb}) ในดินชนิดเดียวกัน ความชื้นดังกล่าวจะ
ขึ้นอยู่กับความเข้มฝนเพียงอย่างเดียว โดยจะไม่เปลี่ยนแปลงตามการเปลี่ยนแปลงของความชันลาดดิน
และช่วงเวลาระหว่างพายุ (Inter-storm periods) จากข้อสรุปที่ได้ เมื่อนำไปประเมินระนาบวิบัติด้วย
หลักการลาดดินอนันต์ พบว่า รูปแบบการวิบัติในลาดดินตื้นสามารถจำแนกผ่านดัชนีเสถียรภาพ
(Stability index, $\tan\varphi'/\tan\beta$) หรือสัดส่วนของอัตราการเพิ่มกำลังในดินต่อความชันลาดดินได้ 3
รูปแบบหลัก ประกอบด้วย 1) การวิบัติตามแนวชั้นทึบน้ำ (Along the impervious layer mode) 2) การ
วิบัติระดับตื้น (Shallow depth mode) และ3) การวิบัติแบบส่งผ่าน (Transitional mode) จากรูปแบบการ
วิบัติทั้ง 3 มีเพียงการวิบัติแบบส่งผ่านเท่านั้นที่อ่อนไหวเป็นอย่างมากต่อการเปลี่ยนแปลงดัชนีการซึม
(Infiltration index, i/k_s) หรืออัตราส่วนระหว่างความเข้มฝนต่อความสามารถซึมผ่านได้ของดินที่
สภาวะอิ่มตัวด้วยน้ำ ส่งผลให้ตำแหน่งของระนาบวิบัติสามารถเกิดขึ้นได้ที่ทุกระดับความลึกในลาดดิน
สำหรับการเตือนภัยเบื้องต้น กรอบแนวคิดเบื้องต้นเกี่ยวกับการจำแนกรูปแบบการวิบัติในงานวิจัยนี้
สามารถนำใช้ประโยชน์ในการระบุตำแหน่งที่เหมาะสมต่อการติดเครื่องมือเพื่อเฝ้าระวังดินโคลนถล่ม
ระดับตื้นได้ในอนาคต
        ส่วนที่สองของวิทยานิพนธ์นำเสนอผลการวิเคราะห์เชิงตัวเลขเพื่อศึกษาปัจจัยที่ส่งผลกระทบ
ต่อดินโคลนถล่มระดับตื้นและกราฟน้ำฝนวิกฤติหรือความสัมพันธ์ระหว่างความเข้มฝนและเวลาที่ลาด

ดินเริ่มเกิดการวิบัติ (Rainfall intensity-duration thresholds for initiation of slope failures, ID thresholds) ซึ่งเป็นที่นิยมใช้กันอย่างแพร่หลายในการเตือนภัยเบื้องต้น ผลการวิเคราะห์เชิงตัวเลข พบว่า อัตราการลดลงของเสถียรภาพลาดดินจะเพิ่มขึ้นตามการเพิ่มของปริมาณความเข้มฝน แต่จะคงที่เมื่อความเข้มฝนมากกว่าหรือเท่ากับความสามารถในการซึมผ่านได้ของดินที่สภาวะอิ่มตัวด้วยน้ำ ($i \geq k_s$) นอกจากนี้ความสามารถในการซึมผ่านได้ของดินที่สภาวะอิ่มตัวด้วยน้ำยังแสดงบทบาทสำคัญต่อกราฟน้ำฝนวิกฤติในการความคุมปริมาณความเข้มฝนที่สามารถกระตุ้นการวิบัติของลาดดิน กล่าวคือ เมื่อปริมาณความเข้มฝนอยู่ในช่วงต่ำกว่าความสามารถในการซึมผ่านได้ของดินที่สภาวะอิ่มตัวด้วยน้ำ เวลาในการวิบัติของลาดดินนั้นจะเร็วขึ้นตามปริมาณความเข้มฝนที่เพิ่มขึ้น แต่เมื่อไหร่ก็ตามที่ปริมาณความเข้มฝนมีค่าสูงกว่าหรือเท่ากับความสามารถของดินดังกล่าว เวลาในการวิบัติของลาดดินจะไม่เปลี่ยนแปลงสำหรับความชันลาดดินและช่วงเวลาระหว่างพายุจะแสดงบทบาทหลักต่อการควบคุมเสถียรภาพเริ่มต้นของลาดดิน โดยที่เสถียรภาพเริ่มต้นของลาดดินจะลดลงตามความชันที่เพิ่มขึ้นและการลดลงของช่วงเวลาระหว่างพายุ ดังนั้น จึงทำให้สองปัจจัยนี้ส่งผลกระทบต่อความสัมพันธ์ของกราฟน้ำฝนวิกฤติเช่นกัน

สาขาวิชาวิศวกรรมโยธา

ปีการศึกษา 2559

ลายมือชื่อนักศึกษา_____

ลายมือชื่ออาจารย์ที่ปรึกษา_____

SOMJAI YUBONCHIT : INFLUENCE INDICES FOR RAINFALL-INDUCED SHALLOW SLOPE FAILURES IN VIEW OF WARNING SYSTEM IMPLEMENTATION. THESIS ADVISOR : ASSOC. PROF. AVIRUT CHINKULKIJNIWAT, Ph.D., 185 PP.

SHALLOW LANDSLIDES/EARLY WARNING SYSTEM/SLOPE STABILITY/ FINITE ELEMENT ANALYSIS/HYDRO-MECHANICAL RESPONSES

This thesis consists of two main parts. In first part, a series of experiments were undertaken to evaluate the hydrological responses of shallow slopes of varying steepness subjected to varying intensities, periods, and inter-storm periods of rainfall. An analysis of infinite slopes were also undertaken to develop a fundamental understanding of rainfall-induced shallow landslide characteristics. The hydrological and physical responses were characterized in the infiltration and saturation phases. During the infiltration phase, the maximum water content was found behind the wetting front, termed as the water content behind the wetting front (θ_{wb}). For a certain soil type, the magnitude of θ_{wb} was found to be dependent on the magnitude of rainfall intensity, regardless of the slope gradient and initial water content. Based on the relative depth of the failure plane, the failure can be categorized by three prime modes: 1) along the impervious layer mode, 2) shallow depth mode, and 3) transitional mode. These modes can be characterized by the magnitude of a stability index termed as $\tan\varphi'/\tan\beta$ ratio. An infiltration index termed as i/k_s ratio was found to play a role in the depth of failure plane only for the transitional mode. Based on

those failure modes, primary methodology for monitoring device installations to build up physically-based warning system was introduced.

Second part presents a sets of parametric study performed via finite element modeling to investigate the effect of saturated permeability of soil, slope angle and antecedent rainfall on instability of a shallow slope. It was found that the rate of reduction in safety factor increases with an increasing the intensity of rainfall, only in a range of lower than the infiltration capacity at soil saturated state. As such the saturated permeability of the soil, which is equal to the infiltration capacity at soil saturated state, plays an important role in the shallow slope failure. The saturated permeability was found also to govern a range of applicability of the rainfall intensity-duration thresholds (ID thresholds) for initiation of slope failure. If the rainfall intensity is not greater than the infiltration capacity at soil saturated state, the rainfall duration to failure (T_{rf}) can be read from the ID thresholds. Slope angle and antecedent rainfall were found to play significant roles on instability of shallow slopes, as they control the initial stability of slope, which results in the different linear relationship of ID thresholds. In addition, the slope angle might accelerate the rate of rain water infiltration, and hence it reflects the slope of the ID thresholds.

School of <u>Civil Engineering</u>   Student's Signature _____

Academic Year 2016   Advisor's Signature _____

ACKNOWLEDGEMENTS

Jothityangkoon, Assistant Professor Dr. Pornpot Tanseng and Associate Professor Dr. Panich Voottipruex for serving as Ph.D. thesis examiners.

Finally, my doctoral study would not be completed, if I lacked spirit, power, inspiration, love and tireless supports from my beloved family. Deeply thanks to my parents Mr. Janda Yubonchit and Mrs. Mai Yubonchit. I am grateful to my younger brother and sister for very well taking care of our parents during my study. They are always in my mind.

Somjai Yubonchit

LIST OF TABLES

TABLE OF CONTENTS

TABLE OF CONTENTS (Continued)

3 HYDROLOGICAL RESPONSES AND STABILITY ANALYSIS OF SHALLOW SLOPES WITH COHESIONLESS SOIL SUBJECTED TO CONTINUOUS RAINFALL

TABLE OF CONTENTS (Continued)

TABLE OF CONTENTS (Continued)

LIST OF FIGURES

LIST OF FIGURE (Continued)

LIST OF FIGURE (Continued)

LIST OF FIGURE (Continued)

LIST OF FIGURE (Continued)

LIST OF FIGURE (Continued)

SYMBOLS AND ABBREVIATIONS

a	=	curvature of ID thresholds
c	=	intercept of ID thresholds
c'	=	effective cohesion of soil
$C(h)$	=	rate of change in the volumetric water content with respected to the pressure head
E'	=	effective modulus of elasticity
FS	=	safety factor
h	=	pressure head
i	=	rainfall intensity
I_f	=	rainfall intensity at state of slope failure
k_{sat}	=	saturated permeability of soil
$k_x(h)$	=	unsaturated permeability of soil in direction of x
$k_y(h)$	=	unsaturated permeability of soil in direction of y
$k_z(h)$	=	unsaturated permeability of soil in direction of z
m	=	gradient of ID thresholds
n	=	rate of water extraction from the soil once the air entry has been exceeded
S_e	=	effective saturation
S_{eb}	=	effective saturation behind wetting front
S_r	=	degree of saturation

SYMBOLS AND ABBREVIATIONS (Continued)

S_s = specific storage of a porous media or soil

t_b = between rainfall storm period

T_{rf} = time to slope failure

u_a = pore air pressure

u_w = pore water pressure

u_{wi} = pore water pressure

v' = effective Poisson´s ratio

Z_w = vertical depth at failure plane

Z_{wf} = critical depth

Z_t = total depth of soil layer

α = air-entry value of soil

β = slope angle

γ = unit weight of soil

γ_{sat} = total unit weight

γ_{unsat} = dry unit weight

θ_e = effective volumetric water content

θ_{fc} = volumetric water content at field capacity

θ_w = volumetric water content

SYMBOLS AND ABBREVIATIONS (Continued)

θ_{wi} = initial volumetric water content

θ_r = residual volumetric water content

θ_{sat} = saturated volumetric water content

θ_{wb} = volumetric water content behind wetting front

θ = volumetric water content

σ' = effective stress

σ^s = suction stress

σ_n = total normal stress

τ = shear strength of unsaturated soil

φ' = internal soil friction angle

χ = coefficient of effective stress

ψ_{max} = maximum pressure head

i/k_s = infiltration index

$\tan\varphi'/\tan\beta$ = stability index

CHAPTER I

INTRODUCTION

1.1   Statement of problem

Rainfall-induced failures in a shallow soil slope, which is defined by relatively thin thickness of a soil layer comparing with a slope length frequently result in natural disasters in many countries. One of the worst natural disasters in Thailand due to failure of the soil slope was in 1988. Extremely rainfall in the southern part of Thailand in 1988 resulted in widespread slope failures and caused more than 240 deaths, as well as the destruction of 1560 bridges and 5694 km of roads (Oh et al. 2008). Another great tragedy in Thailand was due to a slope failure on 10 August 2001 in Phetchabun province when a rainfall intensity of 100 mm/day induced hundreds of slope failure and sequential mudflows resulting in 136 deaths as well as economic damages of more than 15 million USD (Yumuang 2006).

An early warning system represents effective tool widely used to manage rainfall-induced disasters, including landslides, floods, and debris flows (Brand et al., 1984; Keefer et al., 1987; Wilson et al., 1993; Sirangelo and Braca, 2004). In Thailand, 1,052 early warning stations has been established by the Department of Water Resources since in 2004, which covers all 3,207 hazardous villages in Thailand. Monitoring devices including automatic thermometer, rain gauge and soil moisture sensor have been installed at warning stations to collect real-time temperature, rainfall and soil water content. The real-time

rainfall data are typically evaluated through the risk thresholds to interpret the disaster risk. The risk thresholds is usually critical rainfall triggering the initiation of rainfall-induced landslides, in which it has been empirically recognized as the cumulative rainfall of 100-300 mm in a day (the Department of Mineral Resources, 2004). The real-time rainfall data of 50-65%, 65-80%, and >80% of the critical rainfall are considered as immunity, caution and evacuation levels of the disaster risk, respectively.

The advantage of using critical rainfall thresholds as a part of early warning is its ease for fast assessment of rainfall-induced landslides. However, the rainfall thresholds has been empirically obtained by analyzing historical data of the landslides. Several factors such as soil's hydraulic properties (Pradel and Raad 1993; Rahimi et al. 2010; Ma et al. 2011; Li et al. 2013), slope geometries (Rahardjo et al. 2007; Cho 2009; Ali et al. 2014a) and antecedent rainfall conditions (Rahardjo et al. 2001; Rahimi et al. 2011; Cuomo and Della Sala 2013) that affect hydro-mechanical interactions and hence landslide characteristics are neglected. In addition, the real-time soil water content read from moisture sensor is useless, because only real-time rainfall is used to assess the risk disaster in Thailand. Previous literatures also reveal that the installation of monitoring devices (i.e., moisture sensor, tensiometors and inclinometer) can be effectively used to establish physically-based warning system (e.g., Tohari et al., 2007; Gallage and Uchimura, 2010; Greco et al. 2010), in which warning levels can be directly interpreted via real-time responses from those devices. Nevertheless, prior to install those devices, a suitable location for monitoring of rainfall-induced landslides needs to be examined.

This thesis therefore attempts to examine the factors influencing landslide characteristics and hence the critical rainfall thresholds. The aim is also to determine a primary framework of the monitoring device installations used to enhance warning system. The outcomes of thesis would provide comprehensive understanding of rainfall-induced shallow landslide mechanisms and subsequently a guideline for building up powerful warning system based on monitoring device installations.

1.2   Objectives of the study

1.2.1   To determine primary framework for installation of monitoring device used to enhance warning system for rainfall-induced shallow landslides.

1.2.2   To examine factors influencing rainfall-induced shallow landslide characteristics and the critical rainfall thresholds used for early warning system.

1.3   Outlines of thesis

This thesis consists of five chapters and outlines of each chapter are presented as follows:

Chapter II presents an overview of the theories and review of the literatures on rainfall-induced landslides. The classical methods and theories used in slope stability analysis are firstly presented. The second and third parts contain of the advance theories related to shear strength and flow behavior of unsaturated soil. Afterwards, reviews of previous researches related with rainfall-induced slope instability subjected to field

investigation, laboratory study as well as analytical and numerical simulations are discussed. Finally, various prediction methods that are commonly implemented to the warning systems are reviewed and discussed.

Chapter III presents the influences of rainfall intensity, slope angle and antecedent moisture content on hydraulic responses in shallow slopes with cohesionless soil by physical slope model. Based on comprehensive understanding achieved from laboratory experiments, the infinite slope stability analysis was developed to examine the slope stability and critical depth related to the variations of concerned factors. The results from the slope stability analysis were subsequently classified as different modes of shallow slope failures, and then the suitable locations for early warning system based on installation of the monitoring devices involved with the modes of shallow landslides was primary introduced in this chapter.

Chapter IV presents factors influencing rainfall-induced shallow landslide characteristics and critical rainfall thresholds based on finite element analysis. The numerical experiments were divided into three series to investigate the influence of rainfall intensity, slope angle and periodical rainfall. The rainfall periods in each series were prescribed as 24 hr and until slope failure initiation. Some results from the analysis were deducted to explain the mechanisms of the rainfall-induced shallow landslides. Subsequently, the numerical results subjected to 24 hr rainfall were plotted to examine influence of the concerned factors on the slope stability characteristics. Finally, the critical rainfall thresholds based on variation of concerned factors were presented by plotting rainfall intensity and duration at the initiation of the slope failures.

Chapter V concludes the present work based on two main objectives of this thesis. The findings obtained from chapter III were summarized to fulfill the first objective of this thesis. Secondly, the summary of comprehensive knowledge gained from chapter IV was illustrated. Finally, the recommendations of further research based on incompletion of present work were suggested.

1.4   Scope and limitation

Because slope failure is a wide problem, the study in the field is most difficult to install the measurement devices and to control the several factors affecting on obtained results. Therefore, the investigation of the hydraulic responses as well as the stability of shallow slope in this study is performed under the large-scale laboratory test, limit equilibrium analysis and finite element method.

1.5   References

Ali A, Huang J, Lyamin AV, Sloan SW, and Cassidy MJ. 2014a. **Boundary effects of rainfall-induced landslides.** Computers and Geotechnics 61: 341-354.

Brand EW, Premchitt J, and Phillipson HB. 1984. **Relationship between Rainfall and Landslides in Hong Kong.** In Proceedings of the 4th International Symposium on Landslides, Toronto, Canada 1: 377 - 384.

Cho SE. 2009. **Infiltration analysis to evaluate the surficial stability of two-layered slopes considering rainfall characteristics.** Engineering Geology 105: 32-43.

Cuomo S, and Della Sala M. 2013. **Rainfall-induced infiltration, runoff and failure in steep unsaturated shallow soil deposits.** Engineering Geology 162: 118-127.

DMR (Department of Mineral Resource), Thailand. 2004. Landslide risk map of Thailand.

Gallage C, and Uchimura T. 2010. **Investigation on parameters used in warning systems for rain-induced embankment instability.** In: Proceedings from the 63rd Canadian Geotechnical Conference (GEO2010), 12 - 16 September 2010, Calgary, Alberta.

Greco R., Guida A, Damiano E, and Olivares L. 2010. **Soil water content and suction monitoring in model slopes for shallow flowslides early warning applications**. Physics and Chemistry of the Earth 35(3-5): 127-136.

Keefer DK., Wilson RC, Mark RK, Brabb EE, Brown III WM, Ellen SD, Harp EL, Wieczorek GF, Alger CS and Zatkin RS. 1987. **Real-time landslide warning during heavy rainfall.** Science 238: 921–925.

Li WC, Lee LM, Cai H, Li HJ, Dai FC, and Wang ML. 2013. **Combined roles of saturated permeability and rainfall characteristics on surficial failure of homogeneous soil slope.** Engineering Geology 153: 105-113.

Ma K-C, Tan Y-C, and Chen C-H. 2011. **The influence of water retention curve hysteresis on the stability of unsaturated soil slopes.** Hydrological Processes 25: 3563-3574.

Oh H-J, Lee S, Chotikasathien W, Kim CH, and Kwon JH. 2008. **Predictive landslide susceptibility mapping using spatial information in the Pechabun area of Thailand.** Environmental Geology 57(3):641-651.

Pradel D, and Raad G. 1993. **Effect of permeability on surficial stability of homogeneous slope.** Journal of Geotechnical Engineering 119: 315-332.

Rahardjo H, Nio AS, Leong EC, Song NY. 2010. **Effects of groundwater table position and soil properties on stability of slope during rainfall.** Journal of Geotechnical and Geoenvironmental Engineering 136: 1555-1564.

Rahardjo H, Rezaur RB, Leong EC. 2007. **Factors controlling instability of homogenous soil slopes under rainfall.** Journal of Geotechnical and Geoenvironmental Engineering 133: 1532.

Rahimi A, Rahardjo H, Leong E-C. 2010. **Effect of hydraulic properties of soil on rainfall-induced slope failure.** Engineering Geology 114: 135-143.

Rahimi A, Rahardjo H, and Leong E-C. 2011. **Effect of Antecedent Rainfall Patterns on Rainfall-Induced Slope Failure.** Journal of Geotechnical and Geoenvironmental Engineering, 137(5): 483-491.

Sirangelo B, Braca G. 2004. **Identification of hazard conditions for mudflow occurrence by hydrological model.** Application of FLaIR model to Sarno warning system. Engineering Geology 73: 267–276.

Tohari A, Nishigaki M, and Komatsu M. 2007. **Laboratory rainfall-induced slope failure with moisture content measurement.** Journal of Geotechnical and Geoenvironmental Engineering 133(5): 575-587.

Wilson RC, Mark RK, Barbato G. 1993. **Operation of a real-time warning system for debris flows in the San Francisco Bay area, California.** In: Conference Hydraulics Division, ASCE, vol. 2, pp. 1908-1913.

Yumuang S. 2006. **2001 debris flow and debris flood in Nam Ko area, Phetchabun province, central Thailand.** Environmental Geology 51(4):545-564.

CHAPTER II

THEORETICAL BACKGROUND

AND LITERATURE REVIEW

2.1   Introduction

A soil slope can be defined as unrestrained soil ground placed at an angle with the horizontal that is either naturally occurring or made by humans (Das 2005). Gravitational forces are always acting on the mass of soil beneath a slope. The soil mass will always be in equilibrium, as long as the strength of the mass is greater than the gravitational driving forces. Slope failures are often initiated by processes that increase driving shear stresses and/or decrease shear strengths of the soil mass (Abramson et al. 2002). The slope instability might trigger soil movements in the different forms, for example creep, falls, slides, avalanches, or flows.

In tropical regions, rainfall has been widely recognized as the main factor triggering landslides (Anderson and Sitar 1995; Au 1998; Dai et al. 1999; Gasmo et al. 2000; Ng and Shi 1998; Toll 2001). Some researchers have reported that most landslides occur in the rainy season and result in damage to infrastructure, economic and human casualties (Sweeney and Robertson 1979; Chipp et al. 1982; Pitts 1983, 1985; Brand et al. 1984; Brand 1984; Tan et al. 1987; Johnson and Sitar 1990; Fredlund and Rahardjo 1993; Lim et al. 1996; Ng & Shi 1998; Yumuang 2006; Oh et al. 2008). Chowdhury et al. (2010) also stated that the influence of rainfall must be considered in landslide hazard assessments.

This chapter provides an overview of the theories and reviews of the literatures on rainfall-induced landslides. In the first part, the classical methods and theories used in slope stability analysis are presented. The second and third parts contain of the advance theories related to shear strength and flow behavior of unsaturated soil, respectively, which are necessary in slope stability analysis. Afterwards, reviews of previous researches related with rainfall-induced slope instability subjected to field investigation, laboratory study as well as analytical and numerical simulations are presented. Various prediction methods those are implemented to the warning system are reviewed and discussed.

2.2   Slope stability analysis

The analytical and numerical methods are broadly employed for slope stability analysis. The classical method is analytical based on the limit equilibrium method (LEM) because of its simplicity and wide-range of applications (Cheng and Lau 2008; Abramson et al. 2002). The finite element method (FEM) is a relatively modern method, which allows engineers to perform 2D or 3D slope stability assessment. Despite its complexity, FEM is likely to be used in geotechnical computer software since it has ability to model soil slopes with a very high degree of realism (e.g., complex geometry, loading sequences, reinforcement, water flow and complex soil behavior), and to visualize the deformations of soil slopes.

2.2.1 Limit Equilibrium Method (LEM)

The limit equilibrium method (LEM) is a method that assumes the slope safety factor as a constant parameter for the entire failure surface. The safety factor (*FS*) is used to define the stability of the slope, which can be determined by using the force or moment equilibrium as illustrated in Figure 2.1. In general, moment equilibrium is used for the analysis of rotational landslides, while force equilibrium is applied to translational or rotational failures composed of planar or polygonal slip surfaces (Cheng and Lau 2008).

$$FS = \frac{S_u}{\tau_{required}} \quad \text{(Total stress)}$$

$$FS = \frac{c' + \sigma' \tan\varphi'}{\tau_{required}} \quad \text{(Effective stress)}$$

LIMIT EQUILIBRIUM

$$FS = \frac{\text{Summation of resisting force}}{\text{Summation of mobilized force}}$$

FORCES

$$FS = \frac{\text{Resisting moment}}{\text{Overturning moment}} = \frac{R \int S_u \, ds}{Wx}$$

MOMENTS
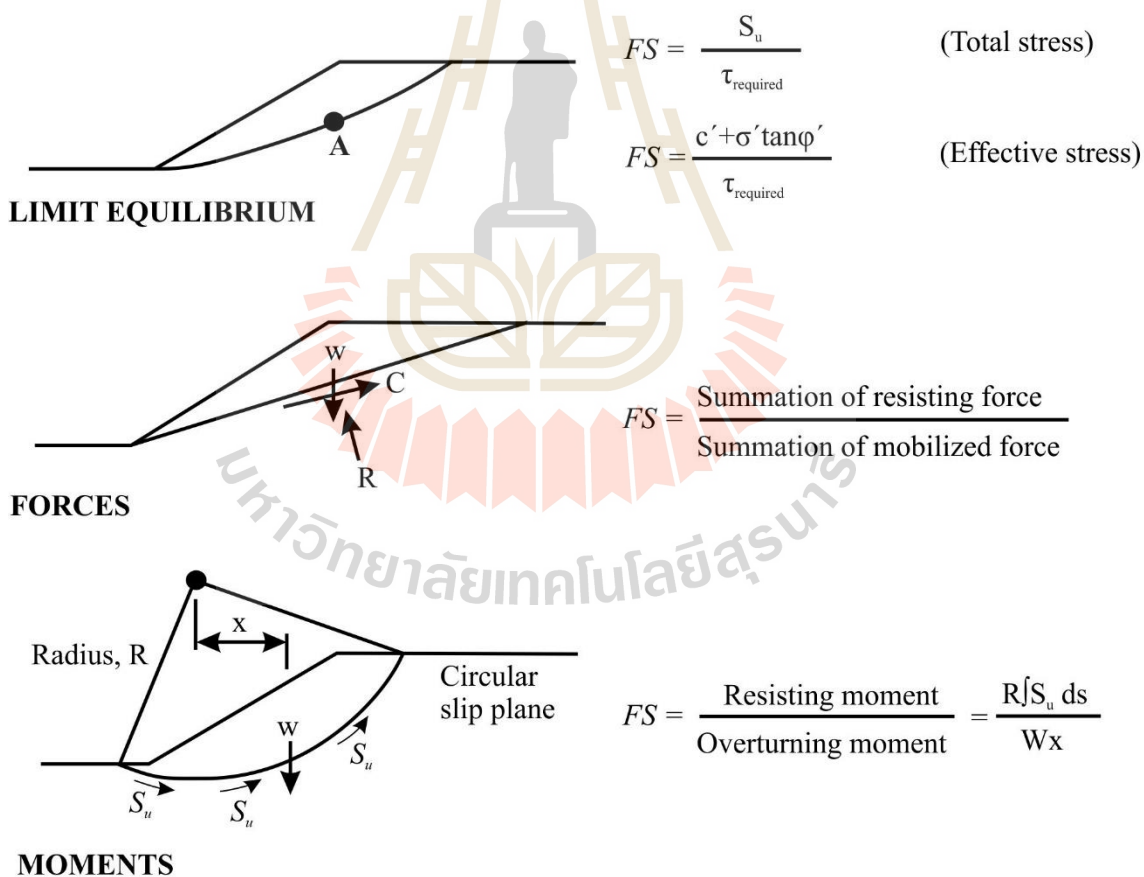
Figure 2.1   Definitions of safety factor (*FS*) (adopted from Abramson et al. 2002)

A soil slope is usually considered unstable when *FS* is lower than 1.0. However, many natural slopes have been found to be still stable even their *FS* obtained from LEM is less than 1.0. Cheng and Lau (2008) stated that this inconsistent phenomenon is due to some common processes in the analysis, such as applying an additional safety factor on the soil parameters, considering 2D analysis rather than 3D analysis and ignoring an additional stabilization due to vegetation or soil suction.

Various types of stability analysis with the limit equilibrium concepts have been used to correspond with the typical modes of failure. In the following paragraphs, some of them are briefly reviewed including, the block analysis, the infinite slope analysis, the planar surface analysis, the circular surface analysis and the popular method of slices.
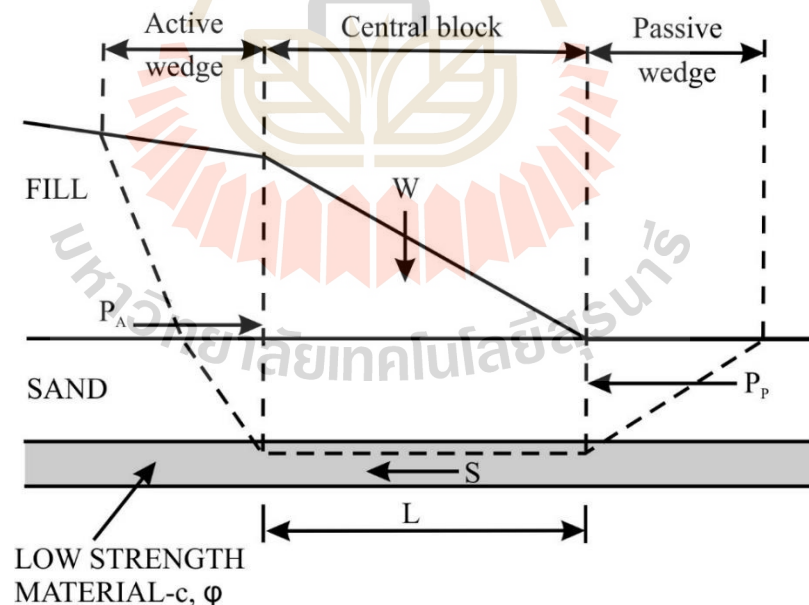
Figure 2.2   Sliding Block Analysis (adopted from Abramson et al. 2002)

A block/wedge analysis assumes a soil slope to be a compacted block. For the analysis, an active force (P_A) or a passive force (P_P) is applied to determine the magnitude of *FS*. This analysis is usually used to estimate the *FS* against sliding in situations where the shear strength of the embankment fill is greater than that of the foundation soils as illustrated in Figure 2.2.

U is pore water force.
N′ is effective normal force.
W is weight of the slice.
T is driving force.
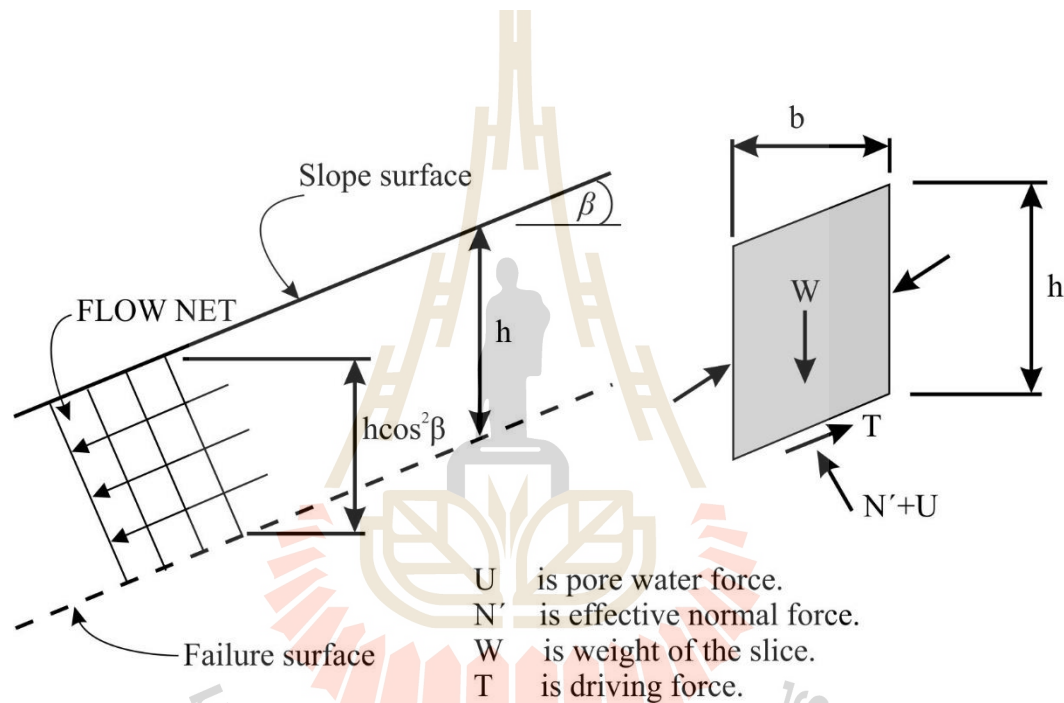
Figure 2.3 Infinite slope failure with parallel seepage (adopted from Abramson et al. 2002).

Infinite slope analysis is used for a slope that extends for a relatively long distance and has a consistent subsoil profile. In this analysis, the failure plane is assumed to be parallel to the slope surface in which the limit equilibrium method can be readily applied. For example, Figure 2.3 illustrates the infinite slope failure in a saturated soil

slope, where N′ is effective normal force, U is pore-water pressure force, W is the weight

of the slice, and T is driving force. The magnitude of FS in this case can be computed by

the ratio of available shear strength to mobilized shear force along the failure plane. Noted

that the shear strength can be computed based on the Mohr-Coulomb failure criteria for

saturated soil.
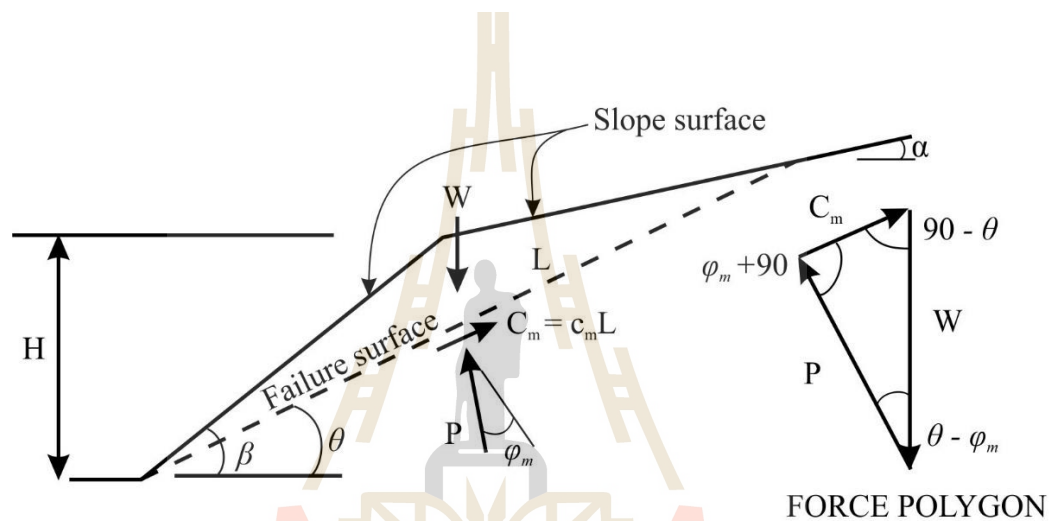
Figure 2.4   Planar Failure Surface (adopted from Abramson et al. 2002)

Planar surface analysis is used for slopes with a thin layer of soil that have

relatively low strength comparing to the overlaying materials. A planer failure surface can

be readily analyzed with a closed form solution, which is depended on the slope geometry

and the shear strength of soil along the failure plane. Figure 2.4 shows a planar failure with

three force components including weight of sliding mass (W), mobilized shear force (C_m)

and normal force (P), which are necessary to be determined for the stability evaluation

(Abramson, 2002). For the typical analysis, the procedure for computing FS requires a trial

and error solution for a $c - \varphi$ soil so that the magnitudes of FS with respect to cohesion (

$FS_c = c/c_m$) and friction ($FS_m = \tan\varphi/\tan\varphi_m$) are equal ($FS = FS_c = FS_m$), where c is

soil cohesion, φ is soil friction angle, c_m and φ_m are mobilized cohesion and friction angle,

respectively.

In homogeneous soil slopes, critical failure surfaces are formed in circular

shape. Two analytical methods for circular failure plane are common used including 1) the

circular arc method ($\varphi_u = 0$ method), and 2) the friction method ($\varphi > 0$ method). The

circular arc method is simplest circular analysis can be applied only for the soil slopes

under undrained condition. While the friction circle method can be applied for the soil

slope under both drained and undrained conditions. In other words, this method is equally

suitable for total and effective stress analysis in the soil slopes.
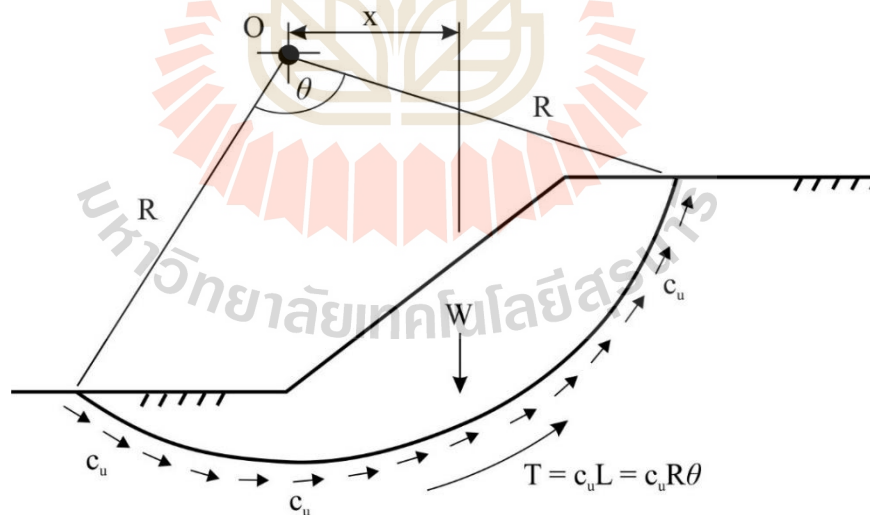
Figure 2.5   Circular failure surface in a $\varphi_u = 0$ soil (adopted from Abramson et

al. 2002)

The circular arc method ($\varphi_u = 0$ method) is based on the assumptions that a rigid cylindrical block will fail by rotation about its center, and the shear strength along the failure surface is defined by the undrained strength. As illustrated in Figure 2.5, the *FS* in the circular arc method can be defined as ratio of overturning to resisting moments following:

$$FS = \frac{c_u LR}{Wx} \tag{2.1}$$

where c_u is undrained shear strength, R is radius of circular surface, W is weight of sliding mass, x is horizontal distance between circle center, O, and the center of the sliding mass.
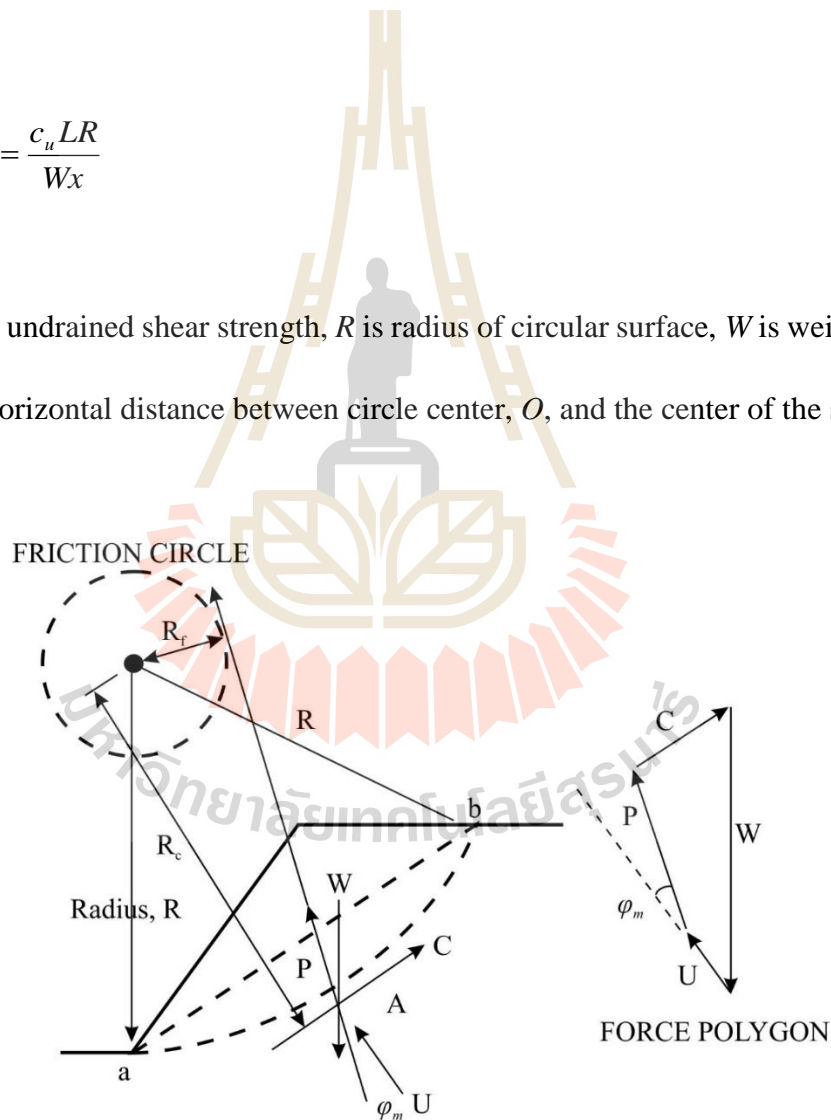
Figure 2.6   Friction circle procedure (adopted from Abramson et al. 2002)

The friction method attempts to satisfy the requirement of complete equilibrium condition. In Figure 2.6, the direction of resultant force (P) is assumed, in which P is the resultant of normal and frictional component of strength along the failure surface. The assumed direction corresponds to a line that is formed by a point of a tangent to the friction circle with a radius R_f to point A located at the intersection of all relevant forces. Based on this assumption, the value of the mobilized shear force (C_m) for computing the FS can be obtained when the force polygon is closed as shown in Figure 2.6, where W is the weight of the slice, U is pore-water pressure force. The final FS can then be computed based on assumption $FS = FS_c = FS_m$ and trial and error solution.
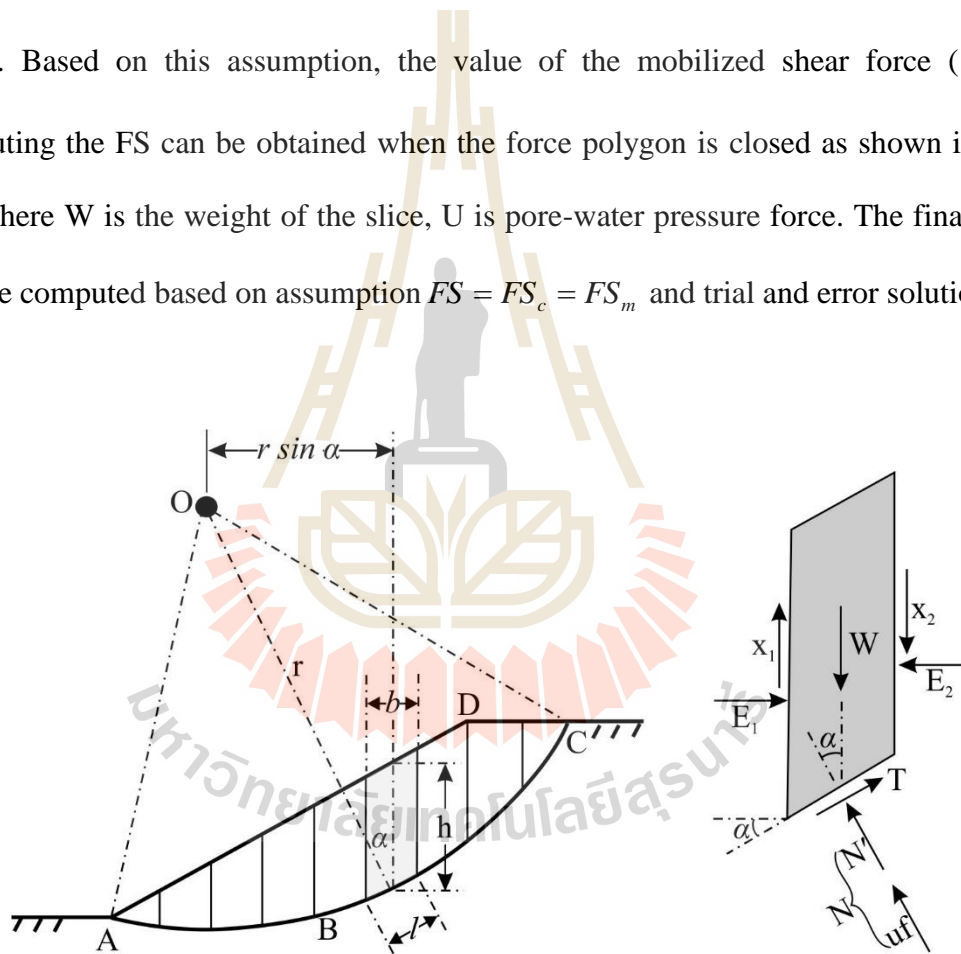
Figure 2.7   The method of slices (adopted from Craig 2004)

The most popular method for circular failure analysis is the method of slices. The soil mass (ABCD) above a trial failure surface (AC) is divided by vertical planes

into many of slices as shown in Figure 2.7, if number of slice is high enough, it is acceptable to assume a straight baseline at the slice bottom. For any slice, α is an inclined angle of the baseline, and h is the height measured on its centerline. *FS* is defined as the ratio of summations of the available shear strength (τ_f) to the mobilized shear stress (τ_m).

The method of slices has gained in popularity in the methods of analysis, due to its ability to accommodate complex geometrics and variety of soil types and pore-water pressure conditions (Terzaghi and Peck 1967). Subsequently, many models based on this concept had been introduced (Wright 1969). Comparison among the methods was discussed (Fredlund and Krahn 1977) and summarized in Table 2.1.

Fredlund and Krahn (1977) summarized that all methods have the same formation of the normal force equation with the exception of the Ordinary method. The differences in the various methods are the different assumptions relating to the inter-slice forces. The Ordinary method ignores inter-slice forces. The Simplified Bishop's method assumes that inter-slice forces are horizontal. The Spencer's method assumes that all inter-slice forces are parallel with an unknown inclination, which is computed through iterations. The Morgenstern and Price's method assumes that the shear force relates to the normal force.

The Ordinary method, Bishop's simplified and Janbu's simplified ignore vertical inter-slice forces. Due to the assumption, effective normal and pore pressure forces do not affect the moment equilibrium since they are directed through the center of the circle. Therefore, Ordinary method, Bishop's simplified and Janbu's simplified should not be used to compute an *FS* for noncircular failure surfaces (Abramson et al. 2002).

Table 2.1 Methods of slides comparisons (adapted from Fredlund and Krahn 1977; Corps of Engineers 2003)

Method	Safety Factor (FS)		Inter-slice Force Assumption (H=horizontal, V=vertical)
	Force Equilibrium	Moment Equilibrium	
Ordinary (Swedish or USBR) (Fellennius 1936)	-	✓	Ignore both H, V
Bishop's Simplified (Bishop 1955)	-	✓	V ignored, H considered
Janbu's Simplified (Janbu 1954; 1957; 1973)	✓	-	V ignored, H considered
Janbu's Generalized (Janbu 1954; 1957; 1973)	✓	-	Both H, V considered
Spencer (Spencer 1967; 1973)	✓	✓	Both H, V considered
Morgestern-Price (Morgestern and Price 1965)	✓	✓	Both H, V considered
Lowe-Karafiath (Lowe and Karafiath 1960)	✓	-	Both H, V considered
Corps of Engineers (Corps of Engineers 1982)	✓	-	Both H, V considered

Bishop's method does not satisfy the horizontal force equilibrium, and Janbu's method does not satisfy the moment equilibrium. On the other hand, Spencer's method or the Morgensters-Price's method satisfies both force and moment equilibrium. However, FS from Bishop's method and Janbu's method yield about $\pm$ 15 % difference to the FS from Spencer's method or the Morgensters-Price's method (Abramson et al. 2002).

The difference between Spencer's and Morgenstern's methods is the assumption on the direction of the inter-slice forces between each slide.

The Lowe and Karafiath's method and Corps of Engineers method determine *FS* using force equilibrium, and assume that the inter-slice force are inclined. Both methods then do not satisfy the moment equilibrium. In addition, the Corps of Engineers method presents an overdetermined system (Abramson et al. 2002).

The general limit equilibrium (GLE) method (Fredlund et al. 1981; Chugh 1986) satisfies both force and moment equilibrium. It can be used for analyzing either circular or noncircular failure surfaces. Furthermore, the GLE has the ability to model an either discrete version of the Morgenstern and Price (1965) procedure, and to implement the Spencer's method directly by using a constant inter-slice force function (Abramson et al. 2002).

Conclusively, it is important for geotechnical engineers to have a comprehensive understanding for the basic concept and limitation of various limit equilibrium methods. Variety of method requires a comprehensive knowledge to choose the most suitable method for a particular slopes.

2.2.2 Strength reduction technique based on Finite Element Method (FEM)

The Finite Element Method (FEM) can be applied to solve differential equations in engineering (Abramson et al. 2002; Hammouri et al. 2008). This method was firstly introduced to geotechnical engineering by Clough and Woodward (1967). The FEM divides the soil continuum into discrete units called finite elements, which are

interconnected at their nodes and predefined boundaries of the continuum. Typically, the displacement method formulation of the FEM is used for application in geotechnical engineering and presents the results in the form of displacements, stresses, and strains at the nodal points (Abramson et al. 2002). Previous literatures have presented reasonable agreement between the FEM analysis and the LEM analysis (e.g., Smith and Hobbs 1974; Zienkiewicz et al. 1975; Griffith 1980).
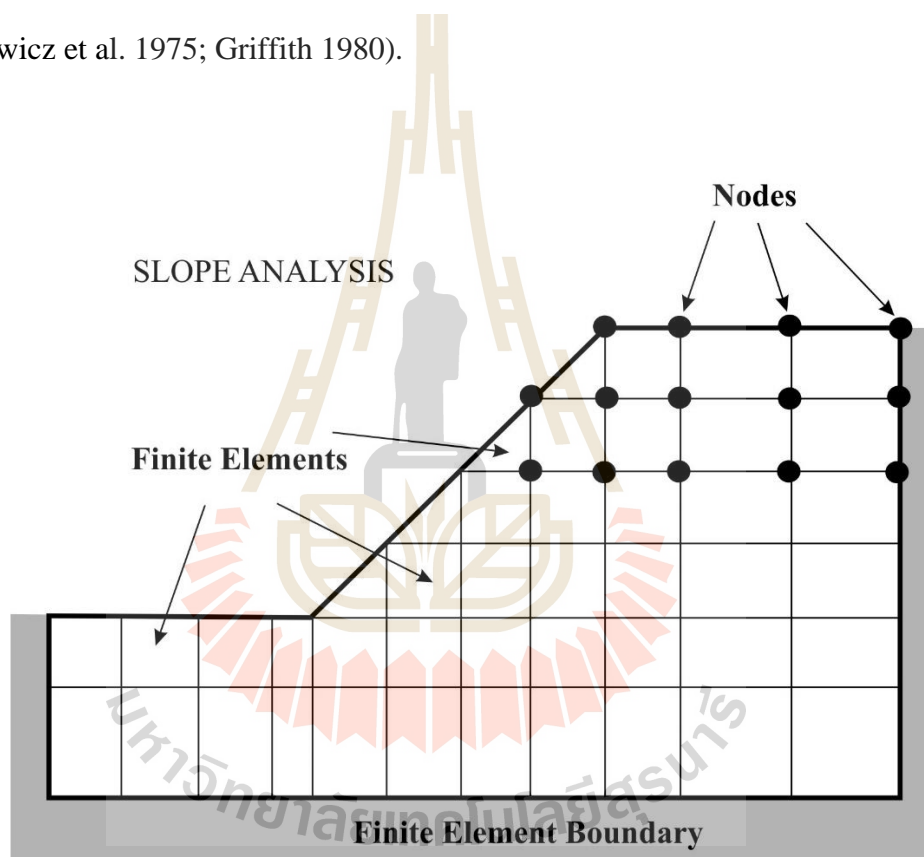
Figure 2.8 Terms in Finite Element Method (FEM) (adopted from Abramson et al. 2002)

The FEM has advantages in the slope stability analysis over LEM in the absence of assumptions for shape or location of the failure surface, slice side forces, and

their direction (Abramson et al. 2002). Complex slope configurations and soil deposits can be modelled by FEM to investigate virtually all types of mechanisms in two or three dimensions. Zaki (1999) also suggested that the real benefits are offered by FEM relative to LEM. Rocscience Inc. (2001) has confirmed that equilibrium stresses, strains, and associated shear strengths in the soil mass can be accurately computed. The critical failure mechanism can be in any shape, not just simple circular or logarithmic spiral arcs. In addition, the FEM is more practical for use in comparing the results of various LEMs. Griffith and Lane (1999) mentioned that FEM has ability to observe progressive failure, such as overall shear failure, and in providing results related to deformations at working stress levels. They also applied FEM to produce operating charts for an assessment of the slope stability under drawdown conditions (Lane and Griffiths 2000).

Rocscience Inc. (2001) stated that two approaches including: 1) the gravity loading increase to failure and 2) the strength reduction to failure can be applied for analyzing the slope stability in the FEM, potentially. The gravity loading approach generates the initial stress state of the problem by assembling calculated element forces from designed load increasing into a global force vector of the finite element mesh. The strength reduction technique is applied to determine factored shear strength parameters related to Mohr-Coulomb criterion (e.g. Matsui and San 1992; Griffith and Lane 1999) as given by the following equation:

$$C_f = \frac{c}{SRF} \tag{2.2}$$

$$\varphi_f = \tan^{-1}\left(\frac{\tan\varphi}{SRF}\right) \quad\quad\quad (2.3)$$

where C_f is factored cohesion (C), φ_f is factored friction angle(φ) and *SRF* is strength reduction factor.

Despite of the advantage of FEM, it still has drawbacks due to its uncertainties failure criteria as mentioned by Wong (1984). In FEM, the failure condition occurs progressively as a consequence of discrete elements of the soil model. Since not all elements fail simultaneously, a wide range of failure spans can be extended from the first occurrence of the yield point to the final failure of all elements. According to Wong (1984), some popular failure criteria include the bulging of slope line (Snitbhan and Chen 1976), shear limit (Duncan and Dunlop 1969), and non-convergence of the solution (Zienkiewicz 1971). Detail on these failure criteria has been described by Abramson et al. (2002), who also concluded that the interpretation of FEM results still depends on the experience and intuition in predicting the behavior of the real physical model, based on the numerical model. Hammouri et al. (2008) concluded that FEM seems to be unable to locate the critical slip surface in cases of an undrained clay slopes. They also concluded that FEM could not adequately reflect the significance when some tension cracks were modelled at different locations. In conclusion, geotechnical analysis using FEM has the benefit in presenting more detail information of slope stability regarding the stress state in the soil. However, the uncertainties in slope stability need to be emphasized to obtain valid analysis.

2.3   Shear strength of unsaturated soil

Terzaghi's principal effective stress (Terzaghi 1943) has been widely used for assessment of the slope stability. This principle states that the controlling variable for the mechanical behavior of earth materials is effective stress, which is defined as the difference between total stress and positive pore water pressure. However, rainfall-induced slope failures in natural soil slope in which rainfall infiltration results in the variations of pore-water pressures and subsequently the soil-shear strength are in unsaturated Terzaghi's effective stress principle is not applicable for assessing the state of stress as it neglects the contribution of soil suction to the soil-shear strength (e.g., Rahardjo et al. 1995; Terlien, 1998; Van Asch et al. 1999; Hornbaker et al. 1997; Mitarai and Nori 2006).

The shear strength of a soil is its ability to resist the shearing stresses taken place in the soil body. Shear failure occurs when the stresses between the particles are such that they slide or roll over other. The conventional Mohr-Coulomb (M-C) failure criterion is widely used to describe the state of stress on surfaces where failure occurs (Lambe and Whiteman 1979; Cernica 1995), which can be expressed as:

$$\tau = c' + (\sigma_n - u_w)\tan\varphi' \tag{2.4}$$

where τ is the soil-shear strength, c' is the effective soil cohesion, σ_n is the normal stress, u_w is the pore-water pressure and φ' is the effective angle of internal friction. The term $(\sigma_n - u_w)$ represents the effective stress for saturated soil (Terzaghi 1943).

Unlike the saturated soil, the pore volume in the unsaturated soil is filled by water and air phases. There are currently three approaches: 1) the independent stress state variable approach (Fredlund and Morgenstern 1977); 2) the modified effective stress approach (Bishop 1959); and 3) the effective stress under suction stress approach (Lu and Lakos 2006), for explaining the state of stress in unsaturated soil.

2.3.1   Shear strength based on independent stress variables

Fredlund and Morgenstern (1977) proposed independent stress state variable approach in term of net normal stress $(\sigma_n - u_a)$ and matric suction $(u_a - u_w)$. These stress variables are treated independently in terms of their roles in the mechanical behavior of unsaturated soil. As for shear strength, Fredlund et al. (1978) formulated an extended M-C criterion to explain the shear strength of unsaturated soil in the space of the stress variables $\sigma_n - u_a$ and $u_a - u_w$ as follows:

$$\tau = c' + (\sigma_n - u_a)\tan\varphi' + (u_a - u_w)\tan\varphi^b \qquad (2.5)$$

where u_a is the air-pore pressure, $(\sigma_n - u_a)$ is net normal stress, $(u_a - u_w)$ is matric suction and φ^b is an additional variable to describe the increase in shear strength with increasing matric suction (Fredlund et al. 1978). In equation 2.5, the shear strength of saturated soil can be described by the first two terms on the right-hand side of the equation. The third term explains the shear strength of unsaturated soil, which increase with increasing matric

suction. The 3-dimensional failure surface based on the extended M-C criterion in space ($\sigma_n - u_a$)- τ -($u_a - u_w$) is shown in Figure 2.9.

As for the parameter φ^b has been reported as a nonlinear function of matric suction in literatures (e.g., Gan et al. 1988; Escario et al. 1989; Vanapalli et al. 1996). The value of φ^b for a given soil is varied from a value equal or close to the internal friction angle φ' at near zero suction level (i.e., near the saturation state) to about 0° or even negative values for the suction level closed to the residual saturation state.
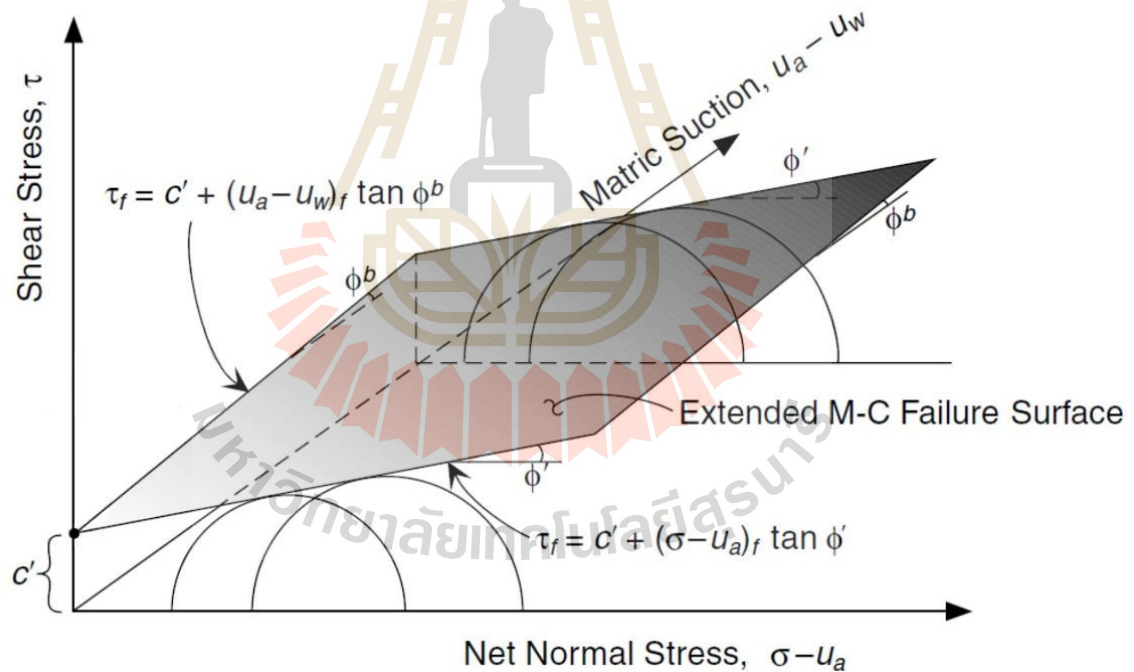
Figure 2.9   Extended Mohr-Coulomb failure surface based on independent stress variables(adopted form Lu and Lakos 2004)
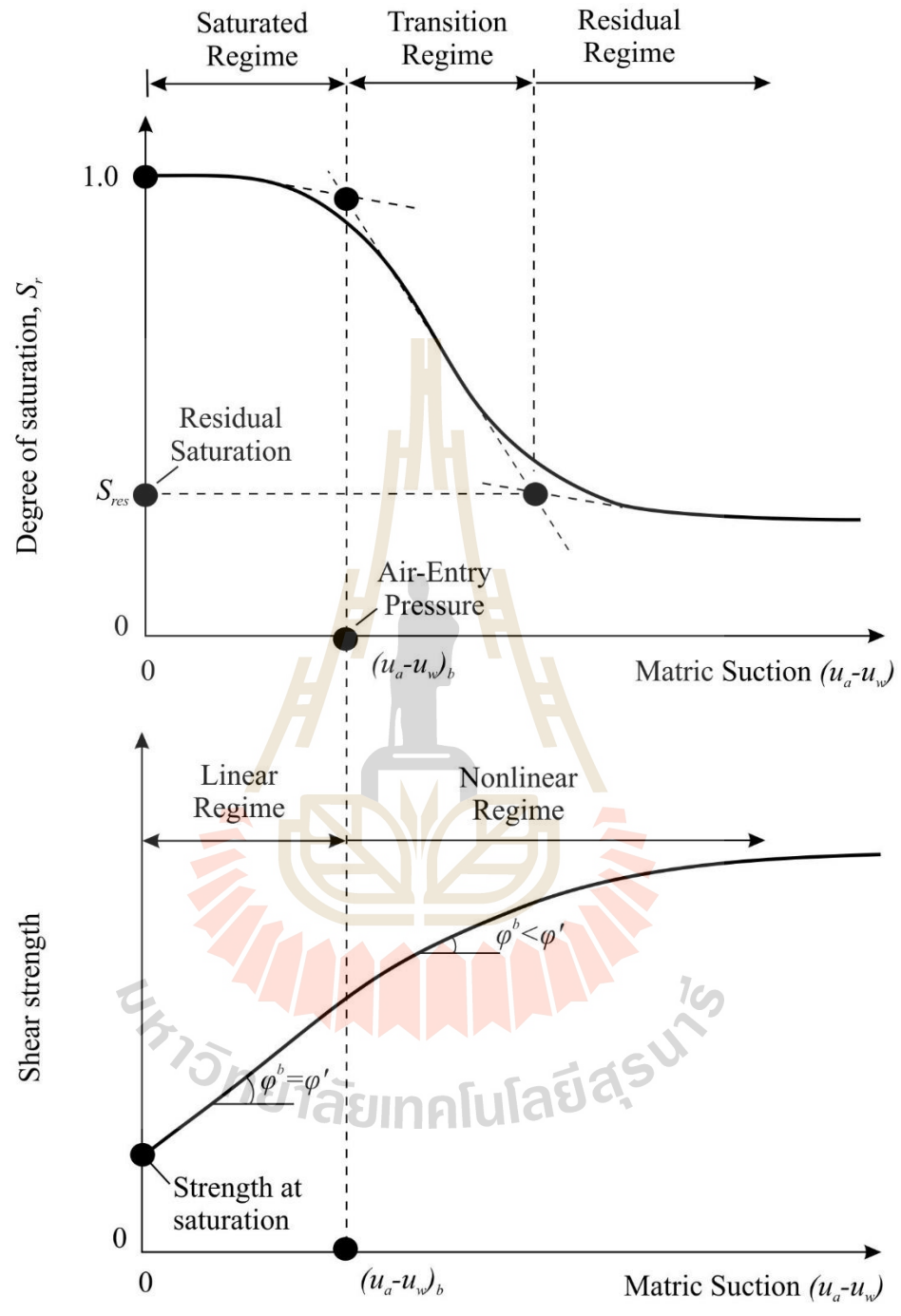
Figure 2.10 Conceptual relationship between soil-water characteristic curve and

unsaturated shear strength envelope (adopted form Lu and Lakos 2004)

The nonlinear shear strength with respect to matric suction can be explained through the soil-water characteristics curve (SWCC) as shown in Figure 2.10. Within the region prior to the air-entry pressure, the soil pores are fully filled with water, the shear strength envelop is approximately straight line, and the φ^b is equal to the internal friction angle φ'. Beyond the air-entry pressure (transition region), the nonlinear shear strength envelop is observed. In this region, the geometries of the interparticle pore menisci change, dramatically. It is therefore affecting the resultant interparticle forces, which contribute to the stresses on the soil skeleton and ultimately contribute to the shear strength. The reduction in the pore water volume reduces the shear strength contribution due to matric suction.

In engineering practices, anticipated suction values are expected to extend beyond the regime where φ^b is independent of suction, the general validity and applicability of the extend M-C approach is questioned. For analysis proposes, Fredlund et al. (1987) suggest that the nonlinearity in the relationship between shear strength and matric suction may be handled in one of several ways: (1) by dividing the failure envelop into two linear portions, the first extending from the point of saturation (zero suction) to air-entry pressure with a slope equal to φ', and the second extending beyond the air-entry pressure with a slope equal to φ^b, (2) by neglecting the nonlinearity and adopting a conservative envelope over the entire suction range with a slope equal to φ^b, where $\varphi^b < \varphi'$, or (3) by discretizing the envelope into several linear segments with varying φ^b angles (Lu and Likos 2004).

2.3.2 Shear strength based on effective stress approach

Bishop (1959) has modified Terzaghi's classical effective stress as the single-valued effective stress equation for unsaturated soil, which can be written as:

$$\sigma' = (\sigma_n - u_a) + \chi(u_a - u_w) \tag{2.6}$$

where σ' is the effective stress for unsaturated soil, χ is the effective stress parameter, which depends on the degree of saturation or matric suction. The matric suction term as $(u_a - u_w)$ contributes to the interparticle stress depending on saturated conditions. For saturated soil, u_a is zero, u_w is positive, χ is equal to one, and equation (2.6) reduces to Terzaghi's classic effective stress equation $\sigma' = (\sigma_n - u_w)$. For completely dry soil, χ is equal to zero and the effective stress is equal to the net normal stress $(\sigma_n - u_a)$. In geotechnical practice, u_a is always at atmospheric pressure, and hence σ' is the total stress. Shear strength can be described by incorporating the single-valued effective stress expression into the classical Mohr–Coulomb failure criterion as:

$$\tau = c' + [(\sigma_n - u_a) + \chi(u_a - u_w)]\tan\varphi' \tag{2.7}$$

For the effective stress parameter χ, it may not be measured or controlled through experiments, directly. However, Bishop (1954) proposed an indirect way to obtain χ from the stresses measured in the soil specimens at failure. The matric suction at failure

may be used to indirectly define the degree of saturation by the way of the soil-water characteristic curve, a one-to-one relationship between χ and degree of saturation can be established. Following this general strategy, Bishop (1959) proposed a nonlinear form of χ based on direct shear tests taken to failure shown as a function of degree of saturation in Figure 2.11.
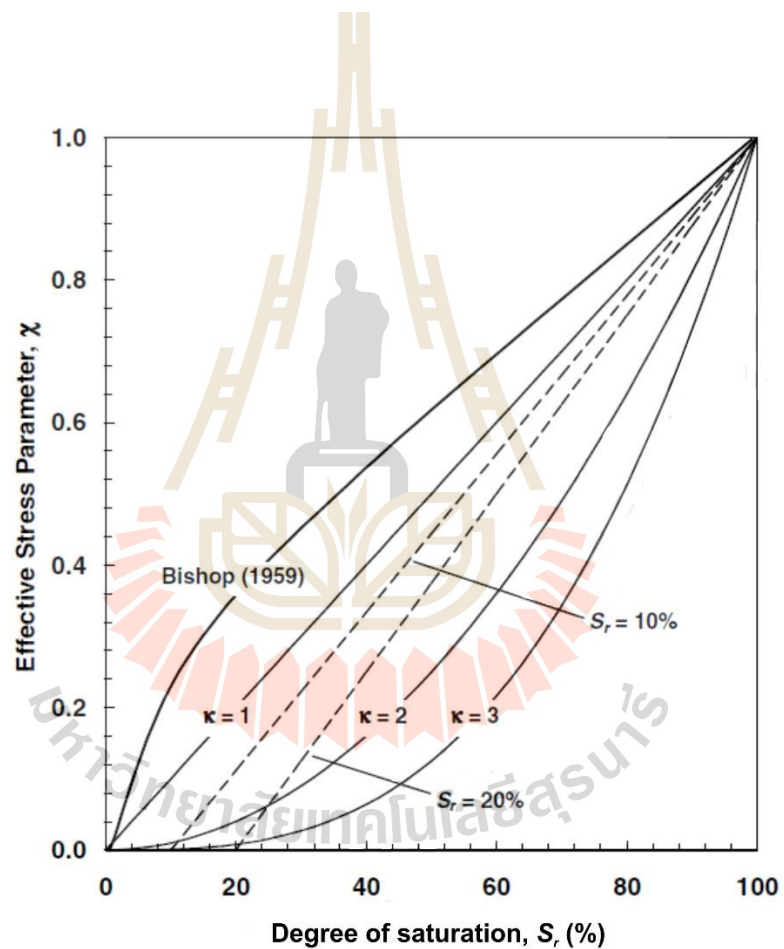
Figure 2.11   Various forms of effective stress parameter χ as function of degree of saturation

Other measurements and mathematical representations of χ have been reported as a function of degree of saturation or as a function of matric suction. Based on a best fit to the experimental data, Khalili and Khabbaz (1998) proposed a form of χ as a function of suction ratio $(u_a - u_w)/u_e$ as follows:

$$\chi = \left(\frac{u_a - u_w}{u_e} \right)^{-0.55} \qquad \text{for } u_a - u_w > u_e \qquad (2.8a)$$

$$\chi = 1 \qquad \text{for } u_a - u_w \leq u_e \qquad (2.8b)$$

where u_e is a suction value marking the transition between saturated and unsaturated states, being the air-explosion pressure for a wetting process and the air-entry pressure for a drying process. A fit of the equations to the experimental data shown is illustrated in Figure 2.12.

The validity of several forms of χ as a function of the degree of saturation was also examined by Vanapalli and Fredlund (1996) using a series of shear strength test results for statically compacted mixtures of clay, silt, and sand from Escario and Juca (1989). For matric suction ranging between 0 and 1500 kPa, the following expressions (equations 2.9 and 2.10) show good fit to the experimental results:

$$\chi = S^{\kappa} = \left(\frac{\theta}{\theta_{sat}} \right)^{\kappa} \qquad (2.9)$$

$$\chi = \frac{S - S_r}{1 - S_r} = \left(\frac{\theta - \theta_r}{\theta_{sat} - \theta_r} \right) \tag{2.10}$$

where S is the degree of saturation, θ is volumetric water content, θ_{sat} is saturated volumetric water content, and κ is a fitting parameter optimized to obtain a best fit between measured and predicted values, S_r is residual degree of saturation, θ_r is residual volumetric water content. The nature of equations 2.9 and 2.10 is illustrated in Figure 2.11 for several values of κ and S_r.
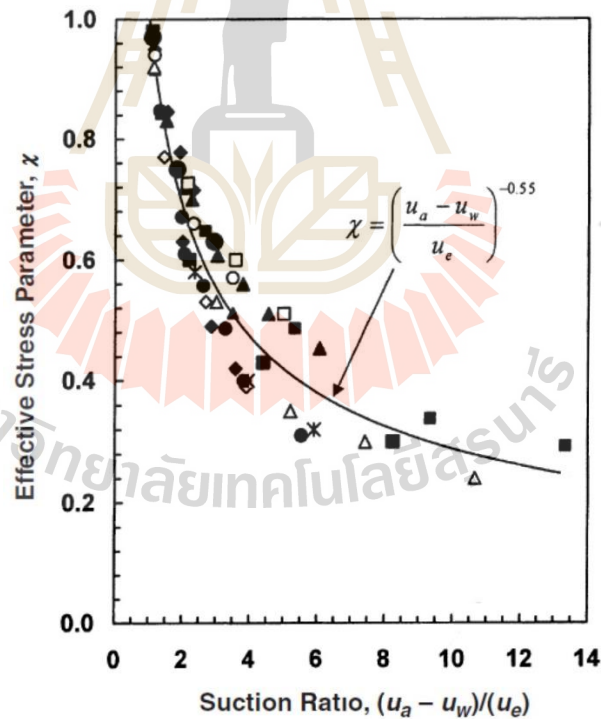
Figure 2.12 Effective stress parameter χ as function of matric suction (after Khalili and Khabbaz 1998)

2.3.3   Shear strength based on suction stress approach

Lu and Lakos 2006 questioned on the effectiveness, validity, and practicality of above two different approaches for describing the state of stress and corresponding behavior of unsaturated soil remain largely uncertain. Difficulties associated with experimentally or theoretically determining the effective stress parameter χ have limited the general applicability of Bishop's approach in research and practice. Experimental studies have suggested the non-uniqueness of $\chi = f(S)$. Similar experimental and conceptual difficulties associated with determining necessary material variables such as φ^b and uncertainties in their uniqueness over a wide range of saturation have limited the practical applicability of the independent stress variable approach. In addition, the major theoretical and practical obstacle faced by the two independent stress state variable approach is that it cannot be reconciled within the context of classical mechanics for saturated soil. In classical soil mechanics, the single stress variable (effective stress) can be used for both shear strength (e.g., limit state) and deformation (e.g., consolidation) analyses. This philosophy has been widely adopted as the design basis in geotechnical practice.

Lu and Likos (2004) and Lu and Likos (2006) have introduced the suction stress characteristic curve to represent the state of stress in unsaturated soil. It is an extension of both Terzaghi's effective stress for saturated soil and Bishop's effective stress for unsaturated soil. Like previous effective stress approaches, the suction stress approach seeks a single stress variable that is responsible for the mechanical behavior of earth materials. However, the suction stress concept differs from Bishop's effective stress,

because it eliminates the need to define the coefficient of effective stress χ, as suction

stress is solely a function of soil suction. The effective stress under suction stress concept

proposed by Lu and Likos (2006) can be written as:

$$\sigma' = (\sigma - u_a) - \sigma^s \tag{2.11}$$

where σ^s is defined as the suction stress characteristic curve of soil with a general

functional form:

$$\sigma^s = -(u_a - u_w) \qquad \text{for} \qquad u_a - u_w < 0 \tag{2.12a}$$

$$\sigma^s = f(u_a - u_w) \qquad \text{for} \qquad u_a - u_w \geq 0 \tag{2.12b}$$

The effective stress is directly defined by the stress variable of suction stress, not by matric

suction or/and another variable such as χ in Bishop's effective stress (Bishop 1959). The

expression for effective stress of this approach is similar to that for Terzaghi's effective

stress. Based on the broad experimental data available in literature and thermodynamic

equilibrium principle, Lu and Godt (2008) and Lu et al. (2010) showed that the suction

stress can be described as:

$$\sigma^s = -(u_a - u_w)\theta_e = -(u_a - u_w)\left(\frac{\theta - \theta_r}{\theta_{sat} - \theta_r}\right) \tag{2.13}$$

The shear strength based on this approach can be expressed as:

$$\tau = c' + (\sigma_n - u_a)\tan\varphi' - (u_a - u_w)\left(\frac{\theta - \theta_r}{\theta_{sat} - \theta_r}\right)\tan\varphi' \tag{2.14}$$

or

$$\tau = c' + c'' + (\sigma_n - u_a)\tan\varphi' \tag{2.15a}$$

$$c'' = -(u_a - u_w)\left(\frac{\theta - \theta_r}{\theta_{sat} - \theta_r}\right)\tan\varphi' \tag{2.16b}$$
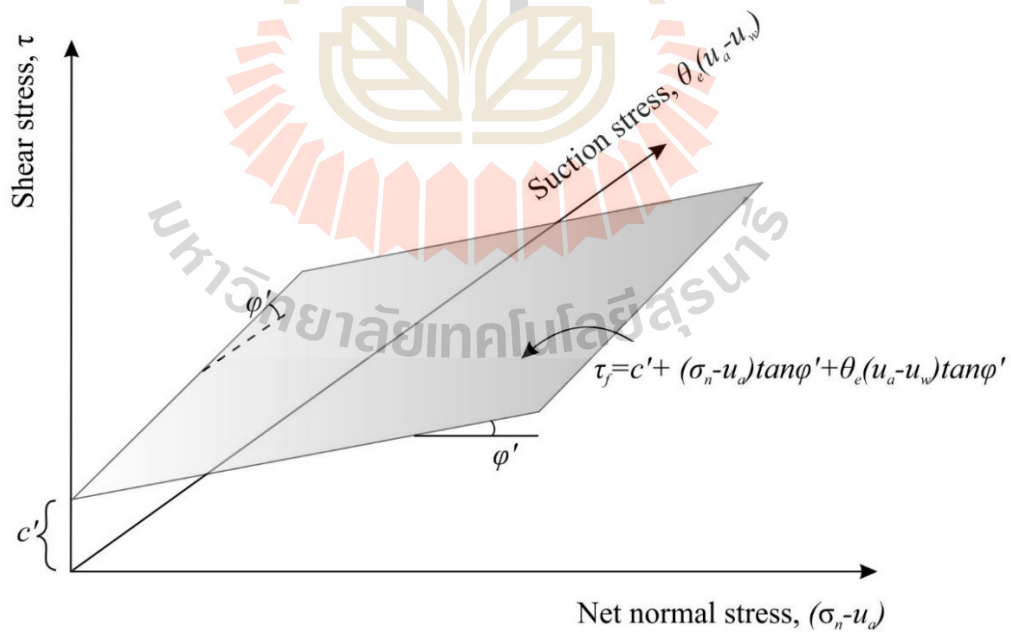
Figure 2.13   Shear strength surface in space of net normal stress, suction stress, and shear

stres

where c' and c'' represent shear strength due to the apparent cohesion in unsaturated soil. The apparent cohesion includes the cohesion term c' and a term c'', which describes shear resistance arising from capillary effects. Physically, capillary cohesion (c'') describes the mobilization of suction stress in terms of shearing resistance.
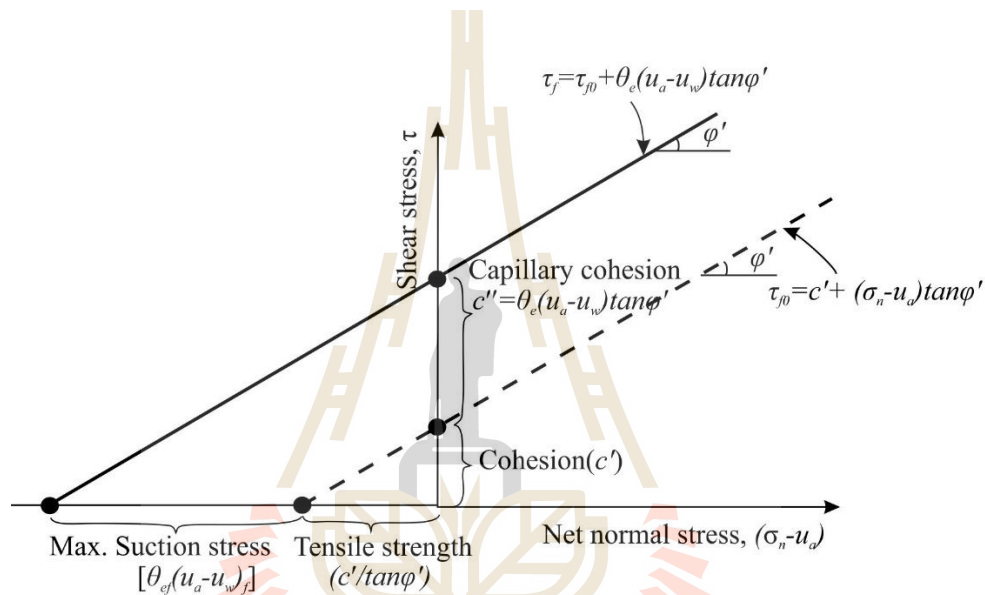
Figure 2.14   Projection of shear strength surface shown in Figure. 2.13 on shear stress-net normal stress plane

The 3-dimensional failure surface based on the concept of suction stress and capillary cohesion in space of ($\sigma_n - u_a$)-σ^s-τ is shown in Figure 2.13. In addition, the failure envelop on ($\sigma_n - u_a$)-τ plane is illustrated in Figure 2.14, which is a projection of Figure 2.13 for two values of suction stress: one for zero suction head and the other for an arbitrary nonzero value. Capillary cohesion (c'') of nonzero suction stress (the upper

envelop) is apparent from the intersection of the envelope with the shear stress axis. The

total intercept value is equal to $c' + c''$, where c' is defined by the intercept of the failure

envelop at zero suction stress. The intersections with the normal stress axis in either case

defines the tensile strength of the soil.

In the suction stress approach, the net normal stress is regarded as an

independent stress state variable and suction stress is a material variable. The definition of

suction stress and capillary cohesion are logical extension of the classical Mohr-Coulomb

criterion and the Terzaghi's effective stress principle. Physically, suction stress is an

internal stress that results specifically from the partial saturation of the soil. Suction stress

originates from the combined effects of negative pore pressure and surface tension (Lu and

Likos 2004).

2.4   Hydrological response in unsaturated soil

It is shown in former section that shear strength of unsaturated soil is varied with

varying matric suction and/or water content in the soil. In natural environment, the

variations of matric suction and water content also depend on several factors including the

soil properties (e.g., the soil-water characteristics and the soil permeability), environmental

factors including (e.g., rainfall and evaporation) and boundary drainage conditions (e.g.,

locations of groundwater level and impervious layer).
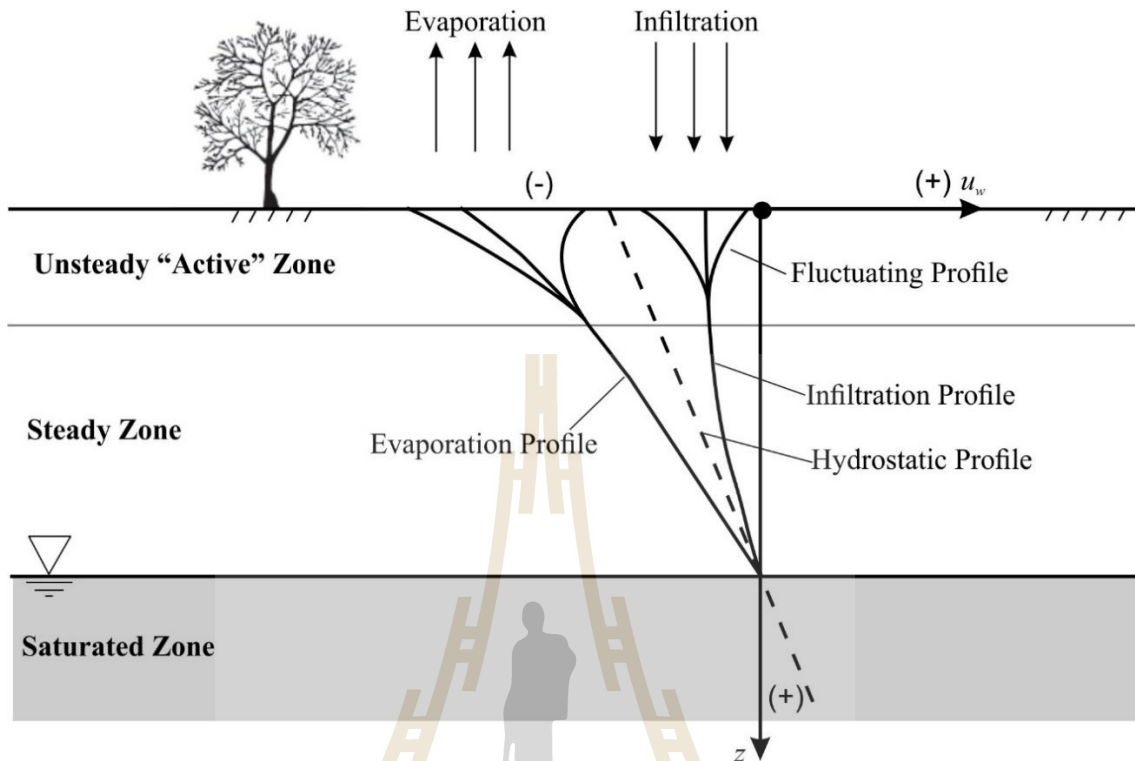
Figure 2.15   Conceptual profiles of matric suction in homogenous deposit under various

surface flux boundary conditions (adopted from Lu and Lakos 2004)

Figure 2.15 shows a typical profile of matric suction in a natural unsaturated soil.

Conceptually, the unsaturated zone can be divided into two zones including a steady-state

zone and a seasonally unsteady-state zone. In steady-state zone, matric suction is relatively

independent of time. While the matric suction profile in unsteady-state zone is fluctuated

depending on time-dependent of water flux (i.e., evaporation and infiltration). The water

flux within the unsaturated zone is a complex function of the soil's hydrologic properties.

The variations of matric suction and water content in unsaturated soil and their responses

under the variation of the water flux have been emphasized in previous and even current

researches. The following sections present a general quantitative description of transient flows through unsaturated soil.

2.4.1 Transient flow through unsaturated soil

In the unsaturated zone, the fluid motion is assumed to obey the classical Richards equation (Richards 1931). The water-mass balance equation for both unsaturated and saturated condition is:

$$-\rho\left(\frac{\partial q_x}{\partial x} + \frac{\partial q_y}{\partial y} + \frac{\partial q_z}{\partial z}\right) = \frac{\partial(\rho\theta)}{\partial t} \tag{2.18}$$

where ρ is the density of water, q_x, q_y, q_z are water fluxes in the x, y, and z directions, respectively, t is the time, and θ is the volumetric water content.

Darcy's law can be generalized to unsaturated fluid flow problems by considering hydraulic conductivity as a function of suction head (i.e., negative pressure head) (Buckingham 1907):

$$q_x = -k_x(h_m)\frac{\partial h_m}{\partial x} \; ; \; q_y = -k_y(h_m)\frac{\partial h_m}{\partial y} \; ; \; q_z = -k_z(h_m)\frac{\partial h_m}{\partial z} \tag{2.19}$$

where h_m is matric suction head and $k(h_m)$ is the unsaturated hydraulic conductivity function. In the absence of an osmotic pressure head, the total head h in unsaturated soil is

the summation of the matric suction head and the elevation head z ($h = h_m + z$). Substituting equation (2.18) into equation (2.19) with the hypothesis of constant water density, yield:

$$\frac{\partial}{\partial x}\left[k_x(h_m)\frac{\partial h_m}{\partial x} \right] + \frac{\partial}{\partial y}\left[k_y(h_m)\frac{\partial h_m}{\partial y} \right] + \frac{\partial}{\partial z}\left[k_z(h_m)\left(\frac{\partial h_m}{\partial z} + 1 \right) \right] = \frac{\partial \theta}{\partial t} \qquad (2.19)$$

The term $\partial\theta/\partial t$ in equation (2.19) can be rewritten in terms of the matric suction head by applying the chain rule:

$$\frac{\partial \theta}{\partial t} = \frac{\partial \theta}{\partial h_m}\frac{\partial h_m}{\partial t} \qquad (2.20)$$

where $\partial\theta/\partial h_m$ is the specific soil water capacity(C) represented by the slope of the relationship between volumetric water content and suction head, which is a function of suction or suction head expressed as follows:

$$C(h_m) = \frac{\partial \theta}{\partial h_m} \qquad (2.8)$$

Substituting equations (2.20) and (2.21) into (2.17), a governing equation for transient unsaturated flow can be written as:

$$\frac{\partial}{\partial x}\left[k_x(h_m)\frac{\partial h_m}{\partial x}\right]+\frac{\partial}{\partial y}\left[k_y(h_m)\frac{\partial h_m}{\partial y}\right]+\frac{\partial}{\partial z}\left[k_z(h_m)\left(\frac{\partial h_m}{\partial z}+1\right)\right]=C(h_m)\frac{\partial h_m}{\partial t} \quad (2.22)$$

Equation (2.22) can also be rewritten as a volumetric water content based equation. Following the chain rule, Darcy's law can be expressed in horizontal direction as follows:

$$q_x=-k_x(\theta)\frac{\partial h_m}{\partial x}=-k_x(\theta)\frac{\partial h_m}{\partial \theta}\frac{\partial \theta}{\partial x}=-D_x\frac{\partial \theta}{\partial x} \quad (2.23)$$

$$q_y=-k_y(\theta)\frac{\partial h_m}{\partial y}=-D_y\frac{\partial \theta}{\partial y} \quad (2.24)$$

$$q_z=-k_z(\theta)\left(\frac{\partial h_m}{\partial z}+1\right)=-D_z\frac{\partial \theta}{\partial z}-k_z(\theta) \quad (2.25)$$

Substituting equations (2.23), (2.24), (2.25) into equation (2.17), yield:

$$\frac{\partial}{\partial x}\left[D_x(\theta)\frac{\partial \theta}{\partial x}\right]+\frac{\partial}{\partial y}\left[D_y(\theta)\frac{\partial \theta}{\partial y}\right]+\frac{\partial}{\partial z}\left[D_z(\theta)\frac{\partial \theta}{\partial z}\right]+\frac{\partial k_z(\theta)}{\partial z}=\frac{\partial \theta}{\partial t} \quad (2.26)$$

where $D(\theta)$ is defined as the ratio of the hydraulic conductivity to the soil water capacity and is called hydraulic diffusivity for unsaturated soil($D=k(h_m)/C(h_m)$).

Equations 2.19 and 2.26 are the Richards' equation represented in term of pressure head and water content based equations. To solve the equations, mathematical descriptions of the soil water characteristic curve (SWCC) and hydraulic permeability function are required.

2.4.2 Hydraulic models

Hydraulic properties of unsaturated soil including Soil-Water Characteristic curve (SWCC) and permeability function of a soil are important input properties for analyzing transient flow through unsaturated soil. SWCC is the relationship representing water storage capacity of the soil with respect to various soil suction. Figure 2.16 shows a typical SWCC of a soil, which is related to some common parameters such as saturated volumetric water content θ_{sat} , residual volumetric water content and air-entry pressure. As shown in the Figure 2.16, θ_{sat} describes the point where all of the available pore space in the soil matrix is filled with water. θ_r presents the condition where the pore water resides primarily as isolated pendular menisci and extremely large changes in suction are required to remove additional water from the system. While air-entry pressure describes the point where air first starts to enter the largest pores of the soil and the soil becomes to unsaturated soil. A pressure plate apparatus is common used to obtain discrete data point of SWCC by measuring water content at steady state according to applied soil suction. To use the discrete data for subsequently applications, such as flow, stress and deformation analyses, a continuous mathematical model is then needed.
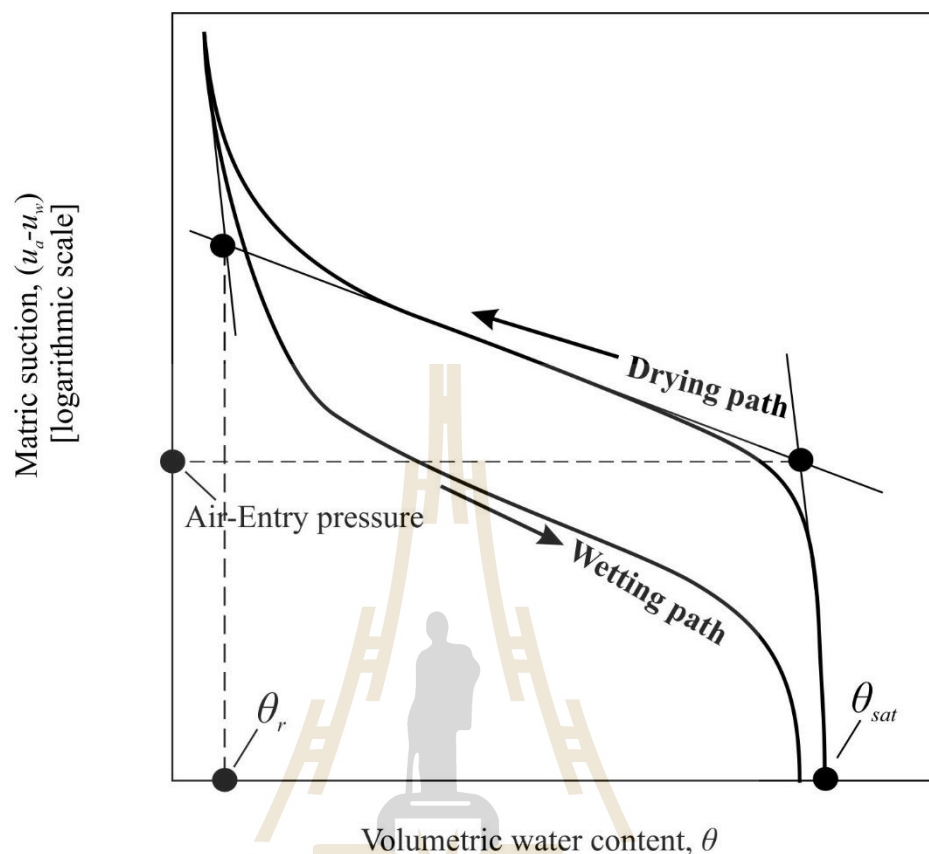
Figure 2.16 Typical soil-water characteristic curve showing approximate locations of residual water content θ_r, saturated water content θ_{sat}, and air entry pressure

Numerous researchers have proposed the mathematical models to represent SWCC. Table 2.2 summarize SWCC models proposed by several researchers (e.g. Gardner 1958; Brooks and Corey 1964; Brutsaert 1966; Campbell 1974; Van Genuchten 1980; Tani 1982; Boltzman 1984; Fermi 1987; Fredlund and Xing 1994; Ruso 1988). The SWCC models are different in term of their parameters used. The parameters used in the various SWCC models are mostly related to physical characteristics of the soil such as pore size distribution(n) and air-entry pressure(α).

Table 2.2   List of proposed SWCC models

Authors	SWCC model	Parameters
Gardner(1958)	$\theta(h) = \theta_r + (\theta_{sat} - \theta_r)\left[1 + (\alpha h)^n\right]^{-1}$	$\theta_r, \theta_{sat}, \alpha, n$
Brooks and Corey(1964)	$\theta(h) = \theta_r + (\theta_{sat} - \theta_r)(\alpha h)^{-\lambda}$	$\theta_r, \theta_{sat}, \alpha, \lambda$
Brutsaert(1966)	$\theta(h) = \theta_r + (\theta_{sat} - \theta_r)\left(1/\left(1 + \frac{h}{\alpha}\right)^n\right)$	$\theta_r, \theta_{sat}, \alpha, n$
Campbell(1974)	$\theta(h) = \theta_{sat}(\alpha h)^{\lambda}$	$\theta_{sat}, \alpha, \lambda$
Van Genuchten(1980)	$\theta(h) = \theta_r + (\theta_{sat} - \theta_r)\left[1 + (\alpha h)^n\right]^{-(1 - 1/n)}$	$\theta_r, \theta_{sat}, \alpha, n$
Tani (1982)	$\theta(h) = \theta_r + (\theta_{sat} - \theta_r)\left[1 + (\alpha h)e^{-\alpha h}\right]$	$\theta_r, \theta_{sat}, \alpha$
McKee and Bumb (1984)	$\theta(h) = \theta_r + (\theta_{sat} - \theta_r)\exp\left(\frac{\alpha - h}{n}\right)$	$\theta_r, \theta_{sat}, \alpha, n$
McKee and Bumb (1987)	$\theta(h) = \theta_r + (\theta_{sat} - \theta_r)\left(1/1 + \exp\left(\frac{\alpha - h}{n}\right)\right)$	$\theta_r, \theta_{sat}, \alpha, n$
Fredlung-Xing(1994)	$\theta(h) = \theta_r + \dfrac{(\theta_{sat} - \theta_r)}{\left[\ln\left(2.7183 + (ah)^n\right)\right]^m}$	$\theta_r, \theta_{sat}, a, n, m$
Ruso(1988)	$\theta(h) = \theta_r + (\theta_{sat} - \theta_r)\left[(1 + 0.5\alpha h)e^{0.5\alpha h}\right]^{\frac{2}{2+n}}$	$\theta_r, \theta_{sat}, \alpha, n$

Noted that *h* is suction head.

Van Genuchten model (Van Genuchten 1980) is widely used in the areas related to unsaturated soil (e.g., rainfall-induced slope failures) because of its flexibility to capture the characteristic curve over a wide range of suction. Furthermore, the fitting parameters used in the van Genuchten model can explained in term of physical meaning (i.e. pore size distribution and air entry pressure). The van Genuchten equation can be expressed as follows:

$$\theta_e = S_e = \left\{ \frac{1}{1 + [\alpha(u_a - u_w)]^n} \right\}^{1 - \frac{1}{n}} \tag{2.27}$$

where θ_e is effective volumetric water content, which is equal to the effective degree saturation (S_e), α is a parameter that approximates the inverse of the air-entry pressure, n is a parameter related to the pore size distribution of the soil

Figures 2.17(a) and 2.17(b) respectively present the influences of changing pore size parameter n and air entry parameter α on the shape of SWCC. As for a certain n value, soils with high air-entry pressure are characterized by smaller values of α. The parameter n controls slope of the SWCC in range of desaturation zone. Soils with a flatter characteristic are captured by greater value of parameter n.

There are mathematical models for predicting the permeability functions of unsaturated soils, which is the relationship between soil suction and soil permeability (Gardner 1958; Brooks and Corey 1964; Van Genuchten 1980; Fredlund et al. 1994). The permeability function proposed by Gardner (1958) is widely used to explain permeability-
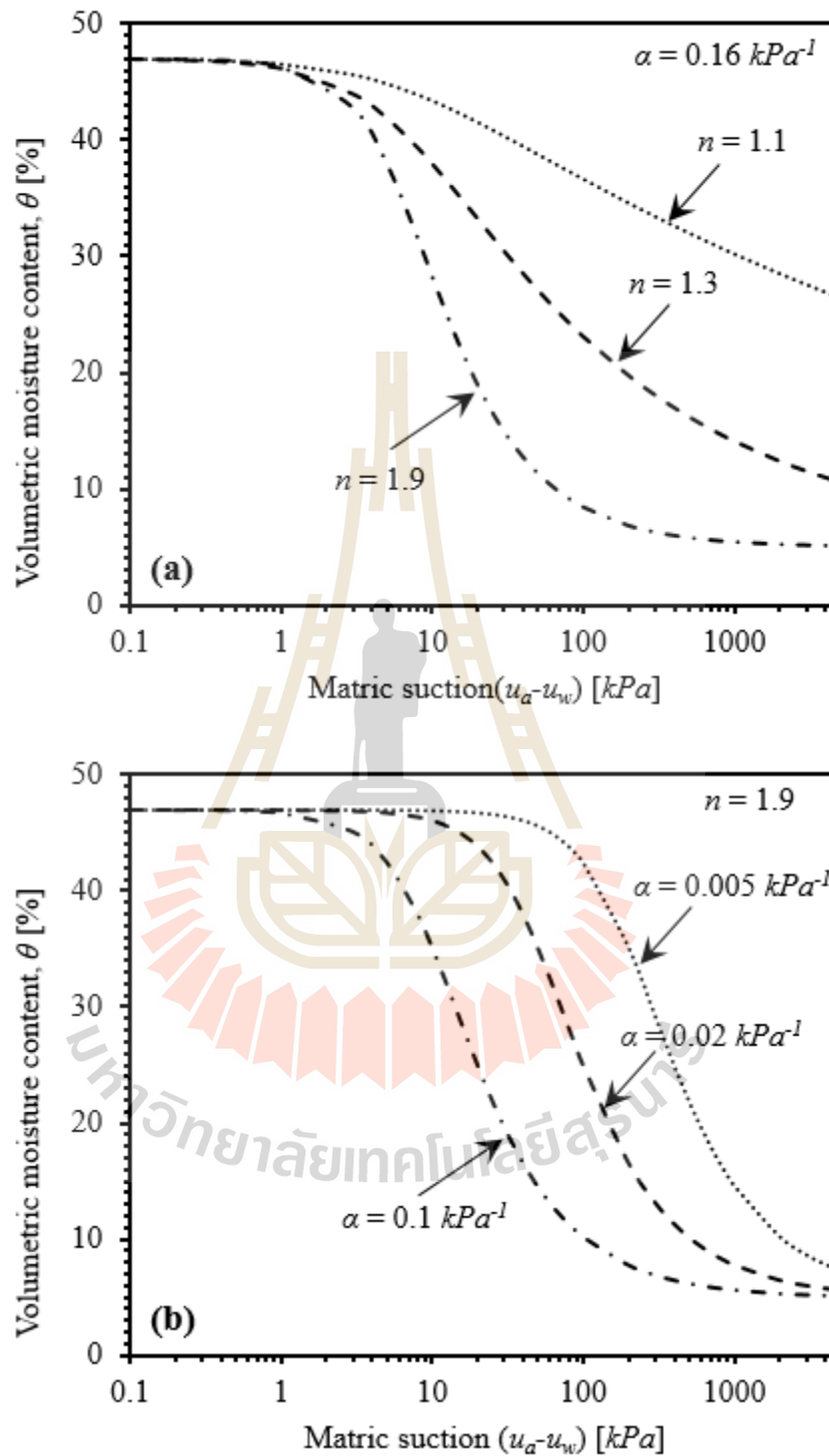
Figure 2.17 Soil-water characteristic curves based on van Genuchten equation showing

effects of changes in (a) the *n* parameter and (b) the α parameter

characteristics of unsaturated soil because of its simplicity. Gardner model requires only one model parameter (α) for exponential function, which can be written as:

$$k(h) = k_{sat} \exp\left[-\alpha(u_a - u_w)\right] \tag{2.28}$$

where k_{sat} is saturated permeability of soil.

Van Genuchten (1980) proposed a more flexible closed-form equation for the permeability function of unsaturated soil by substituting the proposed SWCC model (equation 2.27) into the permeability function proposed by Mualem (1976), subsequently called Mualem-Van Genuchten model. The equation can be expressed as:

$$k(h) = k_{sat} \frac{\left\{1 - \left[\alpha(u_a - u_w)\right]^{n-1}\left\langle 1 + \left[\alpha(u_a - u_w)\right]^n \right\rangle^{\frac{1}{n}-1}\right\}^2}{\left\{1 + \left[\alpha(u_a - u_w)\right]^n\right\}^{\frac{1}{2}-\frac{n}{2}}} \tag{2.29}$$

Equation 2.29 can be also rewritten as a function of effective saturation as follows:

$$k(S) = k_{sat} S_e^{0.5}\left[1 - \left(1 - S_e^{\frac{n}{n-1}}\right)^{\frac{n-1}{n}}\right]^2 \tag{2.30}$$

Equations 2.29 and 2.30 are the permeability equations of unsaturated soil defined as functions of matric suction and effective degree of saturation, respectively.

2.5   A brief reviews on rainfall-induced slope failures

Rainfall-induced landslide is related to hydrological-mechanical interactions within natural soil slopes. Theoretically, rainfall infiltration results in an increase in pore-water pressure and hence lowered soil shear strength. Rainfall-induced slope instability is intently difficult task, due to several factors affect characteristics of the slope instability. Many researchers have attempted to investigate the mechanisms and factors influencing rainfall-induced slope instability using different methodologies including field investigations, laboratory investigations and analytical and numerical simulations. Conclusive results on rainfall-induced slope failures are discussed in the following sections.

2.5.1   Field investigations

Rainfall infiltration has been widely known as the main hydrological process that results in the reduction of the matric suction, shear strength, and subsequently slope stability of an unsaturated soil slope. A number of researchers have investigated the effects of rainfall infiltration on the matric suction in residual soil slopes using in-situ field instrumentations (Duncan 1972; Flyod 1981; Lim et al. 1996; Zhang et al. 2000; Tsaparas

et al. 2003; Rahardjo et al. 2003b). Some of these researchers used a rainfall simulator to apply rainfall to in-situ slopes (Duncan 1972; Flyod 1981; Loch et al. 2001).

Lim et al. (1996) investigated the effects of surface conditions of a residual soil slope on its rainfall-induced instability. In this investigation, a sets of tensiometers were installed to monitor the variations of the matric suction profiles in residual soil slopes with different surface conditions including, a canvas covered grassed surface, a grassed surface, and a bare ground surface. They concluded that the matric suction in the slope with the bare surface decreased rapidly during rainfall infiltration causing the slope unstable.

Zhang et al. (2000) carried out an in-situ infiltration tests on a hillside near the Three Gorges Dam in China. They found that the presence of geological discontinuities can disturb the infiltration pattern, when the slightly inclined joints impeded the water flow in soil and caused the development of perched water above the joints. Meanwhile, lateral drainage of rainwater occurred through the laterally extended joints, which reduced the rise of groundwater due to rainfall infiltration.

Tsaparas et al. (2003) performed a field investigation over 12 months to observe the infiltration characteristics of two residual soil slopes in Singapore. These two locations were instrumented for monitoring the pore-water pressure changes during infiltration. At one of the locations, additional measurements were made for determining water runoff from natural and simulated rainfall. By analyzing the results from the runoff measurements, they stated that rainwater infiltration is affected by the total rainfall and the initial pore-water pressures of the soil slope at the beginning of the rainfall event. Those two parameters can be used as the controlling parameters for observing the changes in the

pore-water pressure within the soil slope during infiltration. Total runoff increases with increases in total rainfall. The runoff measurement also indicated that there is an upper limit on how much rainfall can infiltrate into the soil slope. They also concluded that, for a total rainfall up to 15 mm, the pore-water pressure changes are controlled by the amount of rainfall and unaffected by the initial pore-water pressure. In contrast, for total rainfall greater than 15 mm, the amount of infiltration is highly affected by the initial pore-water pressure conditions.

Rahardjo et al. (2005) investigated the hydrological responses of a residual soil slope to different rainfall conditions. They carried out a field study under natural and simulated rainfall conditions, on a residual slope that was instrumented with pore-water pressure, water content, and rainfall monitoring devices. From their experiment, it was found that a large proportion of the rainfall contributes to infiltration into the residual soil slope. They concluded that smaller magnitude of total rainfall might contribute fully to infiltration, while larger magnitude of total rainfall contributes more to runoff than infiltration. Infiltration and runoff amounts are influenced by the antecedent rainfall in the slope. This rainfall amount also play role on an increment of pore-water pressure. From the results of this experiment, they concluded that it is vital to know the amount of infiltration excluding from runoff water since the infiltrated water plays significant role on stability of the soil slope.

2.5.2 Laboratory investigations

Orense et al. (2004) conducted a series of laboratory experiments on sandy slopes to determine the triggered process of rainfall-induced landslides. Water was percolated into the slope model from the side upslope, and by simulated rainfall on top of the slope model. The pore water pressure, the soil water content and ground deformation in this study were recorded. The results from laboratory experiments were discussed that instability of soil slope occurs only when the water table is allowed to rise during rainfall infiltration and suction decreases. The authors established the following statement based on the displacement analysis, "when the water table approaches the slope surface, especially near the toe, a highly unstable zone is formed in that area and slope failure may be triggered." They also suggested that prediction of slope failure initiation is possible by monitoring degree of saturation, displacements and pore water pressure within the slope.

Huat et al. (2006) performed a physical slope model in a laboratory to investigate the rainfall infiltration characteristics in soil slope. During the test, the slope angle can be adjusted to reach a desired slope angle. Effect of surface covers were investigated by varying different types of cover material during the test. They concluded that type of surface covers plays role on the rainfall infiltration. They also found that rainfall infiltration decreases with increasing the steepness of soil slope.

Tohari et al. (2007) carried out a series of experiments on rainfall-induced failures using physical model tests in a laboratory. To construct a number of homogeneous experimental slopes in this study, two different sandy soils namely river sand and residual granite soil were used. A metal tank with maximum dimensions of 2.0x1.0x1.5 m was used

in this experiment. One side of the tank was constructed by a 20 mm thick acrylic board for allowing simple installation of the instrument system and observation of the deformation process. A rainfall simulator was designed to produce an effective rainfall intensity of approximately 10 cm/h and set approximately 1.0 m above the model slopes to induce the change in volumetric moisture content and instability in the model slope. They concluded that rainfall-induced slope failures are essentially initiated under drained conditions by the loss of lateral support resulting from earlier localized seepage induced failures. This instability of the seepage area may have an effect on the overall stability of the slope. Therefore, monitoring the formation of seepage areas needs to be investigated for the prediction of a particular slope failure hazard during a particular rainfall.

Lee et al. (2011) conducted 1-D soil column and 2-D slope model using rainfall simulator. The tests were conducted on four typical types of residual soils (i.e., sand-gravel, silty gravel, sandy silt, and kaolin), with one and two-layered soil system under various rainfall intensity and duration. The results showed that the suction distributions for the single-layered homogeneous soils obtained from the one-dimensional soil column were almost identical to those obtained from two-dimensional slope model. They found that the lateral flow plays dominant role on suction distributions. In addition, they also concluded that the minimum suction value in soil during infiltration process is governed by the rainfall intensity, rainfall duration, and the saturated permeability of soil.

Tiwari and Lewis (2012) conducted experiments on slope models made of sand at different slope angles, which were later exposed to rainfall-induced infiltration. The variation of suction, moisture content and location wetting front, with time were recorded.

The author also considered the seismic effect on slope stability, on which the soil slope models were shaken with different accelerations before and after the rainfall events. They concluded that for sandy slopes the variation of degree of saturation depends on the steepness of the slope. They reported that the value of seismic acceleration increases with the increase in the distance from the base in dense soil. They also observed that variation of suction after the seismic event also showed a loss in apparent cohesion in saturated sandy soils which created a loss of stability in slopes.

Phi et al. (2013) curried out using two-dimensional slope model in laboratory to examine hydrological responses on hillslope slope system. The slope model were conducted with a uniform slope angle and high permeable soil (k_{sat} = 1.28 cm/min) subjected to various rainfall intensity. They concluded that the responses of pore water pressure in slope model are characterized into two phases. First the wetting front moves vertically downwards at all locations along the slope. The saturation state of the soil in this phase remains unsaturated state as the wetting front passed. Furthermore, the magnitude of negative pore water pressure in this phase depends on both rainfall intensity and soil's saturated permeability. The second phase is related to the upward expansion of the saturated zone when the wetting front arrives impervious layer (simulated bedrock). The accumulation of water generates an increasing in water table, and consequently positive pore water pressure. The findings by Phi et al. (2013) are supported by the previous laboratory investigations including Tohari et al. (2007), Huang et al. (2008, 2010) and Sharma and Nakagawa (2010).

2.5.3 Analytical and numerical analyses

Slope failures in unsaturated soils are often induced by rainfall infiltration. The characteristics of water flow, change of pore-water pressure, and shear strength of soils are the major parameters related to slope stability analysis involving unsaturated soils that are directly affected by the flux boundary condition (i.e., infiltration and evaporation), soil's hydraulic properties and slope geometries.

There are numerical investigations on mechanism of rainfall-induced slope failures (Ng and Shi 1998; Gasmo et al. 2000 and Ng et al. 2001; Cho and Lee 2001; Cai and Ugai 2004; Zhang et al. 2004; Collins and Znidarci 2004; Griffiths and Lu 2005). Ng and Shi 1998 concluded that rainfall infiltration causes a decrease of matric suction and permeability of unsaturated soil. Gasmo et al. (2000) also showed that the matric suction increased over time due to the applied evaporation, and subsequently decreased over time due to rainfall infiltration. As for stability analysis, the slope stability increases slowly due to evaporation and decreases rapidly due to infiltration. In addition, rainfall characteristics (i.e., pattern, intensity and duration of rainfall), soil's hydraulic properties (i.e., soil's saturated permeability and SWCC) and initial degree of saturation have been recognized as a significant influence on pore water pressures, water content, shear strength and thus soil slope stability (Ng et al. 2001; Cho and Lee 2001; Cai and Ugai 2004; Zhang et al. 2004; Griffiths and Lu 2005). The rainfall intensity expressed as a proportion of soil's saturated permeability is also indicated as main factor influencing the matric suction near the ground surface. When the rainfall intensity is equal to or greater than soil's saturated permeability, soil's saturated permeability effectively turns into the upper limit of

infiltration rate (Zhang et al. 2004). Furthermore, Collins and Znidarci (2004) concluded that various triggering mechanisms may occur due to slope geometry, soil strength and infiltration patterns. The rainfall-induced landslides are a complex problem that involves the analysis of seepage forces, infiltration pattern from unsaturated to saturated regimes and soil shear strength.

Factors influencing rainfall-induced slope failures can be clearly confirmed by a sets of parametric study from previous researches (Rahardjo at al. 2007; Rahardjo at al. 2010; Rahimi et al. 2010; Rahimi et al. 2011). Seepage analysis based on finite element method and limit equilibrium method for stability analysis were performed on a homogenous soil slope, where circular failure modes were assumed. Rahardjo at al. 2007 concluded that soil's saturated permeability and rainfall intensity are the primary factors controlling the stability of slopes. While the initial water table location and slope angle play a secondary role, which only governs the initial stability of the slope. The fitting parameters of SWCC affect the slope stability on low permeable soil slopes more significantly than the stability of high permeable soil slopes, which is not sensitive to the variation of SWCC fitting parameters (Rahimi et al. 2010). Rahimi et al. (2011) also stated that the significance of antecedent rainfall on the slope stability depends on soil's permeability.

As for shallow soil slopes, where the thickness of soil layers is thin compared to the slope length and failure plane is parallel to the slope surface, there are stability analyses on the shallow slopes based on infinite stability analysis (Pradel and Raad 1993; Ma et al. 2011; Santoso et al. 2011; Cuomo and Sala 2013; Li et al. 2013; Ali et al.

2014a; Ali et al. 2014b). Pradel and Raad 1993, Santoso et al. 2011 and Ali et al. 2014b have found that soil's permeability plays an important role on shallow slope stability. Cuomo and Sala (2013), Ma et al. (2011) and Li et al (2013) have described that the rainfall characteristics (rainfall intensity and duration), soil's hydraulic properties (soil's saturated permeability and SWCC) and slope angle are predominant factors controlling the hydraulic responses of soil slope, the occurrence time and depth of failure planes. In addition, the boundary conditions defined as fully drained, partially drained, and impermeable boundaries significantly affect the occurrence time and depth of rainfall-induced shallow landslides (Ali et al. 2014a).

2.6 Prediction methods for rainfall-induced landslides

Rainfall-induced landslide is one of the most dangerous disasters frequently found in mountainous regions all around the world, especially regions that routinely experience heavy rainfall (Aleotti and Chowdhury 1999; Guzzetti et al. 1999; Dai et al. 2002; Liao et al. 2006; Yumuang 2006; Oh et al. 2008). These landslides significantly affects nearby community, infrastructure and economic damages (Iverson 2000; Hong et al. 2006; Yumuang 2006; Oh et al. 2008; Kirschbaum et al. 2009a). Therefore, an early warning system is very important tool to mitigate those damages. To build up the system, the methodology for predicting rainfall-induced landslides needs to be implemented as a significant part of the system. The prediction methodology should be normally based on simplicity and ease of usage to get faster real-time assessment of rainfall-induced landslides, and to provide the timely warning for the people living nearby hazardous areas.

In last decades, many researchers have attempted to propose the rainfall-induced landslide prediction methods that are potentially implemented to an existed early warning system. The prediction methods proposed by various researchers can be mainly characterized into two groups including empirically-based method (e.g., Chen et al. 2005; Caine 1980; Marchi et al. 2002; Alieoti 2004; Chen 2005; Giannecchini 2005; Godt et al. 2006; Chleborad et al. 2006; Matsushi and Matsukura 2007; Guzzetti et al. 2007; Caine 1980; Keefer et al. 1987), and a physically-based method (e.g. Osman and Barakbah 2006; Tohari et al. 2007; Baum and Godt 2009; Gallage and Uchimura 2010; Vieira et al. 2010; Pagano et al. 2010; Ren et al. 2010; Lin et al. 2010; Chang and Chiang 2009; Sakellariou and Ferentinou, 2001).

2.6.1 Prediction using empirically-based method

An empirically-based method is mostly expressed as a simply mathematical equations for predicting rainfall-induced landslides. Because rainfall has been widely recognized as main factor triggering slope failures (Anderson and Sitar 1995; Au 1998; Dai et al. 1999; Gasmo et al. 2000; Ng and Shi 1998; Toll 2001), the empirically-based equations have been statistically proposed via interpreting and analyzing historical data or local experiences of rainfall events resulting in the initiation of slope failures. Mostly, the equations are represented as a relationship between rainfall intensity (I) and duration (D) at initiation state of slope failures, which are broadly called "rainfall intensity-duration thresholds for initiation of slope failure (ID thresholds)". The general expression of the ID thresholds can be presented as follows:

$$I_f = a + cT_{rf}^{m} \qquad\qquad (2.31)$$

where a, c and m are the ID thresholds parameters which represent the curvature, intercept and gradient of ID thresholds, respectively.

Table 2.3 summarizes ID threshold proposed by some researchers (e.g., Caine 1980; Calcaterra et al. 2000; Corominas 2000; Crosta and Frattini 2001; Aleotti 2004; Cannon and Gartner 2005; Chien et al. 2005; Guzzetti et al. 2007), which covers all of landslide types. Figure 2.18 plots various ID thresholds on double logarithm scale. It is illustrated that the ID thresholds developed by previous researchers are different. The magnitudes of the thresholds parameters (i.e., a, c and m) are usually obtained by statistical regression analysis from historical data related to rainfall- induced slope failures. The regression results are based on sources of collected data. The various ID thresholds can be classified into three categories based on source of the data used to develop the thresholds (Guzzetti et al. 2007; Muntoha 2008) including:

- Global ID thresholds when historical rainfall-induced landslide data have been collected from many regions world-wide (e.g. Caine 1980; Crosta and Frattini 2001; Cannon and Gartner 2005; Guzzetti et al. 2007).

- Regional ID thresholds when historical rainfall-induced landslide data have been collected from regions with similar meteorological, geological and physiographic characteristics (e.g. Calcaterra et al. 2000; Corominas

2000; Aleotti 2004; Chen et al. 2005; Chien et al. 2005; Giannecchini 2005; Chleborad et al. 2006; Godt et al. 2006).

- Local ID thresholds when historical rainfall-induced landslide data have been recorded from local areas with specific climate regime and geomorphologic settings (e.g. Marchi et al. 2002).

Table 2.3 Summary of ID thresholds proposed by various researchers

Author	Equation	Category/Area	Landslide type
Caine 1980	$I_f = 14.82 \times T_{rf}^{-0.39}$	G/World	Shallow landslide &debris flow
Calcaterra et al. 2000	$I_f = 28.10 \times T_{rf}^{-0.74}$	R/Campania, Italy	All types including: - Shallow landslide - Soil slip - Debris flow
Corominas 2000	$I_f = 17.96 \times T_{rf}^{-0.59}$	R/Pyrenees, Spain	All types
Crosta and Frattini 2001	$I_f = 0.48 + 7.2 \times T_{rf}^{-1.0}$	G/World	Shallow landslide
Aleotti 2004	$I_f = 19.0 \times T_{rf}^{-0.50}$	R/Piedmont, Italy	Shallow landslide
Cannon and Gartner 2005	$I_f = 7.0 \times T_{rf}^{-0.60}$	G/World	Debris flow
Chien et al. 2005	$I_f = 115.47 \times T_{rf}^{-0.80}$	R/Taiwan	All types
Guzzetti et al. 2007	$I_f = 1.96 \times T_{rf}^{-0.32}$	G/World	All types
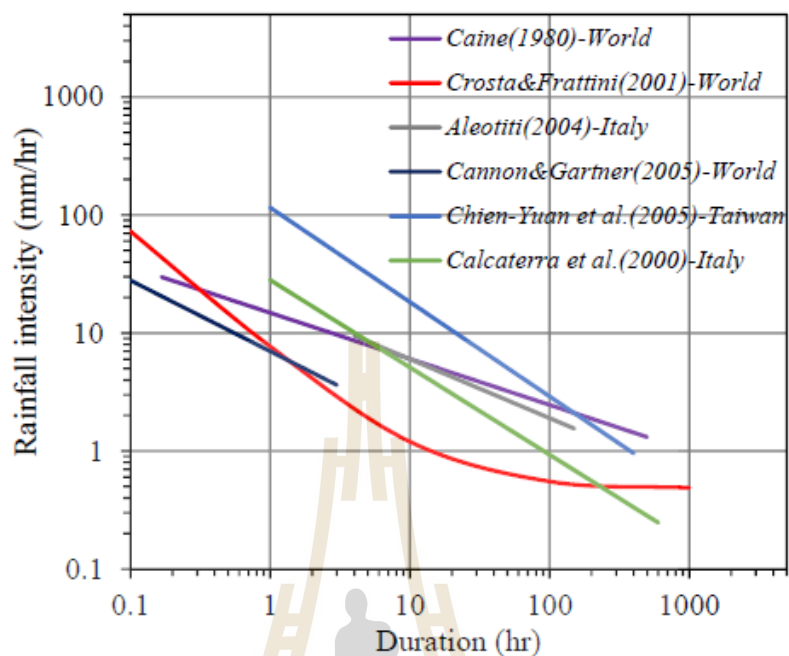
Figure 2.18 ID thresholds for initiation of shallow slope failures proposed by previous researchers

Establishing ID thresholds only needs the historical data of slope failure events and the knowledge for rainfall interpretation. Therefore, due to its simplicity and ease for usage, the ID thresholds is commonly integrated as part of an early warning systems in worldwide, which were adopted by local governments to mitigate the risk related to the rainfall-induced landslides such as the system operated by the Geotechnical Engineering Office of Hong Kong (Brand et al. 1984); the early warning system of San Francisco Bay area, California, USA (Keefer et al. 1987; Wilson et al. 1993); the debris flow warning system of the city of Nagasaki, Japan (Iwamoto 1990); the system ''Rio-watch'', developed for the city of Rio de Janeiro, Brazil (D´Orsi et al. 1997); the landslide

warning system adopted by the civil protection agency of Campania, Italy (Versace et al. 2003; Sirangelo and Braca 2004; Sirangelo et al. 2007).

2.6.2 Prediction using physically-based method

Physically-based method is generally established based on comprehensive understanding of the real physical processes of rainfall-induced landslides. Evaluation of the landslides using real-time observations of hydrological and mechanical responses read from monitoring devices (e.g., tensiometer, moisture sensor, inclinometer and rain gauge) installed within concerned soil slope is one of physically-based methods that can be simply used to build up powerful warning system with more accuracy. For most effective system, prior to install those devices, the rainfall-induced landslide mechanisms must be clarified. In last decade, some researchers have undertaken a field investigations and laboratory experiments to clarify the instability mechanism in a soil slope subjected to rainfall, and to propose methodology for monitoring device installations (e.g. Osman and Barakbah 2006; Tohari et al. 2007; Gallage and Uchimura 2010; Greco et al. 2010). Furthermore, some researchers have attempted to determine assessment criteria that might be a guideline for installation of the monitoring devices (e.g., Pagano et al. 2010; Eichenberger et al. 2013).

Osman and Barakbah (2006) has surveyed a several cases of rainfall-induced slope failures along North-South Expressway in Malaysia and analyzed the unique relationships between vegetation attribute parameters to slope stability. They claimed that the stability of a vegetation covered slope could be indicated by soil water content (SWC)

and root length density (RLD) parameters. They also argued that by using these parameters, slope failure can be predicted for the future, potentially.
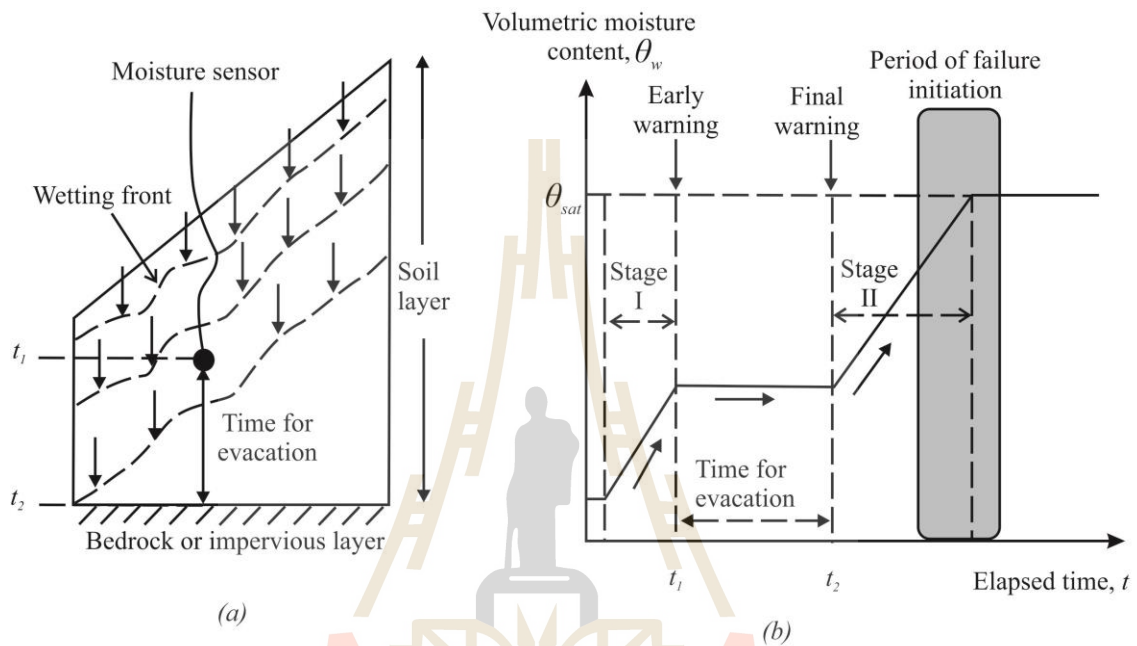
Figure 2.19   The conceptual prediction methodology for rainfall-induces slope failure based on moisture content measurements (adopted from Tohari et al. 2007)

Tohari et al. (2007) conducted a series of large-scale tests on homogeneous slopes to study the rainfall-induced slope failure mechanisms. They reported that most of the failure planes took place near the slope surface and were triggered by the rise in water table. Therefore, they have argued that a methodology of rainfall-induced slope failure assessment could be developed by observing the water content responses in soil slopes as illustrated in Figure 2.19. The monitoring devices (i.e., moisture sensor) should be installed

close to the slope surface. In addition, they also suggested two levels of warning phases, termed as early warning and final warning. The early warning level is initiated when the wetting front moves through the sensor and the final warning level is initiated soon after the wetting front reaches the impervious layer and the water table starts to rise.

(a)   (b)
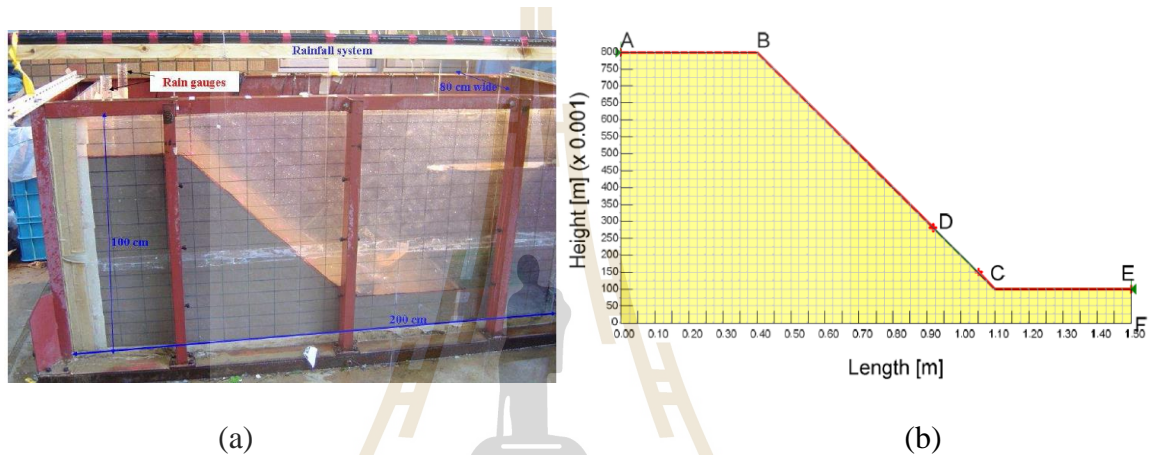
Figure 2.20   Experiment slope models used by Gallage and Uchimura (2010) (a) laboratory experiment and (b) numerical experiment

Gallage and Uchimura (2010) curried out laboratory and numerical experiments (as shown in Figure 2.20) to investigate the mechanism of rainfall-induced embankment failures, and to examine probably parameters that can be used to establish physically-based warning system. Based on the laboratory experiments and slope stability analysis, the results showed that most of slope failures was initiated nearby slope toe due to the rise phase in water table. They suggested that displacement, moisture content and pore-water pressure measurements near the toe of the slope should be used as a physically-based warning system of slope instability. They also mentioned that slope displacement read from

inclinometers provided warning of the slope failure with more accurately. While water content read from moisture sensors and pore-water pressure read from pore pressure sensors provided the warning with adequate accuracy.

Greco et al. 2010 conducted laboratory experiments to get better understanding of the hydraulic processes causing slope failure, and to identify the most useful monitored variables for effective early warning systems. They concluded that most of slope failures was taken place when the soils were unsaturated state, because the soil apparent cohesion contributed by matric suction was lost due to rainfall infiltration. Furthermore, they also suggested that the monitoring of soil volumetric water content was more useful than using the soil suction monitoring for building up early warning systems, because water content grew up smoothly during the entire infiltration processes, while soil suction showed abrupt steep fronts.

Pagano et al. (2010) conducted a simple method by using a simple 1D numerical seepage analysis to determine the critical criteria that might be used to build up early warning system for rainfall-induced landslides. They proposed a preliminary methodology using the values of water content and the pore water pressure at a triggering slope instability condition as an indicator for building up early warning system. In their methodology, the water content and the pore water pressure at triggering point are used as an indicator to evaluate time to slope failure.

Eichenberger et al. 2013 curried out one-dimensional seepage analysis in numerical model and infinite slope stability analysis to quantify the critical variables that might be used to construct an early warning system. They proposed the use of the critical

capillary stress as an indicator to evaluate rainfall-induced shallow slope failures. The critical capillary stress is a function of vertical stress and slope angle as shown in Figure 2.21, and it is defined as multiple of degree of saturation and matric suction by concerning safety factor of 1.0 in slope stability analysis. They also suggested that the critical capillary stress can be probably used to calculate critical matric suction levels, which can be subsequently applied to a local early warning system based on vertically distributed borehole instrumentation for matric suction or water content measurements.
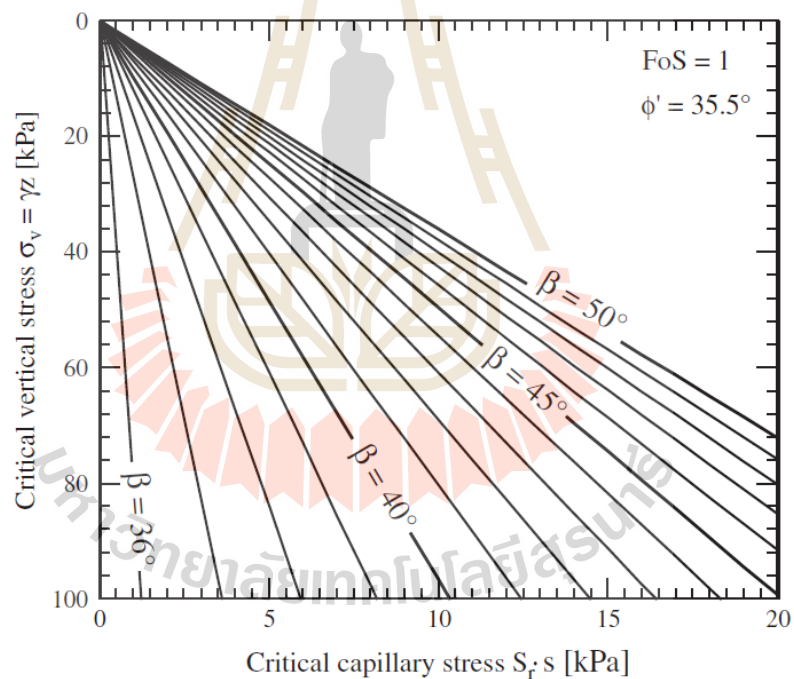
Figure 2.21   The critical capillary stress chart proposed by Eichenberger et al. 2013

2.7   Summary

This thesis aims to examine prediction methods that can be integrated as a part of early warning system to manage the rainfall-induced shallow slope failures. Both empirically-based and physically-based methods have reviewed. There are some important point yet to be addressed:

- Most of ID thresholds has been empirically proposed by using statistical analysis of historical data of rainfall-induced shallow landslides. Therefore, some relevant factors such as soil hydraulic properties, slope geometries and antecedent rainfall conditions influencing the slope failure characteristics have been neglected by the thresholds (Pradel and Raad 1993; Rahimi et al. 2010; Ma et al. 2011; Santoso et al. 2011; Cho and Lee 2002; Rahardjo et al. 2007; Cho 2009; Ali et al. 2014a; Rahardjo et al. 2001; Rahimi et al. 2011; Cuomo and Della Sala 2013; Zhan et al. 2013).

- Methodology for early warning system based on monitoring device installations has been proposed with the specific slope geometry (Tohari et al. 2007; Gallage and Uchimura 2010; Pagano et al. 2010; Eichenberger et al. 2013). In Thailand, shallow slope are occupied in many mountainous area. None of previous attempts has been devoted to characterize the rainfall-induced shallow slope failure taking warning system into account. Suitable location of monitoring device installations for early warning system has not been clearly examined yet, and remained gap to the knowledge.

Both insufficient points related to using empirically-based and physically-based predictions as part of early warning system will be examined in this thesis. The outcomes of this work would provide preliminary frameworks for building up early warning system based on comprehensive understanding of physical process of rainfall-induced shallow landslides.

2.8 References

Abramson LW, Lee TS, Sharma S, and Boyce GM. 2002. **Slope Stability and Stabilization Methods**. John Wiley & Sons. New York.

Aleotti P. 2004. **A warning system for rainfall-induced shallow failures.** Engineering Geology 73(3-4):247-265.

Aleotti P, and Chowdhury R. 1999. **Landslide Hazard Assessment: Summary Review and New Perspectives.** Bulletin of Engineering Geology and the Environment 58: 21–44.

Ali A, Huang J, Lyamin AV, Sloan SW, and Cassidy MJ. 2014a. **Boundary effects of rainfall-induced landslides.** Computers and Geotechnics 61:341-354.

Anderson SA, and Sitar N. 1995. **Analysis of Rainfall-Induced Debris Flows.** J. Geotech. Engrg. 121(7):544-552.

Au SWC. (1998). **Rain-induced Slope Instability in Hong Kong.** Engineering Geology 51:1 – 36.

Bishop AW. 1954. **The use of pore water coefficients in practice.** Geotechniqe 4(4):148–152.

Bishop AW. 1955. **The use of the Slip Circle in the Stability Analysis of Slopes.** Geotechniqe 5(1):7–17.

Bishop AW. 1959. **The principle of effective stress.** Tek. Ukebl. 106(39):859–863.

Brand EW. 1996. **Keynote Paper: Slope Instability in Tropical Areas.** Proc. Of 7th International Symposium on Landslides, Trondheim, 2031 – 2051.

Brand EW, Premchitt J, and Phillipson HB. 1984. **Relationship between Rainfall and Landslides in Hong Kong.** In Proceedings of the 4th International Symposium on Landslides, Toronto, Canada 1:377 - 384.

Brooks RH, and Corey AT. 1964. **Hydraulic Properties of Porous Media.** Chapter 7: Conclusion and Recommendations 225.

Brutsaert W. 1966. **Probability laws for pore-size distributions.** Soil Science 101(2):85-92.

Buckingham E. 1907. **Studies on the movement of soil moisture. US Department of Agriculture Bureau of Soils.** Government Printing Office, Bulletin 38, Washington DC.

Cai F, and Ugai K. 2004. **Numerical analysis of rainfall effect on slope stability.** International Journal of Geomechanics 4(2):69–78.

Caine N. 1980. **The rainfall intensity-duration control of shallow landslides and debris flows.** Geografiska Annaler Series A-physical Geography 62:23-27.

Calcaterra D, Parise M, Palma B, and Pelella L. 2000. **The influence of meteoric events in triggering shallow landslides in pyroclastic deposits of Campania.** Proceedings 8th International Symposium on Landslides, (Bromhead E, Dixon N, Ibsen ML, eds) Cardiff: AA Balkema. Vol. 1, pp. 209-214.

Campbell GS. 1974. **A simple method for determining unsaturated conductivity from moisture retention data.** Soil Science 117:311-314.

Cannon SH, and Gartner JE. 2005. **Wildfire-related debris flow from a hazards perspective.** In: Debris flow Hazards and Related Phenomena (Jakob M, Hungr O, eds), Springer Berlin Heidelberg. pp. 363-385.

Cernica JN. 1995. **Geotechnical engineering: soil mechanics.** John Wiley and Sons New York, 453 pp.

Chen C, Chen T, Yu F, Yu W, and Tseng C. 2005. **Rainfall Duration and Debris-flow initiated Studies for Real-time Monitoring.** Environmental Geology 47:715–724.

Cheng YM, and Lau CK. 2008. **Slope Stability Analysis and Stabilization.** New York: Routledge.

Chien YC, Tien CC, Fan CY, Wen CY, and Chun CT. 2005. **Rainfall duration and debrisflow initiated studies for real-time monitoring.** Environmental Geology 47: 715-724.

Chipp PN, Henkel DJ, Clare, DG, and Pope RG. 1982. **Field measurement of suction in colluvium covered slopes in Hong Kong.** In Proceedings of the Seventh Southeast Asian Geotechnical Conference, November 22-26 Hong Kong: 49-62.

Chleborad AF, Baum RL, and Godt JW. 2006. **Rainfall thresholds for forecasting landslides in the Seattle, Washington, area-Exceedance and probability.** U.S. Geological Survey Open-File Report 2006, 1064.

Cho SE. 2009. **Infiltration analysis to evaluate the surficial stability of two-layered slopes considering rainfall characteristics.** Engineering Geology 105(1-2):32-43.

Cho SE, and Lee SR. 2001. **Instability of Unsaturated Soil Slopes due to Infiltration.** Computer and Geotechnics 28:185 – 208.

Cho SE, and Lee SR. 2002. **Evaluation of surficial stability for homogeneous slopes considering rainfall characteristics.** Journal of Geotechnical and Geoenvironmental Engineering Geology 128:756-763.

Chowdhury R, Flentje P, and Bhattacharya G. 2010. **Geotechnical Slope Analysis.** Taylor & Francis Group. London.

Chugh AK. 1986. **Variable Interslice Force Inclination in Slope Stability Analysis.** Chapter 7: Conclusion and Recommendations 227.

Clough RW, and Woodward RJ. 1967. **Analysis of Embankment Stresses and Deformations.** Journal of Geotechnical Division, ASCE, 529-549.

Collins BD, and Znidarcic D. 2004. **Stability analyses of rainfall induced landslides.** Journal of Geotechnical and Geoenvironmental 130(4):362–372.

Corominas J. 2000. **Landslides and climate.** Keynote lecture- In: Proceedings 8th International Symposium on Landslides, (Bromhead E, Dixon N, Ibsen ML, eds) Cardiff: AA Balkema. Vol. 4, pp. 1-33.

Corps of Engineers. 1982. **Slope Stability.** Engineering Manual EM 1110-2-1902, Washington DC, Department of the Army, Office of the Chief of Engineers.

Corps of Engineers. 2003. **Slope Stability.** Engineering Manual, EM 1110-2-1902. Department of the U.S Army Corps of Engineers.

Crosta GB, and Frattini P. 2001. **Rainfall thresholds for triggering soil slips and debris flow.** In: Proceedings 2nd EGS Plinius Conference on Mediterranean Storms (Mugnai A, Guzzetti F, Roth G, eds) Siena. pp. 463–487.y, 128:756-763.

Cuomo S, and Della Sala M. 2013. **Rainfall-induced infiltration, runoff and failure in steep unsaturated shallow soil deposits.** Engineering Geology 162:118-127.

Dai FC, Lee CF, and Ngai YY. 2002. **Landslide Risk Assessment and Management-an Overview.** Engineering Geology 64:65–87.

Dai FC, Lee CF, Wang SJ, and Feng YY. 1999. **Stress-strain Behaviour of a Loosely Compacted Volcanic-derived Soil and its Significance to Rain-induced Fill Slope Failures.** Engineering Geology 53:359 – 370.

Das BM. 2005. **Fundamentals of Geotechnical Engineering (Second Edition).** Toronto: Thomson.

D'Orsi RN, d'Avila C, Ortigão JAR, Dias A, Moraes L, and Santos MD, 1997. **The Riode Janeiro landslide watch system.** In: 2nd Pan-American Symp. on Landslides, Rio de Janeiro, vol. 1, pp. 21–30.

Duncan MJ. 1972. **The Performance of A Rainfall Simulator and A Investigation of Plot Hydrology.** Master Thesis. University of Canterbury, New Zealand.

Duncan JM, and Dunlop P. 1969. **Slopes in stiff-fissured clays and shales.** Proceeding ASCE Journal of Soil Mechanics and Foundation Division, 95(2), 467-492. 228 Chapter 7: Conclusion and Recommendations.

Eichenberger J, Ferrari A, and Laloui L. 2013. **Early warning thresholds for partially saturated slopes in volcanic ashes.** Computers and Geotechnics 49: 79-89.

Escario D, and Juca J. 1989. **Strength and Deformation of partly saturated soils.** Proceedings of the 12th ICSMFE, Rio de Janeiro, vol.3: 43-46.

Flyod CN. 1981. **Mobile Rainfall Simulator for Small Plot Field Experiment.** Jounal Agriculture Eng. Res. 26:307.

Fredlund DG, and Krahn J. 1977. **Comparison of slope stability methods of analysis.** Canadian Geotechnical Journal 14(3):429 439

Fredlun DG, Krahn J, and Pufahl DE. 1981. **The Relationship between Limit Equilibrium Slope Stability Methods.** In Proceeding of the International Conference on Soil Mechanics and Foundation Engineering 3:409-416. Stockholm.

Fredlund DG, and Morgenstern NR. 1977. **Stress State Variables for Unsaturated Soils.** ASCE, Journal of Geotechnical Engineering Division 103(5):447-466.

Fredlund DG, Morgenstern NR, and Widger RA. 1978. **The Shear Strength of Unsaturated Soils.** Canadian Geotechnical Journal 15(3):313-321.

Fredlund DG, and Rahardjo H. 1993. **Soil Mechanics for Unsaturated Soils.** New York: John Wiley & Sons, Inc.

Fredlund DG, and Xing A. 1994. **Equations for the Soil-Water Characteristic Curve.** Canadian Geotechnical Journal 31:521 – 532.

Fredlund DG, Xing A, and Huang S. 1994. **Predicting the Permeability Function for Unsaturated Soils using the Soil-Water Characteristic Curve.** Canadian Geotechnical Journal 31(3):521–532.

Gallage C, and Uchimura T. 2010. **Investigation on parameters used in warning systems for rain-induced embankment instability.** In: Proceedings from the 63rd Canadian Geotechnical Conference (GEO2010), 12 - 16 September 2010, Calgary, Alberta.

Gan JKM, and Fredlund DG. 1988. **Multistage direct shear testing of unsaturated soils.** American Society for Testing Materials, Geotechnical Testing Journal 11(2):132-138.

Gardner WR. 1958. **Some Steady State Solutions of the Unsaturated Moisture Flow Equation with Application to Evaporation from a Water Table.** Soil Science 85(4):228–232.

Gasmo JM, Rahardjo H, and Leong EC. 2000. **Infiltration Effects on Stability of a Residual Soil Slope.** Computer and Geotechnics 26:145–165.

Giannecchini R. 2005. **Rainfall triggering soil slips in the southern Apuan Alps (Tuscany, Italy).** Advances in Geosciences 2:21-24.

Godt, JW, Baum RL, and Chleborad AF. 2006. **Rainfall Characteristics for Shallow Landsliding in Seattle,Washington, USA.** Earth Surface Processes and Landforms 31:97–110.

Greco R, Guida A, Damiano E, and Olivares L. 2010. **Soil water content and suction monitoring in model slopes for shallow flowslides early warning applications.** Physics and Chemistry of the Earth 35(3-5):127-136.

Griffiths DV. 1980. **Finite element analyses of walls, footing and slopes.** Phd thesis, Department of Engineering, University of Manchester.

Griffiths DV, and Lane PA. 1999. **Slope Stability analysis by finite elements.** Geotechnique 49(3):387-403.

Griffiths DV, and Lu N. 2005. **Unsaturated slope stability analysis with steady infiltration or evaporation using elasto-plastic finite elements.** Int. J. Numer. Anal. Methods 29:249–267.

Guzzetti F, Carrara A, Cardinali M, and Reichenbach P. 1999. **Landslide Hazard evaluation: a Review of Current Techniques and their application in a Multi-scale Study, Central Italy.** Geomorphology 31:181–216.

Guzzetti F, Peruccacci S, Rossi M, and Stark CP. 2007. **Rainfall thresholds for the initiation of landslides in central and southern Europe.** Meteorology and Atmospheric Physics 98: 239-267.

Hammouri NA, Malkawi AIH, and Yamin MMA. 2008. **Stability analysis of slopes using the finite element method and limiting equilibrium approach.** Bulletin of Engineering Geology and the Environment 67(4):471-478.

Hornbaker DJ, Albert R, Albert I, Barabasi AL, and Schiffer P.1997. **What keeps sandcastles standing?** Nature 387:765.

Hong Y, Adler R, and Huffman G. 2006. **Evaluation of the Potential of NASA Multi-Satellite Precipitation analysis in Global Landslide Hazard Assessment.** Geophys Res. Lett., 33.

Huang C-C, Lo C-L, Jang J-S, and Hwu L-K. 2008. **Internal soil moisture response to rainfall-induced slope failures and debris discharge.** Engineering Geology 101(3-4):134-145.

Huang C-C, and Yuin S-C. 2010. **Experimental investigation of rainfall criteria for shallow slope failures.** Geomorphology 120(3-4):326-338.

Huat BBK, Ali FH, and Low TH. 2006. **Water Infiltration Characteristics of Unsaturated Soil Slope and its Effect on Suction and Stability.** Geotechnical and Geological Engineering 24:1293–1306.

Iwamoto M. 1990. **Standard amount of rainfall for warning from debris disaster.** In: ALPS 90, 6th International Conference Field Workshop on Landslides, Milano, pp. 77–88.

Iverson RM. 2000. **Landslide Triggering by Rain Infiltration.** Water Resources Research. 36(7):1897–1910

Janbu N. 1954. **Application of Composite Slip Surface for Stability Analysis.** European Conference on Stability of Earth Slopes, Stockholm, Sweden.

Janbu N. 1957. **Stability Analysis of Slopes with Dimensionless Parameters.** Harvard University Soil Mechanics Series, No.46.

Janbu N. 1973. **Slope Stability Computations in Embankment-Dam Engineering.** New York, Wiley, pp. 47-86.

Johnson KA, and Sitar N. 1990. **Hydrologic conditions leading to debris-flow initiation.** Canadian Geotechnical Journal 27:789–801.

Keefer DK, Wilson RC, Mark RK, Brabb EE, Brown WM, Ellen SD, Harp EL, Wieczorek GF, Alger CS, and Zatkin RS. 1987. **Real-time Landslide Warning during Heavy Rainfall.** Science 238:921-925.

Khallili N, and Khabbaz MH. 1998. **A unique relationship for the determination of the shear strength of unsaturated soils.** Geotechnique 48(5): 681-687.

Kirschbaum DB, Adler R, Hong Y, Hill S, and Lerner-Lam AL. 2010. **A Global Landslide Catalog for Hazard Applications: Method, Results and Limitations.** Natural Hazards 52:561-575.

Lambe TW, and Whitman RV. 1979. **Soil mechanics, SI version.** John Wiley & Sons, Chichester, 553 pp.

Lane P, and Griffiths D. 2000. **Assessment of stability of slopes under drawdown conditions.** Journal of Geotechnical and Geoenvironmental Engineering 126 (5):443-450.

Lee LM, Kassim A, and Gofar N. 2011. **Performances of two instrumented laboratory models for the study of rainfall infiltration into unsaturated soils.** Engineering Geology 117(1-2):78-89.

Li WC, Lee LM, Cai H, Li HJ, Dai FC, and Wang ML. 2013. **Combined roles of saturated permeability and rainfall characteristics on surficial failure of homogeneous soil slope.** Engineering Geology 153:105-113.

Liao HJ, Ching JY, Lee WF, and Wei J. 2006. **Landslide along mountain road in Taiwan.** In L-G Tham and K-T Chau (eds), Proceeding of the Seminar on the state-of-the practice of Geotechnical Engineering in Taiwan and Hong Kong, 75-99.

Lim TT, Rahardjo H, Chang MF, and Fredlund DG. 1996. **Effect of Rainfall on Matric Suction in a Residual Soil Slope.** Canadian Geotechnical Journal 33(2):618–628.

Loch RJ, Robotham BG, Zeller L, Masterman N, Orange DN, Bridge B, Sheridan G, and Bourke JJ. 2001. **A Multi-purpose Rainfall Simulator for Field Infiltration and Erosion Studies.** Aust. J. Soil Res. 39:599.

Lowe J, and Karafiath L. 1960. **Stability of Earth Dams Upon Drawdown.** Proceeding of the 1st Pan American Conference on Soil Mechanics and Foundation Engineering, Mexico City, pp. 537-552.

Lu N, and Godt JW. 2008. **Infinite-slope stability under steady unsaturated conditions.** Water Resources Research 44:W11404 doi:10.1029/2008WR006976.

Lu N, Godt J, and Wu DT. 2010. **A closed-form equation for effective stress in unsaturated soil.** Water Resources Research 46:W05515.

Lu N, and Likos WJ. 2004. **Unsaturated soil mechanics.** John Wiley and Sons, Inc.

Lu N, and Likos WJ. 2006. **Suction stress characteristic curve for unsaturated soil.** Journal of Geotechnical and Geoenvironmental Engineering 123:131–142.

Ma K-C, Tan Y-C, and Chen C-H. 2011. **The influence of water retention curve hysteresis on the stability of unsaturated soil slopes.** Hydrological Processes 25(23):3563.

Marchi L, Arattano M. and Deganutti AM. 2002. **Ten years of debris-flow monitoring in the Moscardo Torrent (Italian Alps).** Geomorphology 46:1-17.

Matsui T, and San KC. 1992. **Finite element slope stability analysis by shear strength reduction technique.** Soils and Foundations 32(1):59-70.

Maulem Y. 1976. **A New Model for Predicting the Hydraulic Conductivity of Unsaturated Porous Media.** Water Resources Research 12:513–522.

McKee CR, and Bumb AC. 1984. **The importance of unsaturated flow parameters in designing a monitoring system for hazardous wastes and environmental emergencies.** In Proceedings of the Hazardous Materials Control Research Institute National Conference, Houston, Tex., March 1984. pp. 50–58.

McKee CR, and Bumb AC. 1987. **Flow-testing coalbed methane production wells in presence of water and gas.** Society of Petroleum Engineers (SPE), Richardson, Tex. Formation Evaluation No. 1, pp. 599–608.

Mitarai N, and Nori F. 2006. **Wet granular materials.** Advances in Physics 55:1–45.

Morgenstern NR, and Price VE. 1965. **The Analysis of the Stability of General Slip Surfaces.** Geotechnique 15(1):77-93.

Muntohar AS. 2008. **An Integrated Infiltration and Slope Stability Model for Predicting Rainfall Induced Landslides along a Mountain Road in Taiwan (PhD dissertation).** The National Taiwan University of Science and Technology.

Ng CWW, and Shi Q. 1998. **A Numerical Investigation of the Stability of Unsaturated Soil Slopes Subjected to Transient Seepage.** Computer and Geotechnics 22 (1):1–28.

Ng CWW, Wang B, and Tung YK. 2001. **Three-dimensional Numerical Investigations of Groundwater Responses in an Unsaturated Slope Subjected to Various rainfall Patterns.** Canadian Geotechnical Journal 38:1049–1062.

Oh H-J, Lee S, Chotikasathien W, Kim CH, and Kwon JH. 2008. **Predictive landslide susceptibility mapping using spatial information in the Pechabun area of Thailand.** Environmental Geology 57(3):641-651.

Orense RP, Shimoma S, Maeda K, and Towhata I. 2004. **Instrumented model slope failure due to water seepage.** Journal of Natural Disaster Science 26(1):15–26.

Osman N, and Barakbah SS. 2006**. Parameters to predict slope stability – Soil water and root profiles.** Ecological Engineering Journal 28:90-95.

Pagano L, Picarelli L, Rianna G, and Urciuoli G. 2010. **A Simple Numerical Procedure for Timely Prediction of Precipitation-induced Landslides in Unsaturated Pyroclastic Soils.** Landslides 7:273-289.

Phi S, Clarke W, and Li L. 2013. **Laboratory and numerical investigations of hillslope soil saturation development and runoff generation over rainfall events.** Journal of Hydrology 493:1-15.

Pitts J. 1983. **The Form and Causes of Slope Failures in an Area of West Singapore Island.** Singapore Journal of Tropical Geography 4(2): 162-168.

Pradel D, and Raad G. 1993. **Effect of permeability on surficial stability of homogeneous slopes.** Journal of Geotechnical and Geoenvironmental Engineering, 119(2): 315-332.

Rahardjo H, Lee TT, Leong EC, and Rezaur RB. 2005. **Response of a residual soil slope to rainfall.** Canadian Geotechnical Journal 42:340–351.

Rahardjo H, Lim TT, Chang MF, and Fredlund DG. 1995. **Shear-strength.** Chapter 7: Conclusion and Recommendations 237.

Richards LA. 1931. **Capillary conduction of liquids in porous mediums.** Physics 1:318–333.

Rahardjo H, Ong TH, Rezaur RB, and Leong EC. 2007. **Factors controlling instability of homogeneous soil slopes under rainfall.** Journal of Geotechnical and Geoenvironmental Engineering 133(12):1532-1543.

Rahardjo H, Nio AS, Leong EC, and Song NY. 2010. **Effects of Groundwater Table Position and Soil Properties on Stability of Slope during Rainfall.** Journal of Geotechnical and Geoenvironmental Engineering 136(11):1555-1564.

Rahimi A, Rahardjo H, and Leong E-C. 2010. **Effect of hydraulic properties of soil on rainfall-induced slope failure.** Engineering Geology 114(3-4):135-143.

Rahimi A, Rahardjo H, and Leong E-C. 2011. **Effect of Antecedent Rainfall Patterns on Rainfall-Induced Slope Failure.** Journal of Geotechnical and Geoenvironmental Engineering 137(5):483-491.

Rocscience Inc. 2001. **Application of the Finite Element method to Slope Stability.** Toronto.

Russo D. 1988. **Determining soil hydraulic properties by parameter estimation: on the selection of a model for the hydraulic properties.** Water Resources Research 24 (3):453–459.

Santoso AM, Phoo, K-K, and Quek S-T. 2011. **Effects of soil spatial variability on rainfall-induced landslides.** Computers and Structures 89(11-12):893-900.

Sharma RH, and Nakagawa H. 2010. **Numerical model and flume experiments of single- and two-layered hillslope flow related to slope failure.** Landslides 7(4):425-432.

Sirangelo B, and Braca G. 2004. **Identification of hazard conditions for mudflow occurrence by hydrological model. Application of FLaIR model to Sarno warning system.** Engineering Geology 73:267-276.

Sirangelo B, Versace P, and De Luca DL. 2007. **Rainfall nowcasting by at site stochastic model PRAISE.** Hydrology and Earth System Science 11:1341–1351.

Smith IM, and Hobbs R. 1974. **Finite element analysis of centrifuged and built-up slopes.** Geotechnique 24(4):531-559.

Snitbahn N, and Chen WF. 1976. **Finite element analysis of large deformation in slopes.** In C.S. Desai (Ed.), Proceeding ASCE Conference on Numerical Method in Geomechanics. Virginia Polytechnic Institute.

Spencer E. 1967. **A Method of Analysis of the Stability of Embankments Assuming Parallel Inter-Slice Forces.** Geotechnique 17:11-26.

Spencer E. 1973. **Thrust Line Criterion in Embankment Stability Analysis**. Geotechnique 23:85-100.

Sweeney DJ, and Robertson PK. 1979. **A Fundamental Approach to Slope Stability problems in Hong Kong.** Hong Kong, 35-44.

Tan SB, Lim TL, Tan SL, and Yang KS. 1987. **Landslide Problems and their Control in Singapore.** In: 9th Southeast Asian Geotechnical Conference, Chapter 7: Conclusion and Recommendations 239.

Tani M. 1982. **The properties of a water-table rise produced by a one-dimensional, vertical, unsaturated flow.** Journal of Japan Forestry Society 64:409–418.

Terlien MTJ. 1998. **The determination of statistical and deterministic hydrological landslide-triggering thresholds.** Environmental Geology 35:124-130.

Terzaghi K. 1943. **Theoretical Soil Mechanics.** John Wiley and Sons, New York.

Terzaghi K, and Peck RB. 1967. **Soil Mechanics in Engineering Practice (2nd edition).** John Wiley and Sons, New York.

Tiwari B, and Lewis A. (2012). **Experimental modeling of rainfall and seismic activities as landslide triggers.** Geocongress 2012:471-478.

Tohari A, Nishigaki M, and Komatsu M. 2007. **Laboratory Rainfall-Induced Slope Failure with Moisture Content Measurement.** Journal of Geotechnical and Geoenvironmental Engineering 133(5):575-587.

Toll DG. 2001. **Rainfall-induced Landslide in Singapore.** Geotechnical Engineering 149(4), 211–216.

Tsaparas I, Rahardjo H, Toll DG, and Leong E. 2003. **Infiltration Characteristics of Two Instrumented Residual Soil Slopes.** Canadian Geotechnical Journal 40:1012–1032.

Van Asch ThWJ, Buma J, and Van Beek LH. 1999. **A view on some hydrological triggering systems in landslides.** Geomorphology 30:25–32.

Van Genuchten MT. 1980. **A Closed-form Equation for Predicting the Hydraulic Conductivity of Unsaturated Soils.** Soil Science Society of America Journal 44: 892–898.

Vanapalli SK, Fredlund DG, Pufahl DE, and Clifton AW. 1996. **Model for the prediction of shear strength with respect to soil suction.** Canadian Geotechnical Journal 33(3):379-392.

Versace P, Sirangelo B, and Capparelli G. 2003. **Forewarning model of landslides triggered by rainfall.** 3rd International Conference on Debris-flow Hazards Mitigation: Mechanics, Prediction and Assessment, Davos, Switzerland 2:1233–1244.

Wilson RC, Mark RK, and Barbato G. 1993. **Operation of a real-time warning system for debris flows in the San Francisco Bay area, California.** International Conference Hydraulics Division, ASCE 2:1908-1913.

Wong FS. 1984. **Uncertainties in FE Modelling of Slope Stability.** Computers and Structures 19(5/6):777-791.

Wright SG. 1969. **A Study of Stability and Undrained Shear Strength of Clay Shales**. (PhD Dissertation). University of California, Berkeley, California.

Xie M, Esaki T, and Cai M. 2004. **A time-space based approach for mapping rainfall induced shallow landslide hazard.** Environmental Geology 46(6):840-850.

Xue J, and Gavin K. 2008. **Effect of rainfall intensity on infiltration into partly saturated slopes.** Geotechnical and Geological Engineering 26(2):199-209.

Yumuang S. 2006. **2001 debris flow and debris flood in Nam Ko area, Phetchabun province, central Thailand.** Environmental Geology 51(4):545-564.

Zaki A. 1999. **Slope stability analysis overview.** University of Toronto.

Zhang LL, Fredlund DG, Zhang LM, and Tang WH. 2004. **Numerical study of soil conditions under which matric suction can be maintained.** Canadian Geotechnical Journal 41(4):569–582.

Zhang LL, Zuo ZB, Ye GL, Jeng DS, and Wang JH. 2013. **Probabilistic parameter estimation and predictive uncertainty based on field measurements for unsaturated soil slope.** Computers and Geotechnics 48:72-81.

Zhang J, Jiao JJ, and Yang J. 2000. **In Situ Rainfall Infiltration Studies at a Hillside in Hubei Province, China.** Engineering Geology 57:31 – 38.

Zienkiewicz OC. 1971. **The Finite Element Method in Engineering Science.** New York: McGraw-Hill.

Zienkiewicz, OC, Humpheson C, and Lewis RW. 1975. **Associated and non-associated viscoplasticity and plasticity in soil mechanics.** Geotechnique 25:671-689.

CHAPTER III

HYDROLOGICAL RESPONSES AND STABILITY ANALYSIS OF SHALLOW SLOPES WITH COHESIONLESS SOIL SUBJECTED TO CONTINUOUS RAINFALL

3.1   Statement of problem

Some literatures as reviewed in previous chapter (Tohari et al. 2007; Gallage and Uchimura 2010; Greco et al. 2010; Eichenberger et al. 2013) revealed that the physically-based prediction can be used to build up an early warning system, interestingly. In the method, the warning levels are evaluated via the real-time hydraulic responses read from a set of monitoring devices. The common monitoring devices are moisture sensors, piezometers and tensiometers. Location of instrumentation is vital for early warning systems to be effective. Few attempts have been made to date on the study of suitable instrumentation locations for effective early warning systems. Tohari et al. (2007) conducted a series of large-scale tests on homogeneous slopes to understand the triggered mechanism of rainfall-induced slope failures and reported that most of the failure planes took place near the slope surface and were triggered by the rise in water table. Consequently, Tohari et al. (2007) suggested that the monitoring devices should be installed close to the slope surface and suggested two levels of warning phases, termed as early warning and final warning. The early warning is initiated when the wetting front moves through the

sensor and the final warning is initiated soon after the wetting front reaches the impervious layer and the water table starts to rise. However, this recommendation is based on a homogeneous soil slope, where the dominant failure mode is a shallow noncircular sliding failure. However, for shallow slopes, where the thickness of the soil slope is thin compared to the length of the slope, the dominant mode of failure is translational sliding failure, which is different from the failure mechanisms reported by Tohari et al. (2007).

Insight into the development of seepage responses on shallow slopes during rainfall period will further enhance the efficiency of physical warning systems. Pradel and Raad (1993), Lee et al. (2009), Li et al. (2013), and Ali et al. (2014b) reported that the increment of pore pressure depends on an infiltration index, termed as a ratio of rainfall intensity (i) to the saturated permeability of the soil (k_s). The higher the infiltration index, the more likely the failure occurs during the period of downward advance of wetting front termed the infiltration phase, and hence the shallower the depth of failure, and vice versa. Though works have been undertaken to study the hydrological responses in shallow slope due to rainfall, few of the previous attempts has incorporated the angle of slope into consideration. Lee et al. (2011) conducted a set of laboratory experiments on one-dimensional soil columns on a 18° tilted slope model to investigate the hydrological response of 4 soil types subjected to two magnitudes of rainfall intensity (3.35 x 10^{-6} m/sec. and 1.85 x 10^{-5} m/sec.) and rainfall period (1 hr. and 24 hr). Li et al. (2013) conducted numerical experiments with 2 computational cases; 1) one dimensional flow, and 2) two dimensional flow with a single slope angle. Although these researchers included the slope angle to their investigations, comparisons were carried out only on the hydrological responses

between one dimensional and two dimensional flows with single slope angle. There has been no known studies to date involving a series of laboratory experiments to evaluate the hydrological responses due to rainfall on shallow slopes, whereby the slope angle is conclusively taken into consideration.

In landslides, there is an interaction between the slope angle and the soil frictional angle (Ma et al. 2011; Eichenberger et al. 2013; Li et al. 2013; Ali et al. 2014b). Li et al. (2013) derived a close form solution and presented the interaction between the slope angle and the soil frictional angle on failure mechanisms including the depth of failure plane. They showed that the slope might fail through either the advance of wetting front or the rise of water table depending on the magnitudes of soil frictional angle and the slope angle. These varying failure mechanisms might lead to different depth of failure plane. Through it is realized that knowledge on the location failure plane is vital for enhancing the efficiency of the early warning system, no attempt has been devoted to explain the effect of the relevant factors (such as rainfall intensity, slope angle, soil frictional angle, etc.) on the location of failure plane.

This paper is systematically divided into two parts: 1) laboratory experiments and 2) stability analysis of the slope. A physical slope model was constructed to evaluate the hydrological responses on various steepness of soil slopes when subject to various rainfall intensities and periods. Subsequently, a series of infinite slope analysis was conducted to develop a fundamental understanding of the characteristics of failure planes in shallow slopes when subjected to varying rainfall conditions.

3.2 Infinite slope

A limit-equilibrium approach (Skempton and DeLory 1957) is a most common method to assess the stability of infinite slopes when subjected to varying rainfall conditions (Cho and Lee 2002; Tsai et al. 2007; Lu and Godt 2008; Cho 2009; Lee et al. 2009; Ma et al. 2011; Li et al. 2013; Zhan et al. 2013; Zhang et al. 2013; Ali et al. 2014a; Ali et al. 2014b). Figure 3.1 shows a typical section of infinite slope under rainfall condition. The failure plane is assumed to be parallel to the slope surface. The safety factor (FS) representing slope stability is defined by a term of shear strength (τ_R) over mobilized shear force (τ_M). As natural soil is always not fully saturated, the unsaturated shear strength can be computed based on the Mohr-Coulomb failure criteria for unsaturated soil (Fredlund and Morgenstern 1976; Fredlund et al. 1978; Fredlund and Rahardjo 1993; Vanapalli et al. 1996). In this study, the failure criteria proposed by Lu and Griffiths (2004) and Lu and Likos (2006) was used as:

$$\tau_R = c' + \left[(\sigma - u_a) - \sigma^s\right]\tan\varphi' \tag{3.1}$$

where c' is effective cohesion, φ' is effective frictional angle, σ is total normal stress, u_a is pore-air pressure, σ^s is suction stress defined as:

$$\sigma^s = -\frac{\theta_w - \theta_r}{\theta_{sat} - \theta_r}\left(u_a - u_w\right) = -S_e\left(u_a - u_w\right) \tag{3.2}$$

where θ_w is volumetric water content, θ_r is residual volumetric water content, θ_{sat} is saturated volumetric water content, a soil suction which is equal to the difference between pore-water pressure and pore-air pressure is expressed as $(u_a - u_w)$, and S_e is the effective degree of saturation. As such, FS of the infinite slope shown in Figure 3.1 can be expressed as:

$$FS = \frac{\tau_R}{\tau_M} = \frac{c' + \left[(\sigma - u_a) - \sigma^s\right]\tan\varphi'}{W\sin\beta\cos\beta} \tag{3.3}$$

where β is the slope angle and W is the weight of the soil slice. Because $W = \gamma Z_w$, $\sigma = \gamma Z_w \cos^2\beta$, and $u_a = 0$ for atmospheric pressure, Eq.3 can be rewritten as:
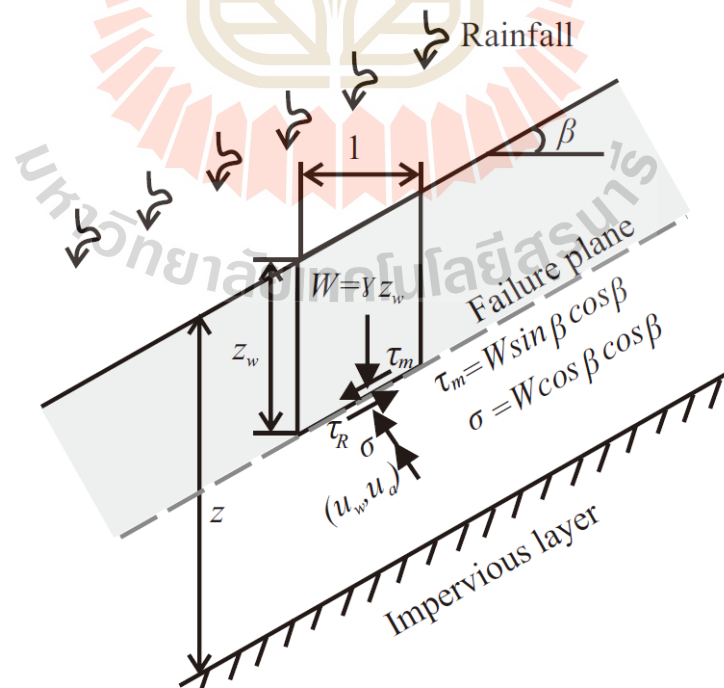
Figure 3.1 Analysis of infinite slope subjected to rainfall event

$$FS = \frac{c' + \left[\gamma Z_w \cos^2 \beta - \sigma^s\right]\tan\varphi'}{\gamma Z_w \sin\beta \cos\beta} = \frac{c' - \sigma^s \tan\varphi'}{\gamma Z_w \sin\beta \cos\beta} + \frac{\tan\varphi'}{\tan\beta} \qquad (3.4)$$

where γ is unit weight of soil, Z_w is vertical depth at failure plane.

Eq. 3.4 is used to assess the stability of shallow soil slopes under either saturated or unsaturated soil conditions. However, the hydrological responses due to flow in unsaturated soil subjected to rainfall should be better understood. As such, a series of laboratory experiments to investigate the hydrological responses on shallow slopes subjected to rainfall conditions was carried out in this research.

3.3   Materials and methods

3.3.1   The physical model

A schematic diagram and photograph of the physical model are shown in Figures 3.2 and 3.3, respectively. The model consists of four components including the rainfall simulator, the experiment box, the box supports, and the chain pulley system. The box supports are pin and roller type supports such that the experiment box can be raised one side to a prescribed inclined angle by the chain pulley.

Figure 3.4 shows details of the experiment box. The box was designed with similar dimensions to previous physical models conducted by Lee et al. (2011) and Phi et al. (2013). The dimensions of this box are 1550 mm length, 1000 mm high, and 200 mm width. The sides and bottom base of the box were made from impervious acrylic plates of 15 mm thick. Five of 5 mm diameter holes were vertically drilled at mid of the side boundary to insert the moisture sensor probes (Decagon 5TE, Decagon Devices Inc. (2007-2010)). Three of 9 mm diameter holes were drilled at bottom of -
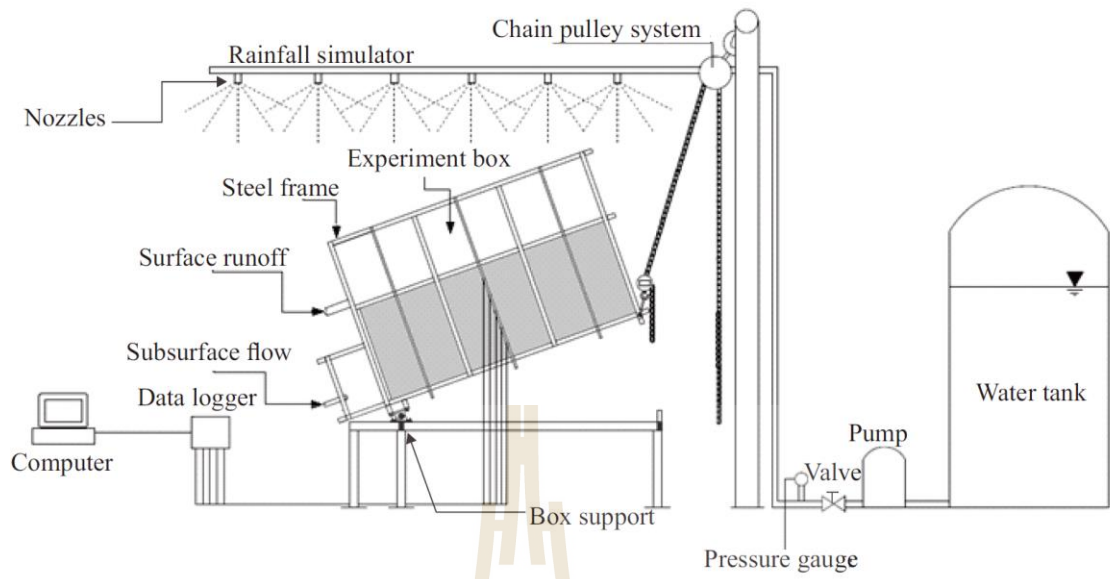
Figure 3.2   Schematic diagram of the physical slope model

Figure 3.3   Photograph of the physical slope model

the experiment box at distances of 375 mm (downslope), 750 mm (middle slope), and 1125 mm (upslope). These holes were used to insert the piezometers. To reduce entrapped air that might be affecting to measurement of the volumetric moisture content (θ_w), three other holes were drilled nearby the piezometer holes to install the opening valves. At downslope, permeable porous concrete overlaid by geotextile was placed to allow free water outflow at nearly saturated state, and to prevent the clogged soil in porous concrete.

A rainfall simulator was installed above the experiment box. The simulator consists of a water tank, a constant pressure pump, a pressure gauge, a set of plastic pipes, a set of small opening nozzles, and a set of control valves. The nozzles were placed in 4 plastic pipes each with spaces of 300 mm, 450 mm, 600 mm, and 900 mm to reproduce various rainfall intensity. The desired rainfall intensities were assigned to the slope model through the rainfall simulator calibrated with the Uniformity Coefficients (CU) (Hall et al. (1989) of greater than 90%.

The calibration was conducted by measuring the volume of water sprayed from the nozzles for 30 minutes. Thirty five cups were placed above the slope surface to collect the nozzled water. Each rainfall intensity, CU was determined to verify the uniformity of rainfall distribution. The expression of CU is written as shown in Eq. 3.5.

$$CU = 1 - \frac{\sum_{i=1}^{n} I_i - I_m}{\sum_{i=1}^{n} I_i} \tag{3.5}$$

where I_i is measured rainfall intensity for the ith cup, I_m is average rainfall intensity

for all cups, and n is total number of cups ($n = 30$).
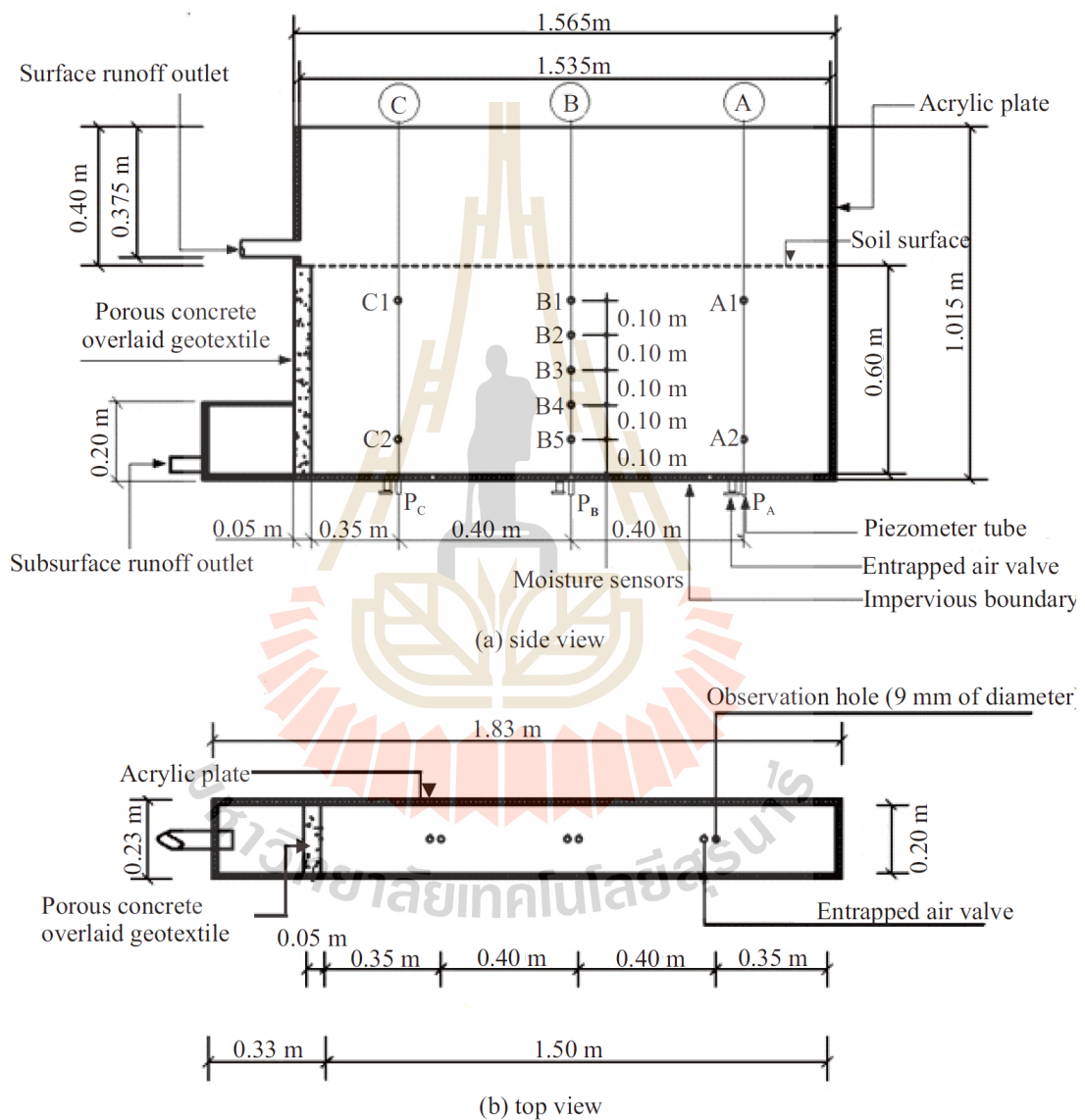
Figure 3.4   Details of the experiment box (a) side view (b) top view

3.3.2 Materials

A local sandy soil was used in this study to prepare the homogeneous soil slope. This soil is classified as poorly-graded sand (SP) according to Unified Soil Classification System (ASTM D2487). Figure 3.5a presents grain size distribution of the soil. Other soil properties such as the specific gravity of the soil (G_s), the saturated permeability (k_s), the strength parameters (φ', c') are presented in Table 3.1. The soil-water characteristic (SWC) determined by the pressure plate (ASTM D 6836-02) is shown in Figure 3.5b. Nonlinear regression was performed to validate the tested data with Eq. 3.6 (van Genuchten 1980). The validated parameters for van Genuchten's model are shown in Table 3.1.

$$S_e = \frac{\theta_w - \theta_r}{\theta_{sat} - \theta_r} = \left\{ \frac{1}{1 + \left[\alpha\left(u_a - u_w\right)\right]^n} \right\}^{1-1/n} \tag{3.6}$$

where S_e is effective degree of saturation, θ_w is water content, θ_r is water content at residual state, θ_{sat} is water content at saturated state, $u_a - u_w$ is matric suction which is different between pore air pressure (u_a) and pore water pressure (u_w), α and n are fitting parameters relating to the inverse of air-entry pressure, and pore size distribution, respectively.

Prior to placement of the soil, the soil was air dried and turned-over every day for 14 days. The soil was then carefully placed into the box to get homogenous soil slopes. Ten layers of 60 mm thick were compacted with a certain weight of dry soil to achieve the dry unit weight and void ratio (e) of 16.9 kN/m³ and 0.59, respectively.

This unit weight of 16.9 kN/m^3 was acquired from the dry soil sample compacted at a standard effort of 600 kJ/m^3 (ASTM-D698). The moisture sensors and piezometers were installed during this process.
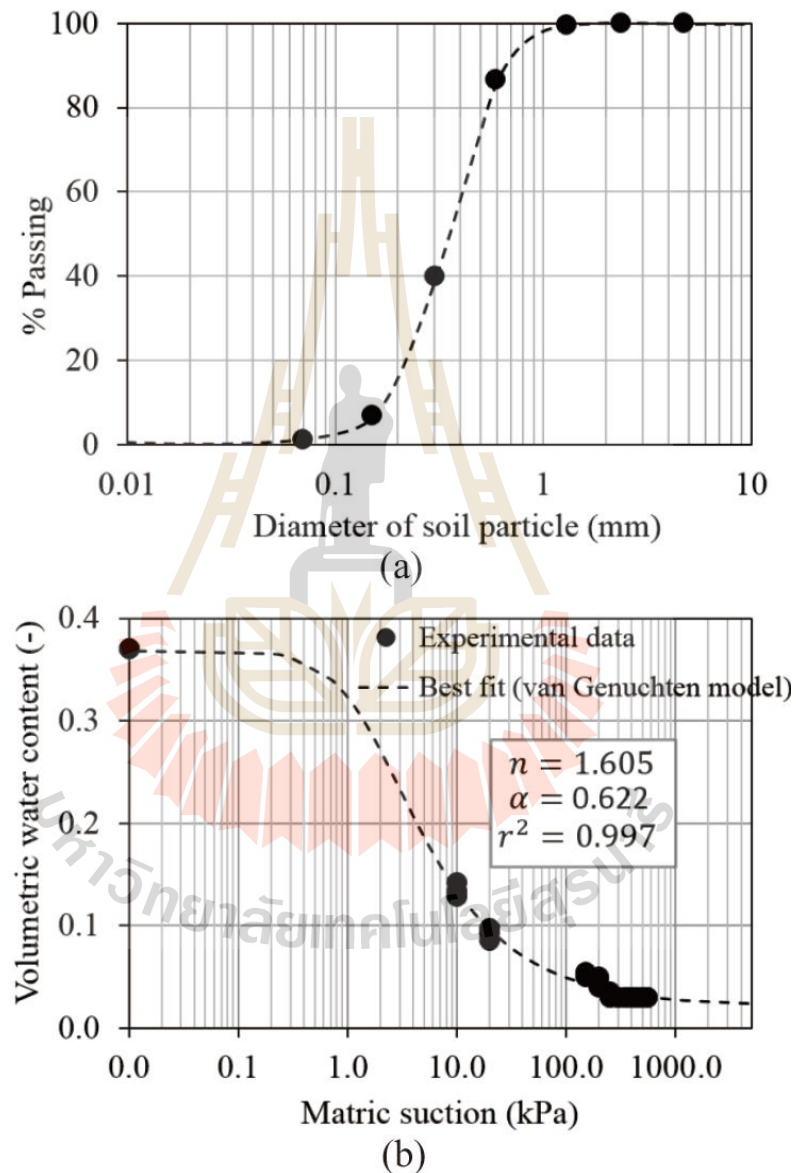
Figure 3.5   Properties of the sandy soil: (a) grain size distribution, and (b) soil-water characteristic (SWC)
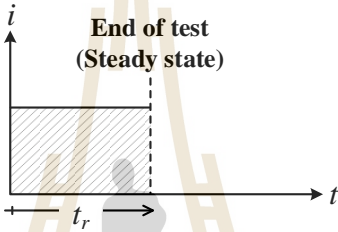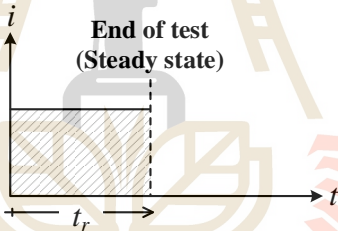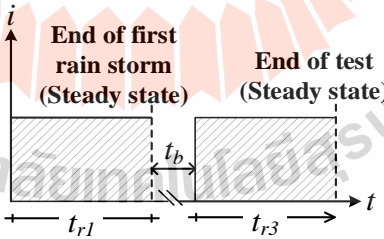
Table 3.1   Summary of the soil properties

Soil properties	Value	Unit
Soil type(USCS Classification)	SP	-
Dry unit weight, γ_d	16.9	kN/m^3
Specific gravity, G_s	2.69	-
Soil hydrologic parameters		
Saturated permeability, k_s	1.54×10^{-4}	*m/sec*
Saturated volumetric water content, θ_{sat}	0.371	-
Residual volumetric water content, θ_r	0.021	-
Fitting parameter, α	0.662	kPa^{-1}
Fitting parameter, n	1.605	-
Soil strength parameters		
Internal friction angle, φ'	38	*deg*
Cohesion, c'	0	*kPa*

3.3.3 Experimental program

Three set of laboratory experiments were conducted as shown in Table 3.2. In total, 13 tests were carried out. Each test, rainfall was continuously applied until the arrival of the steady state which is indicated by the rate of water outflow at slope toe equals to the rainfall intensity. The magnitudes of rainfall intensity assigned to each test were lower than the soil' saturated permeability ($k_s = 1.54 \times 10^{-4}$ m/sec = 554.4 mm/hr), Monitored data were recorded during the test until the steady state (end of each test) was achieved. For sake of ease in experimental setup, rainfall intensity of 100 mm/hr and slope angle of 20° were chosen as a base value. Moreover, if i/k_s is set to be greater than 1.0, the hydraulic responses would not differ from those for $i/k_s = 1.0$ (Lee et al. 2011; Li et al. 2013).

Table 3.2   Experimental programs conducted in this study

Series	Rainfall intensity, i (*mm/hr*)	Slope angle, β *(deg)*	Rainfall sequence	Inter-storm rainfall period, t_b *(day)*
I	45 70 100 130 160	20		-
II	100	5 10 20 30		-
III	100	20		4 7 14 -

The variation of rainfall intensity was conducted in test series I. The rainfall intensities of 45, 70, 100, 130, 160 mm/hr were applied to the model at slope angle (β) of 20°. The variation of slope angle was conducted in the test series II. The slope angles (β) of 5°, 10°, 20° and 30° were assigned to the model subjected to rainfall intensity of 100 mm/hr. The inter-storm rainfall period was assigned to the model in the test series III. This test is to study the effect of antecedent water content from the previous rainfall, which might affect the hydrological responses. The two rainfall events of 100 mm/hr each were applied to the model at slope angle (β) of 20° with the inter-storm period of 4, 7 and 14 days.

3.4   Test results

The volumetric water contents (θ_w) read from the moisture sensors B1, B2, B3, B4, and B5, located at a vertical distance from the impervious surface of 100 mm, 200 mm, 300 mm, 400 mm, and 500 mm, respectively (see Fig. 4a).

Figures 3.6, 3.7 and 3.8 present development of θ_w profile in the soil subjected to rainfall experiment series I, II, and III, respectively. The developments of θ_w profile of all experimental series look similar to each other. The general characters of θ_w profile development were determined as follows:

1) The development of θ_w profile begins since the rainwater starts infiltrating into the soil. During the rainwater infiltration process termed as the infiltration phase, the volumetric water content increases from its initial value (θ_{wi}) to a volumetric moisture content of θ_{wb}, named the volumetric water content behind the wetting front. The θ_{wb} presents a

possible maximum magnitude of θ_w taking place during the infiltration phase.

2) After reaching the impervious boundary of the wetting front, an upward movement of water table begins. This process is called saturation phase. At this phase, θ_w increases from the θ_{wb} to the magnitude of θ_w that closes to θ_{sat}.

The characters of θ_w development summarized above are in accordance with those reported by previous studies (Tohari et al. 2007; Huang et al. 2008; Huang and Yuin 2010; Sharma and Nakagawa 2010; Phi et al. 2013).

Figures 3.6(a) – (e) present the variation of volumetric water content in shallow slope of the experimental series I for rainfall intensity of 45, 70, 100, 130 and 160 mm/hr, respectively. The results show that the θ_w profile development in the infiltration phase clearly depends on the magnitudes of rainfall intensity. The higher rainfall intensity results in the faster move of wetting front, and hence the deeper development of a wetting front. In addition, the results show that the magnitude of θ_{wb} increases with the magnitude of rainfall intensity. This findings are similar to those reported by Lee et al. (2011).

The rainfall intensity also affects the θ_w profile development in the saturation phase. In the plots, the rise of water table is indicated at the magnitude where θ_w reaches θ_{sat}. The level of water table is indicated by the point where the θ_w profile in the saturation phase deviates from θ_{sat}. It is found that the greater rainfall intensity causes the faster rise of water table. In addition, the final level of water table at the

steady state also depend on the rainfall intensity and the greater rainfall intensity yields the higher level of water table at steady state.
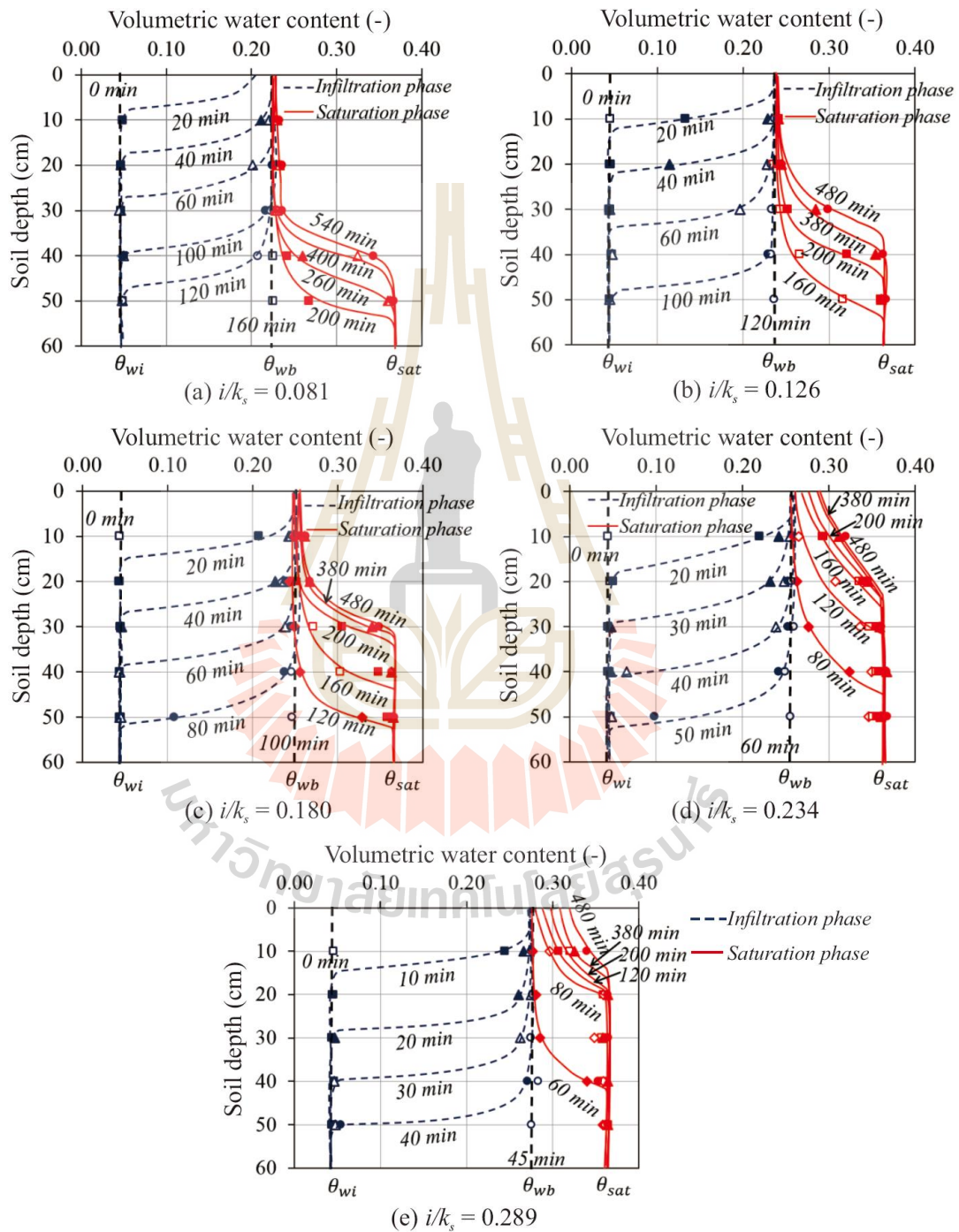
Figure 3.6   Volumetric water content profiles for the test series I: (a) $i/k_s = 0.081$, (b) $i/k_s = 0.126$, (c) $i/k_s = 0.180$, (d) $i/k_s = 0.234$, and (e) $i/k_s = 0.289$
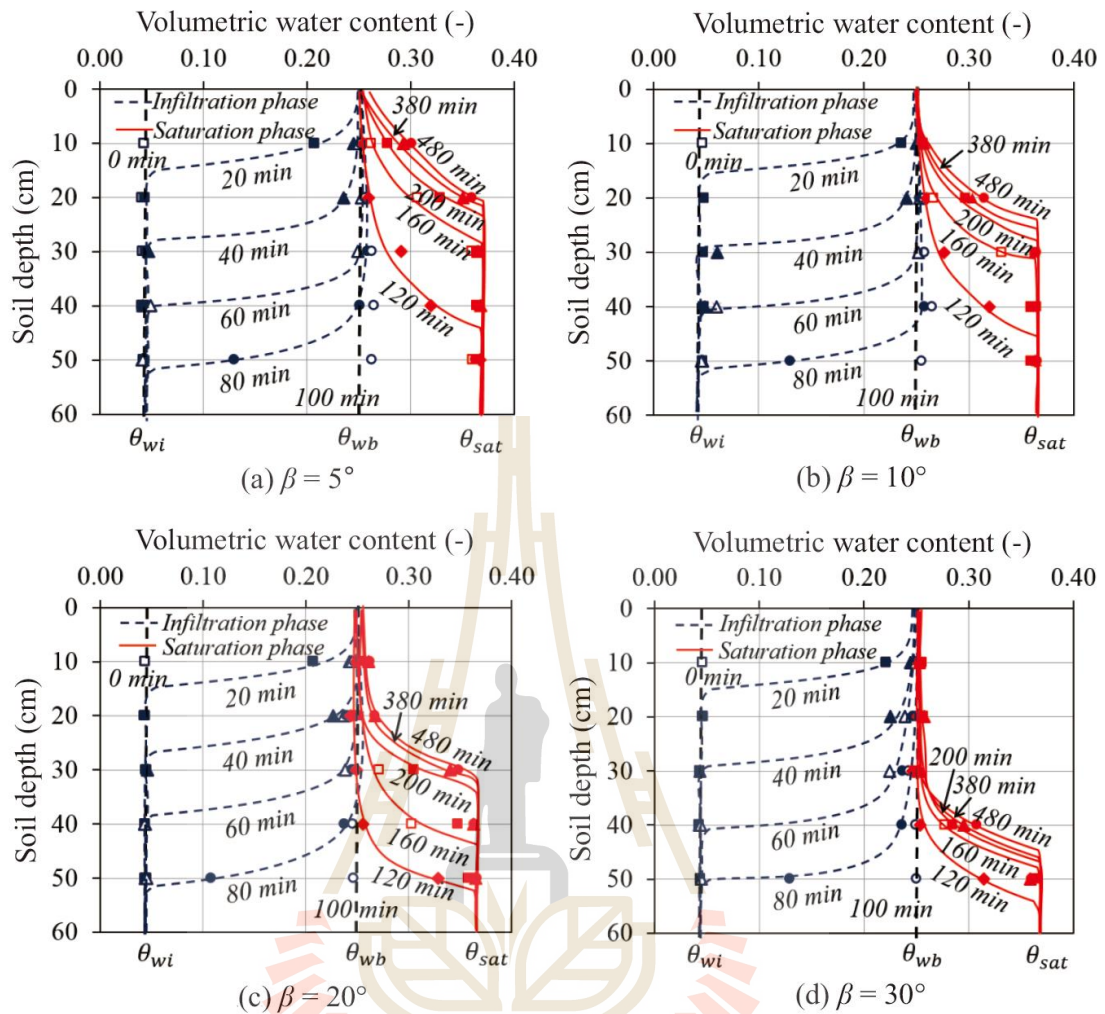
Figure 3.7 Volumetric water content profiles for the test series II: (a) $\beta = 5°$, (b) $\beta = 10°$, (c) $\beta = 20°$, and (d) $\beta = 30°$

Figures 3.7(a)-(d) present variation of volumetric water content in shallow slope of the experimental series II for the slope angle (β) of 5°, 10°, 20° and 30°, respectively. The θ_w development and the magnitude of θ_{wb} in the infiltration phase are not dependent on the slope angle. In other words, within the β range conducted in this study, the magnitude of slope angle β do not affect the hydrological response. It
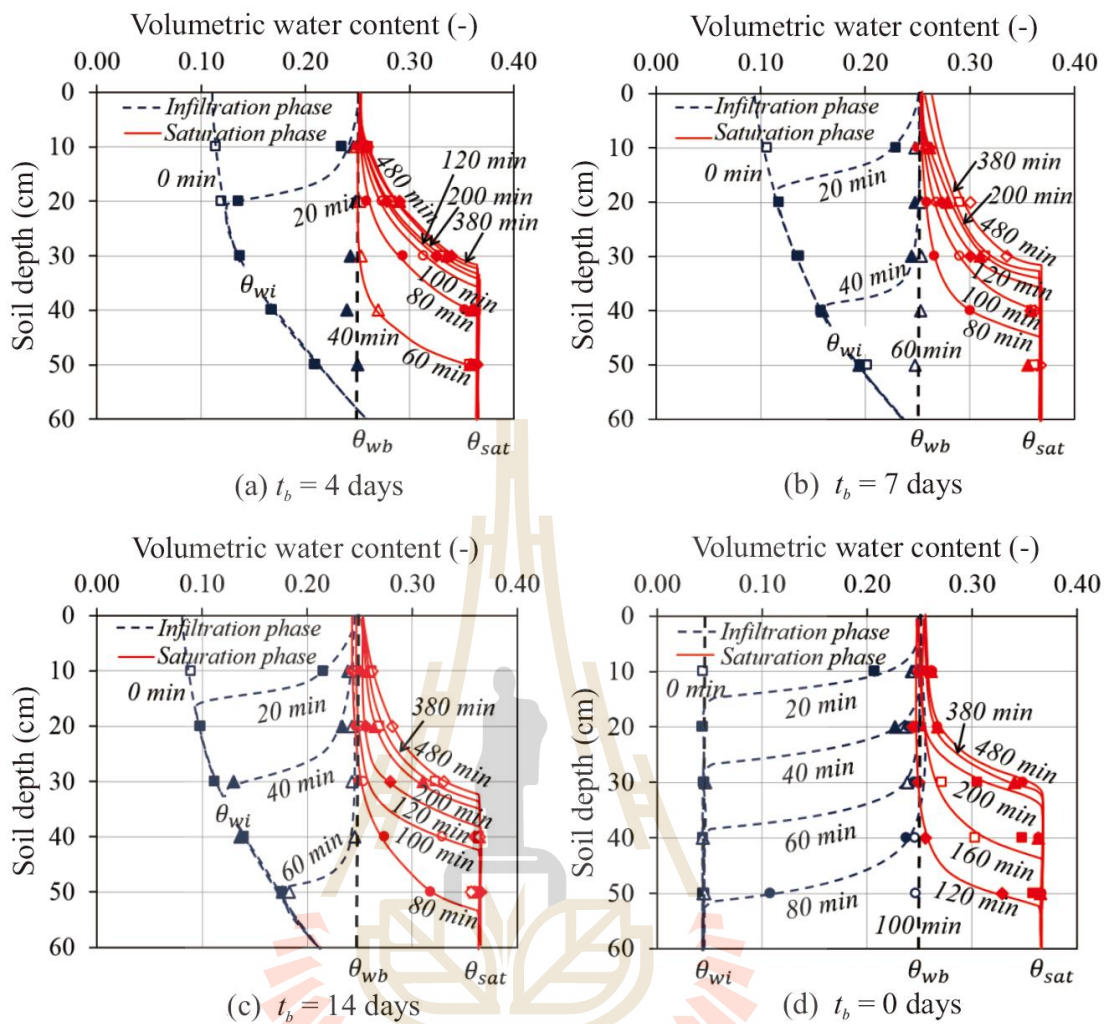
Figure 3.8   Volumetric water content profiles for the test series III: (a) t_b = 4 days,

(b) t_b = 7 days, (c) t_b = 14 days, and (d) continuous storm t_b = 0 days

is due to the vertical seepage flow plays important role to the hydrological responses

in isotropic shallow slope soil during rainwater infiltration process. This finding is

similar to that found by Lee et al. (2011) who conducted two sets of laboratory

seepage flow tests: one-dimensional soil column and 18° tilted slope model. The slope

angle, however, affects the θ_w profile development in the saturation phase. Figures

3.7 (a)-(d) clearly show that the rise of water table depends on the slope angle, the

faster water table development is found at mild slope angle. This results may naturally be attributed to a dominant role of lateral flow along the impervious layer at the soil saturated state. The higher slope angle provides the higher hydraulic gradient and the faster lateral flow, and thus the less accumulated rain water at the impervious boundary.

Figure 3.8 presents variation of volumetric water content in shallow slope of the experimental series III for a continuous storm, and for the different inter-storm period (t_b) of 4, 7, 14 days, respectively. The θ_w development in the infiltration phase depends on the magnitude of t_b as it affects the magnitude of an initial θ_w of the subsequent rainfall (θ_{wi}); the shorter t_b results in the higher magnitude of θ_{wi}. The speed of the wetting front advancement is more rapid for the shorter t_b. Although the variation of t_b significantly affects the wetting front development, it does not affect the magnitude of the volumetric moisture content behind the wetting front (θ_{wb}). In the other word, the magnitude of θ_{wb} is independent of the magnitude of t_b.

3.5 Analytical approach for hydrological responses

The influence factors involving the hydrological responses in shallow slope soil subjected to rainfall events are discussed in the former section. When the rainfall intensity (i) is less than the soil' saturated permeability (k_s), the development of θ_w is divided into two phases: the infiltration and saturation phases. Both phases are characterized by a so-called "steady infiltration profile" on which its magnitude is equal to θ_{wb}.

Figure 3.9 presents a relationship between the measured water content behind the wetting front (θ_{wb}) and the rainfall intensity (i) assigned to the slope model. The permeability function (Gardner, 1958) of the studied soil was plotted in this figure. The point of coincidence between the θ_{wb}-i and permeability function plots indicates that the state at water content of θ_{wb} is a steady infiltration state at which infiltration rate is equal to the rainfall intensity. In addition, the plot shows that the magnitude of θ_{wb} clearly depends on the rainfall intensity, regardless of the variation in slope angle and the inter-storm period.

Based on the relationship between θ_{wb} and i shown in Figure 3.9, development of the steady infiltration profile can be explained. At first, the permeability of the soil layer ($k(\theta_{wi})$) is lower than the magnitude of rainfall intensity (i). Consider a thin surface layer of soil, where $k(\theta_{wi})$ is lower than i. Soon after initiation of the infiltration phase, the infiltrated rainwater is stored in this layer, subsequently leaving and resulting in an increase of its water content, hence an increase in the permeability of this layer. As long as the flux out of the layer is lower than the magnitude of i, the water content continues to increase. When the water content in this layer reaches the magnitude, at which $k(\theta_w) = i$, the rate of water outflow is equal to the rate of water inflow, and there is no further change in water content as long as the rainfall event is continuously applied to the slope. This process takes place successively in each layer as water input continues, producing a descending wetting front at which water decreases more or less abruptly. The water content equals θ_{wb} behind the front and θ_{wi} below it.

Figure 3.9 Relationship between the measure volumetric water content behind the wetting front (θ_{wb}) and the rainfall intensity (i)

Figure 3.9 also presents the other important water content, at a steady infiltration state called the "field capacity" (θ_{fc}), defined as the content of water, on a mass or volume basis, remaining in a soil 2 or 3 days after having been wetted with water and after free drainage is negligible (Soil Science Glossary Terms Committee, 2008). Meyer and Gee (1999) suggested that field capacity (θ_{fc}) occurred when the permeability decreases to between 10^{-9} to 10^{-11} m/sec depending on soil type.

Figure 3.10 presents conceptual idea of the *FS* profile plotted at any time during the infiltration and saturation phases. At a specific time t_1 during the infiltration phase, the variation of θ_w along a vertical depth will vary between its

initial and the steady infiltration profiles. The water content value at the initial infiltration profile is potentially the water content at field capacity (θ_{fc}), while the water content value at the steady infiltration profile is the water content behind the wetting front (θ_{wb}). The variation of *FS* along a vertical depth will vary between two *FS* lines corresponding to the initial θ_w profile and the steady infiltration profile. The minimum magnitude of *FS* possibly occurs along the wetting front profile.

Figure 10d present the *FS* profiledevelopment with wetting front advance. The depth of failure plane, which is later called a critical depth, is located where the magnitude of *FS* reaches 1.0. At a specific time t_2 during the saturation phase, the magnitude of *FS* decreases with increasing depth and the minimum magnitude of *FS* is found at the interface between the soil and the impervious layer. The *FS* profile idealization presented in Figure 3.10 is similar to those reported by previous studies (Santoso et al. 2011; Ali et al. 2014a; Ali et al. 2014b).

As the minimum *FS* possibly occurs along the wetting front, it is vital to take the hydrologic states at steady infiltration profile into consideration for the critical depth calculation. Considering the permeability function proposed by Gardner (1958):

$$k(\theta) = k_s \exp[-\alpha(u_a - u_w)] \tag{3.7a}$$

which can be rewritten in term of $\alpha(u_a - u_w)$ as:

$$\alpha(u_a - u_w) = -\ln\left(\frac{k(\theta)}{k_s}\right) \tag{3.7b}$$
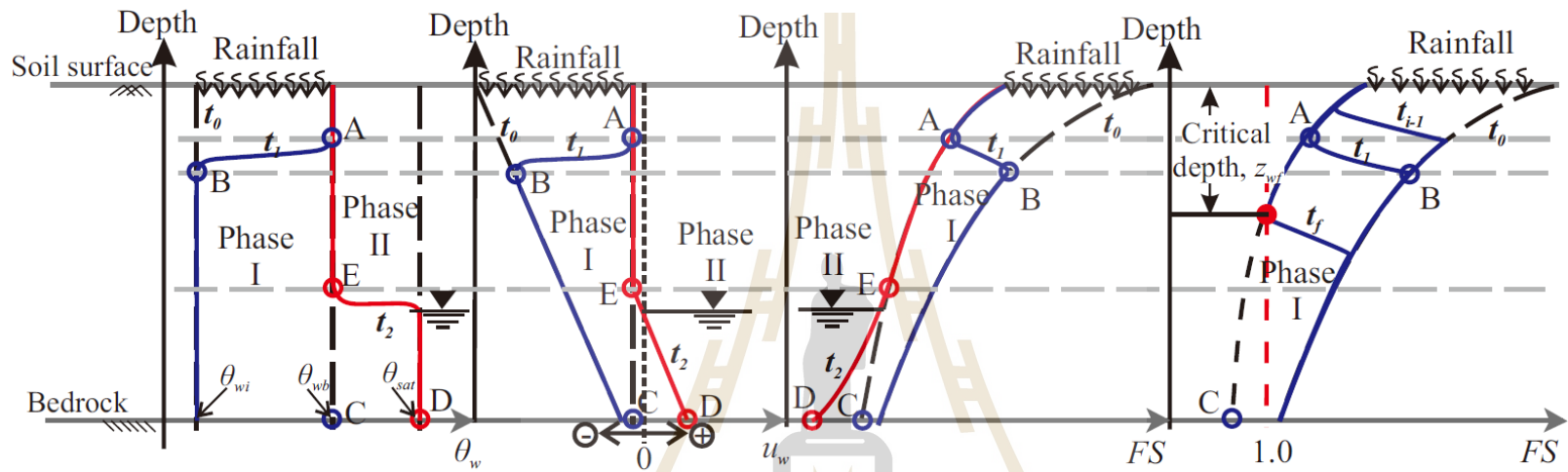
(a) volumetric water content, θ_w (b) pore-water pressure, u_w (c) safety factor, FS (d) determination of critical depth

Figure 3.10   Safety factor characteristics based on hydraulic responses during rainfall event: (a) water content profile,

(b) pore-water pressure profile, (c) safety factor profile, and (d) determination of the critical depth

Replace Eq. 3.7b into Eq. 3.6, yield:

$$S_e = \frac{\theta_w - \theta_r}{\theta_{sat} - \theta_r} = \left\{ \frac{1}{1 + \left[-\ln\left(k(\theta)/k_s\right)\right]^n} \right\}^{1-1/n} \tag{3.8}$$

At $\theta_w = \theta_{wb}$, $k(\theta_{wb}) = i$. Hence, Eq. (3.8) is:

$$S_{eb} = \frac{\theta_{wb} - \theta_r}{\theta_{sat} - \theta_r} = \left\{ \frac{1}{1 + \left[-\ln\left(k(\theta_{wb})/k_s\right)\right]^n} \right\}^{1-1/n} = \left\{ \frac{1}{1 + \left[-\ln\left(i/k_s\right)\right]^n} \right\}^{1-1/n} \tag{3.9a}$$

and the magnitude of suction at $\theta_w = \theta_{wb}$ is:

$$(u_a - u_w)_b = -\frac{1}{\alpha}\ln\left(\frac{i}{k_s}\right) \tag{3.9b}$$

where S_{eb} and $(u_a - u_w)_b$ are the effective saturation and suction behind the wetting front, respectively. Equations 3.9a and 3.9b are the same as the analytical solutions proposed by Lu and Griffiths (2004) and Lu and Likos (2006), to describe the hydrological responses at steady state for one dimensional seepage flow where the ground water table does not exist. The experimental results from the former section show that the volumetric water content at steady (θ_{wb}) is not dependent on the slope angle. As such, the proposed equations are applicable to rainfall infiltration on

unsaturated soil slope. Furthermore, the variations of the S_e and u_w of a certain soil depend only on the magnitude of rainfall intensity.

3.6   Assessment of the stability under rainfall infiltration

Stability prediction of a shallow slope subjected to rainfall infiltration is demonstrated in this section. Properties of the tested soil are reported in this demonstration as summarized in Table 3.1. The soil is 3 m thick and overlaid by an impervious layer. Prior to rainfall event, the ground water table is assumed not to exist. The calculation procedure is as following:

Step 1: Calculate the suction stress ($\sigma^s = S_e(u_a - u_w)$) for a specific rainfall intensity (i). The initial ground water table was assumed to not exist prior to a rainfall event, hence the magnitudes of S_e and $(u_a - u_w)$ at steady state were calculated from Eq. 3.9a and Eq. 3.9b, respectively.

Step 2: Use Eq. 3.4 to perform the slope stability analysis. In the infiltration phase, the magnitude of *FS* was calculated at a line which coincides with the wetting front. This calculation was done at various depths of the wetting front advance. When the wetting front reaches the impervious layer, slope stability analysis for the saturation phase was taken place. The magnitude of *FS* was calculated along the interface between the soil and the impervious layer. This calculation was done at various heights of water table development.

To investigate the effect of rainfall intensity (i) and the slope angle (β) on *FS* of the shallow slope subjected to rainfall event, the above procedures were repeated

for various magnitudes of i and β. Figures 3.11a presents the variation of *FS* according to the wetting front advance Z_w for a 40° inclined slope subjected to various magnitudes of i. Figure 3.11b presents the variation of *FS* according to the wetting front advance Z_w for a various angles of the inclined slope subjected to various magnitudes of i. According to Lu and Griffiths (2004) and Lu and Likos (2006), the hydrological states at steady condition are function of the infiltration index (i/k_s). Hence, the effect of i on the variation of *FS* are presented in term of the infiltration index. The magnitude of *FS* successively decreases with an increasing Z_w for every magnitudes of the infiltration index of lower than 1.0. Since the suction stress σ^s decreases to zero immediately since the initiation of the infiltration phase for the infiltration index of 1.0, the magnitude of *FS* reduces to its lowest value soon after the initiation of the infiltration phase.

For the infiltration index of lower than 1.0, the magnitude of *FS* decreases drastically with small increments of the wetting front advance Z_w. The faster loss of *FS* is found at the greater magnitude of the infiltration index. As the wetting front infiltrates deep enough, the magnitude of *FS* becomes gradually decrease with the increment of Z_w. Figure 3.11b shows that the depth where *FS* gradually decrease with Z_w depends solely on the magnitude of the infiltration index regardless the magnitude of slope angle β which is in accordance with the hydrological responses during the infiltration phase found in the former session.

At the end of the infiltration phase ($Z_w = Z_t$), the volumetric water content in soil is equal to θ_{wb} which is lower than that at the saturated state. However,

immediately after the rainwater starts accumulating along the impervious boundary, i.e. the saturation phase begins, the state of the soil at the impervious boundary changes from unsaturated to saturated states. It results in the drop of *FS* from point B, C and D (the i/k_s of 0.0019, 0.19 and 0.67, respectively) to point A because of the losing in the σ^s. With the rising of water table, the *FS* drops continuously due to the increasing of u_w.
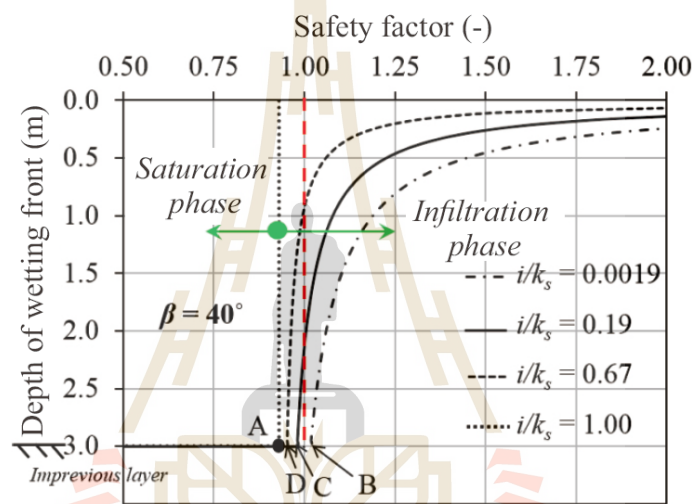
(a)
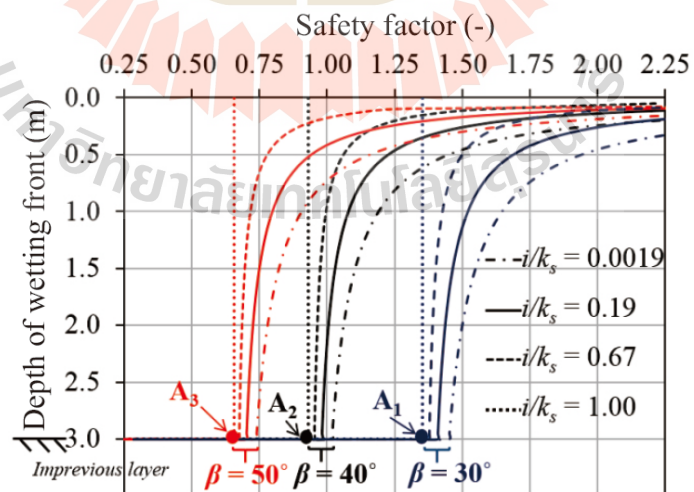
(b)

Figure 3.11　Variation of safety factor with depth: (a) various i values with

$\beta = 40°$, and (b) various values of i and β

Regarding to the calculation of *FS* written in Eq. 3.4, there are three components that contribute to the shear strength of a soil; soil cohesion, suction stress, and the soil frictional components. According to Lu and Griffiths (2004) and Lu and Godt (2008), the suction stress is negative for the soil at the unsaturated state and equals to the magnitude of positive pore water when the state of the soil becomes saturated state. Thus, for a cohesionless soil ($c' = 0$ kN/m^2), the slope failure might take place during either the infiltration or saturation phases, depending on the magnitude of the slope angle compared with the soil frictional angle. The failure state of a steep shallow slope defined by $\beta > \varphi'$ might take place during the infiltration phase. While, the failure state of a mild slope ($\beta \leq \varphi'$) might occur during the saturation phase.
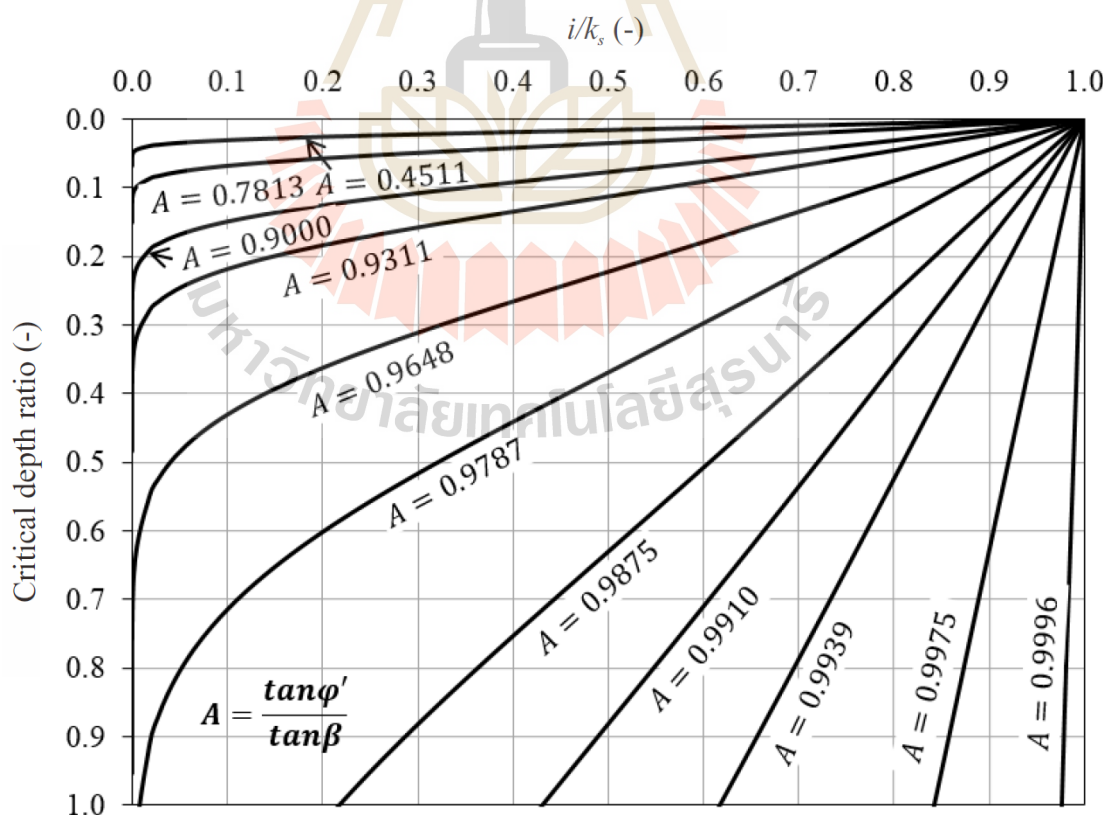
Figure 3.12   Critical depth chart

Location where failure plane takes place is vital for assessment of the slope failure. For the shallow slope failure taken place during the saturation phase, the failure plane always takes place at the interfacial between the soil and the impervious layers. However, the location of failure plane taken place during the infiltration phase might vary from the depth to depth depending on many factors. Figure 3.12 presents the relationships between the normalized critical depth (Z_{wf}/Z_t) and the infiltration index (i/k_s) for various magnitudes of stability index ($\tan\varphi'/\tan\beta$) for this demonstrated case. The vertical distance measured from the slope surface to the failure plane is called the critical depth (Z_{wf}), while the thickness of the shallow slope is denoted as Z_t. For a certain soil, the critical depth decreases with an increasing rainfall intensity. In the other words, the shallower depth of failure plane is encountered in the slope subjected to the greater magnitude of rainfall intensity.

Figure 3.12 shows that the depth of failure plane is very sensitive to the change of rainfall intensity for the stability index ranged from 0.9 to 1.0. The depth of failure plane can occur at any depth depending on the magnitudes of the infiltration and stability indices. However, the depth of failure plane is inert to the change of rainfall intensity for the stability index of lower than 0.9. In addition, in this case the depth of failure plane might take place at very shallow depth ($Z_{wf}/Z_t < 0.2$).

3.7 Categorization of the slope failures

Once the critical depth chart is available, the threshold value can be assigned to the slope based on personal judgment. The threshold is the stability number at which the critical depth is slightly sensitive to rainfall intensity, i.e. the threshold

value used in the illustrated case is 0.9 which is the stability index at which an infiltration index (i/k) to a normalized critical depth(Z_{wf}/Z_t) ratio is no greater than 0.2.

Based on the relative depth of the failure plane, possible modes of slope failure are: 1) along the impervious layer mode, 2) shallow depth mode which occurs very close to the slope surface, and 3) transitional mode which occurs at any depth from the impervious layer to the slope surface. These modes are governed by the stability index ($\tan\varphi'/\tan\beta$) as depicted in Figure 3.13 and summarized below:

1) For the mild slope ($\tan\varphi'/\tan\beta \geq 1.0$), the failure mode is the along the impervious layer mode which is triggered by an increment of positive pore water pressure taking place during the saturation phase.

2) For the steep slope ($\tan\varphi'/\tan\beta < 1.0$), the failure is triggered by the loss of matric suction during the infiltration phase. With the assistance of the critical depth chart, the failure mode is characterized according to the magnitude of $\tan\varphi'/\tan\beta$ ratio.

   - If the slope' stability number ($\tan\varphi'/\tan\beta$) is lower than the threshold (for the illustrated case, the $\tan\varphi'/\tan\beta$ ratio is lower than 0.9), the failure mode is the shallow depth mode which occurs closed to the slope surface.

   - If the slope angle is within a small range between the soil frictional angle and an angle of slightly greater than the soil frictional angle (for the illustrated case shown in the study, the $\tan\varphi'/\tan\beta$ ratio ranges from 0.90 to 1.0), the failure mode is the transitional model. The depth

of the failure plane can occur at any depth in the soil layer depending on the magnitude of infiltration index. A greater $\tan\varphi'/\tan\beta$ ratio results in a more sensitive depth of failure plane relative to the infiltration index.
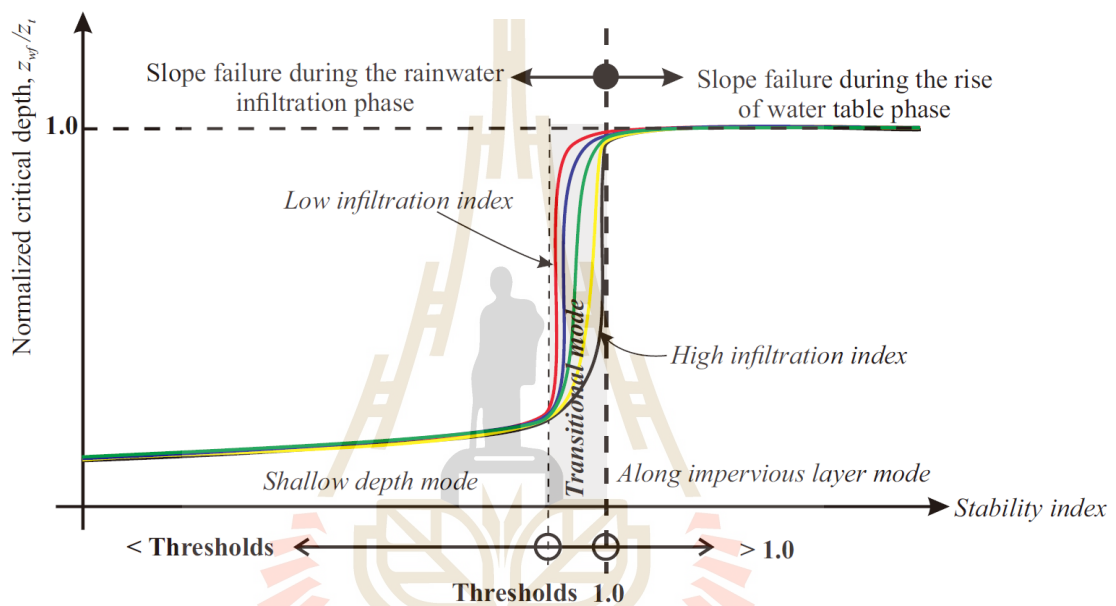
Figure 3.13   Modes of failure in shallow slope classified by the stability number

According to the failure modes shown in Figure 3.13, instrumentations on a specific slope can be characterized by its stability index as conceptually shown in Figure 3.14. In the mild slope ($\tan\varphi'/\tan\beta \geq 1.0$), slope failure will be triggered during the saturation phase. The end of infiltration phase, which is notified by the arrival of θ_{wb} at near interface layer, may be set as the first warning point (Figure 3.14a). For the very steep slope ($\tan\varphi'/\tan\beta \leq$ threshold), the mode of failure is a shallow depth slope failure. Time to reach the failure might occur shortly after a
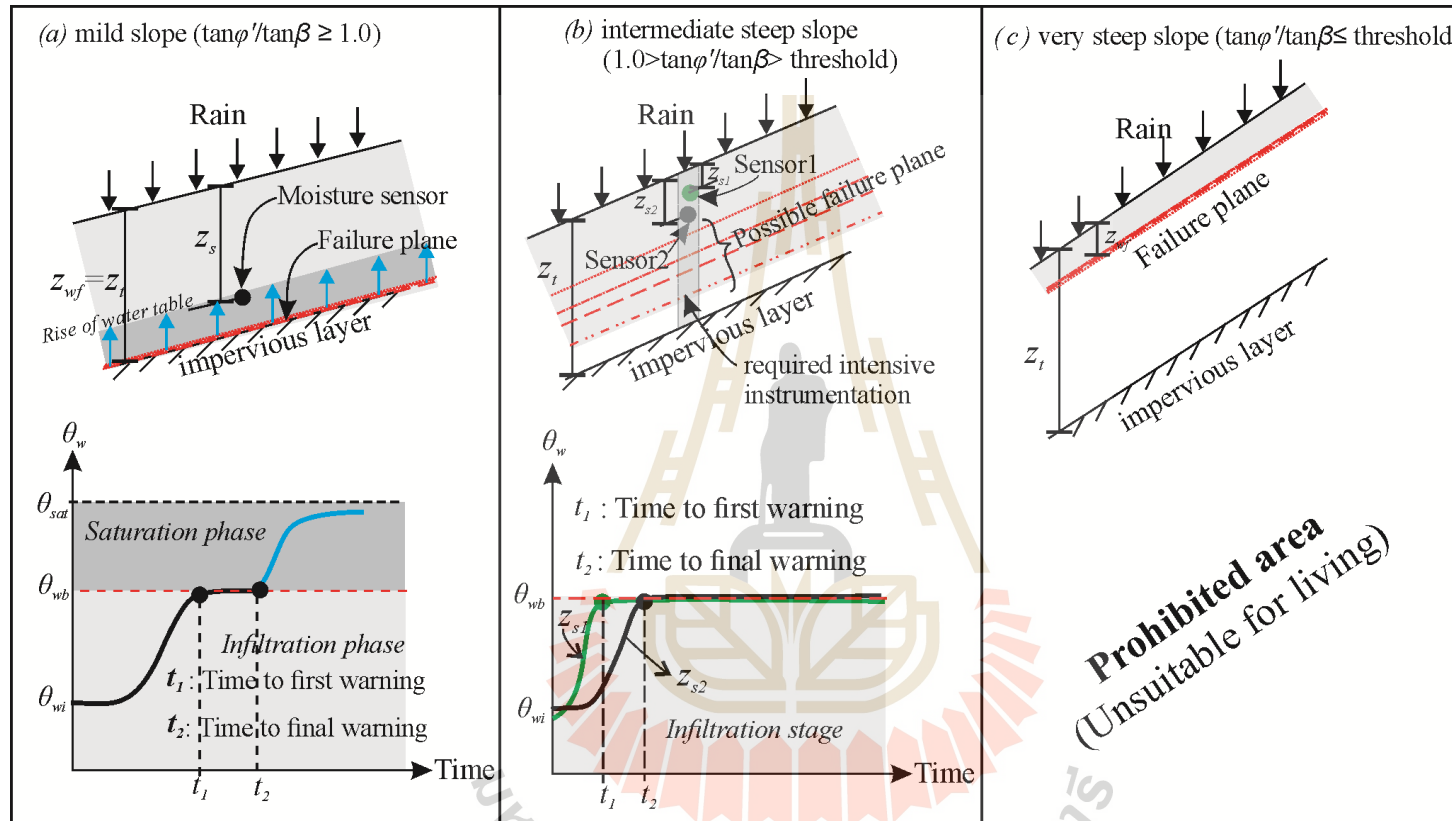
Figure 3.14 Sketch of possible failure planes related to characterized failure modes and conceptual methodology for predicting the slope failures based on water content responses read from moisture sensors; (a) for mild slope($\tan\varphi'/\tan\beta \geq 1.0$), (b) for intermediate steep slope ($1.0 > \tan\varphi'/\tan\beta >$ threshold) and (c) for very steep slope ($\tan\varphi'/\tan\beta \leq$ threshold)

rainfall event. Warning systems might not be suitable for this type of slope. The area and the vicinities should be classified as a sensitive area, in which human activities are prohibited (Figure 3.14b). For an intermediate steep slope ($1.0 > \tan\varphi'/\tan\beta >$ threshold), the failure plane can occur at various depths depending on the stability and infiltration indices. Intensive instrumentation to monitor the rainfall intensity and the development of wetting front must be assigned to this area as typically shown in Figure 3.14c.

3.8   Conclusions

The physical model was conducted in this study to investigate the effect of rainfall intensity, slope angle and inter-storm period on hydrological responses taking place in the soil shallow slope with cohesionless soil, with no water table. The rainfall characteristics used in this study were continuously applied until steady state condition was achieved (end of the test). The magnitudes of rainfall intensity assigned to every test were lower than the soil' saturated permeability ($k_s = 1.54\text{x}10^{-4}$ m/sec = 554.4 mm/hr). The comprehensive understanding of the hydraulic responses gained were leading to simplicity analysis of shallow slope with cohesionless soil subjected to a continuous rainfall of $i < k_s$ and could be concluded that:

1) The hydrological response is characterized by infiltration and saturation phases. During the infiltration phase, the magnitude of volumetric water content increases from its initial value to the final volumetric water content called "volumetric water content behind the wetting front: θ_{wb}". Further increment of the magnitude of volumetric water content will take place

again when the saturation phase begins. At the saturation phase, the magnitude of water content will increase from θ_{wb} to the saturated volumetric water content (θ_s).

2) The magnitude of rainfall intensity (i) affects the volumetric water content on both phases. The higher magnitude of rainfall intensity induces faster movement of wetting front and rise of water table. In addition, the magnitude of θ_{wb} increases with increasing the magnitude of rainfall intensity.

3) The slope angle (β) does not affect the variation of volumetric water content during the infiltration phase. In addition, the magnitude of θ_{wb} does not depend on the magnitude of β. However, the slope angle affects the variation of volumetric water content during the saturation phase. The flatter slope coincide with the faster rise of water table.

4) The inter-storm period affects both stage of θ_w in term of temporal variation. The shorter inter-storm period (t_b) induces the faster movement of wetting front and faster rising in water table. While the magnitude of θ_{wb} is independent with inter-storm period.

5) The failure state of a steep shallow slope with cohesionless soil of $\beta > \varphi'$ might take place during the infiltration phase. While, the failure state of a mild slope of $\beta \leq \varphi'$ might occur during the saturation phase.

6) For the steep slope ($\beta > \varphi'$), the location of the failure plane can occur at any depth varied from the impervious layer to the slope surface, depending on the stability and infiltration indices.

7) The "threshold" which is the stability number at which the critical depth is slightly sensitive to rainfall intensity is vital to categorize a steep slope as a very steep slope. Proper disaster prevention approaches can be implemented based on the threshold and the slope' stability number.

3.9   References

Ali A, Huang J, Lyamin AV, Sloan SW, and Cassidy MJ. 2014a. **Boundary effects of rainfall-induced landslides.** Computers and Geotechnics 61:341-354.

Ali A, Huang J, Lyamin AV, Sloan SW, Griffiths DV, Cassidy MJ, and Li JH. 2014b. **Simplified quantitative risk assessment of rainfall-induced landslides modelled by infinite slopes.** Engineering Geology 179:102-116.

ASTM D2487. 1991. **Standard Classification of Soils for Engineering Purpose (Unified Soil Classification System).** ASTM International, West Conshohocken, PA, USA.

ASTM D698. 1991. **Test Method for Laboratory Compaction Characteristics of Soil Using Standard Effort (12,400 ft-lbf/ft^3 (600 kN-m/m^3)).** ASTM International, Philadelphi, PA, USA.

ASTM D6836-02, 2003. **Test methods for determination of the soil water characteristic curve for desorption using a hanging column, pressure extractor, chilled mirror hygrometer, and/or centrifuge.** ASTM International, West Conshohocken, PA, USA.

Cho SE. 2009. **Infiltration analysis to evaluate the surficial stability of two-layered slopes considering rainfall characteristics.** Engineering Geology 105(1-2):32-43.

Cho SE, and Lee SR. 2002. **Evaluation of surficial stability for homogeneous slopes considering rainfall characteristics.** Journal of Geotechnical and Geoenvironmental Engineering Geology 128:756-763.

Corominas J. 2000. **Landslides and climate.** Keynote lecture- In: Proceedings 8th International Symposium on Landslides, (Bromhead E, Dixon N, Ibsen ML, eds) Cardiff: AA Balkema. Vol. 4, pp. 1-33.

Crosta GB, and Frattini P. 2001. **Rainfall thresholds for triggering soil slips and debris flow.** In: Proceedings 2nd EGS Plinius Conference on Mediterranean Storms (Mugnai A, Guzzetti F, Roth G, eds) Siena. pp. 463–487.

Cuomo S, and Della Sala M. 2013. **Rainfall-induced infiltration, runoff and failure in steep unsaturated shallow soil deposits.** Engineering Geology 162:118-127.

Decagon Devices Inc. 2007-2010. **Operator's Manual version 6**. 2365 NE Hopkins Court Pullman WA 99163.

Eichenberger J, Ferrari A, and Laloui L. 2013. **Early warning thresholds for partially saturated slopes in volcanic ashes.** Computers and Geotechnics 49: 79-89.

Fredlund DG, and Morgenstern NR. 1976. **Constitutive relations for volume in unsaturated soils.** Canadian Geotechical Journal 13:261-276.

Fredlund DG, Morgenstern NR, and Widger RA. 1978. **The shear strength of unsaturated soil.** Canadian Geotechical Journal 15:313–321.

Fredlund DG, and Rahardjo H. 1993. **Soil mechanics for unsaturated soils.** Wiley, New York.

Gardner W. 1958. **Steady state solutions of the unsaturated moisture flow equation with application to evaporation from a water table.** Soil Science 85:228-232.

Greco R, Guida A, Damiano E, and Olivares L. 2010. **Soil water content and suction monitoring in model slopes for shallow flowslides early warning applications.** Physics and Chemistry of the Earth 35(3-5):127-136.

Hall MJ, Johnston PM, and Wheather HS. 1989. **Evaluation of overland flow models using laboratory catchment data. I. An apparatus for laboratory catchment studies.** Hydrological Sciences Journal, 34: 277-288.

Huang C-C, Lo C-L, Jang J-S, and Hwu L-K. 2008. **Internal soil moisture response to rainfall-induced slope failures and debris discharge.** Engineering Geology 101(3-4):134-145.

Huang C-C, and Yuin S-C. 2010. **Experimental investigation of rainfall criteria for shallow slope failures.** Geomorphology 120(3-4):326-338.

Lee LM, Gofar N, and Rahardjo H. 2009. **A simple model for preliminary evaluation of rainfall-induced slope instability.** Engineering Geology 108(3-4):272-285.

Lee LM, Kassim A, and Gofar N. 2011. **Performances of two instrumented laboratory models for the study of rainfall infiltration into unsaturated soils.** Engineering Geology 117(1-2):78-89.

Li WC, Lee LM, Cai H, Li HJ, Dai FC, and Wang ML. 2013. **Combined roles of

saturated permeability and rainfall characteristics on surficial failure of homogeneous soil slope. Engineering Geology 153:105-113.

Lu N, and Godt J. 2008. **Infinite slope stability under steady unsaturated seepage conditions.** Water Resources Research 44(11):1-13.

Lu N, and Griffiths DV. 2004. **Profiles of Steady-State Suction Stress in Unsaturated Soils.** Journal of Geotechnical and Geoenvironmental Engineering Geology 130(10):1063-1076.

Lu N, and Likos WJ. 2006. **Suction Stress Characteristic Curve for Unsaturated Soil.** Journal of Geotechnical and Geoenvironmental Engineering Geology, 132(2):131-142.

Ma K-C, Tan Y-C, and Chen C-H. 2011. **The influence of water retention curve hysteresis on the stability of unsaturated soil slopes.** Hydrological Processes 25(23):3563-3574.

Meyer PD, and Gee GW. 1999. **Flux-based estimation of field capacity.** Journal of Geotechnical and Geoenvironmental Engineering 125(7):595-599.

Phi S, Clarke W, and Li L. 2013. **Laboratory and numerical investigations of hillslope soil saturation development and runoff generation over rainfall events.** Journal of Hydrology 493:1-15.

Pradel D, and Raad G. 1993. **Effect of permeability on surficial stability of homogeneous slopes.** Journal of Geotechnical Engineering 119(2):315-332.

Rahardjo H, Li XW, Toll DG, and Leong EC. 2001. **The effect of antecedent rainfall on slope stability.** Geotechnical and Geological Engineering 19:371-399.

Rahardjo H, Ong TH, Rezaur RB, and Leong EC. 2007. **Factors controlling instability of homogeneous soil slopes under rainfall.** Journal of Geotechnical and Geoenvironmental Engineering 133(12):1532-1543.

Rahimi A, Rahardjo H, and Leong E-C. 2010. **Effect of hydraulic properties of soil on rainfall-induced slope failure.** Engineering Geology 114(3-4):135-143.

Rahimi A, Rahardjo H, and Leong E-C. 2011. **Effect of Antecedent Rainfall Patterns on Rainfall-Induced Slope Failure.** Journal of Geotechnical and Geoenvironmental Engineering, 137(5):483-491.

Santoso AM, Phoon K-K, and Quek S-T. 2011. **Effects of soil spatial variability on rainfall-induced landslides.** Computers & Structures 89(11-12):893-900.

Sharma RH, and Nakagawa H. 2010. **Numerical model and flume experiments of single- and two-layered hillslope flow related to slope failure.** Landslides 7(4):425-432.

Shen S-L, Wang J-P, Wu H-N, Xu Y-S, Ye G-L, and Yin Z-Y. 2015. **Evaluation of hydraulic conductivity for both marine and deltaic deposits based on piezocone testing.** Ocean Engineering, 110: 174-182.

Skempton A, and DeLory F. 1957. **Stability of natural slopes in London Clay.** Proceedings of 4th International Conferrence on Soil Mechanics and Foundation Engineering, Butterworths Scientific Publications, London, 2: 378-381.

Soil Science Glossary Terms Committee. 2008. **Glossary of Soil Science Terms 2008.** Madison: SSSA: pp. 92.

Tohari A, Nishigaki M, and Komatsu M. 2007. **Laboratory rainfall-induced slope failure with moisture content measurement.** Journal of Geotechnical and

Geoenvironmental Engineering 133(5):575-587.

Tsai T-L, Chen H-E, and Yang J-C. 2008. **Numerical modeling of rainstorm-induced shallow landslides in saturated and unsaturated soils.** Environmental Geology 55(6):1269-1277.

Xu Y-S, Shen S-L, and Du Y-J. 2009. **Geological and hydrogeological environment in Shanghai with geohazards to construction and maintenance of infrastructures.** Engineering Geology 109(3-4):241-254.

Yumuang S. 2006. **2001 debris flow and debris flood in Nam Ko area, Phetchabun province, central Thailand.** Environmental Geology 51(4):545-564.

van Genuchten MT. 1980. **A closed-form equation for predicting the hydrualic conductivity of unsaturated soil.** Soil Science Society of America Journal 44: 892-898.

Vanapalli SK, Fredlund DG, Pufahl DE, and Clifton AW. 1996. **Model for the prediction of shear strength with respect to soil suction.** Canadian Geotechical Journal 33(3):379–392.

Zhan TLT, Jia GW, Chen YM, Fredlund DG, and Li H. 2013. **An analytical solution for rainfall infiltration into an unsaturated infinite slope and its application to slope stability analysis.** International Journal for Numerical and Analytical Methods in Geomechanics 37(12):1737-1760.

Zhang LL, Zuo ZB, Ye GL, Jeng DS, and Wang JH. 2013. **Probabilistic parameter estimation and predictive uncertainty based on field measurements for unsaturated soil slope.** Computers and Geotechnics 48:72-81.

CHAPTER IV

INFLUENCE FACTORS INVOLVING RAINFALL-

INDUCED SHALLOW SLOPE FAILURE:

NUMERICAL STUDY

4.1   Statement of problem

An effective tool for mitigating the problems related to slope failures in recent years is the use of the critical rainfall concept. The critical rainfall is usually represented through a relationship between intensity and duration of rainfall for the initiation of slope failure (ID thresholds), e.g. Caine 1980; Calcaterra et al. 2000; Corominas 2000; Crosta and Frattini 2001; Aleotti 2004; Cannon and Gartner 2005; Chien et al. 2005; Guzzetti et al. 2007). The advantages of this concept are their simplicity and rapid assessment. As such, this concept has been widely implemented as a part of an early warning system (Brand 1984, Keefer et al. 1987, Wilson et al. 1993, Sirangelo and Braca 2004).

Although the critical rainfall concept is simple and easy to use to assess the failure of slopes, understanding of the critical mechanism triggering the failure of slope is often neglected. Understanding the rainfall-induced slope failure problem needs coupled flow simulation and mechanical deformation modeling, especially in unsaturated ground water flow environment. Various numerical studies have been undertaken previously, conducting the relevant problems based on conventional theory of ground water flow and mechanical deformation by decoupling the ground water flow field from the mechanical deformation field (Rahardjo et al. 2007, Rahardjo et al. 2010,

Rahimi et al. 2010). However, the rainfall induced slope failure is intrinsically a hydraulic-mechanical interaction between these two fields. Hence, analysis of the relevant problems requires a powerful tool to conduct a series of numerical experiments, which simulate the problem in a coupling of hydrological-mechanical manner (Ng and Shi 1998; Cai and Ugai 2004; Griffiths and Lu 2005; Shen and Xu 2011; Xu et al. 2012; Hamdhan and Schweiger 2013; Khalilnejad et al. 2013; Wu et al. 2015b). None of the previous attempts have conducted the analysis of rainfall-induced shallow slope failure in a fully coupled hydrological-mechanical manner. Moreover, there existed attempts performed the analysis on the slope subjected to a specific period of rainfall. In the other word, analysis on the slope subjected to a certain rainfall continuously until the initiation of slope failure had never been conducted. Therefore, the failure conditions of shallow slope under various conditions of the influence factors have not been investigated to date.

To the author's knowledge, the current gaps of knowledge related to rainfall-induced shallow slope failures are partly discussed below:

- Although, previous attempts devoted to understand the effects of the influence factors; including the soil saturated permeability, the slope angle, and the antecedent rainfall, on circular slope failures, the effects of these influence factors on the stability of shallow slope have not been ascertained.

- None of the previous attempts had described the hydrological related mechanisms of the shallow slope failure in quantitative manner. This paper is the first attempt to presents them in such a manner.

- The common tool for assessment of the critical rainfall in the rainfall induced slope failure is the rainfall intensity-duration thresholds for

initiation of slope failure (ID thresholds). However, as the ID thresholds were established empirically, the effects of the influence factors on the ID thresholds have not examined yet.
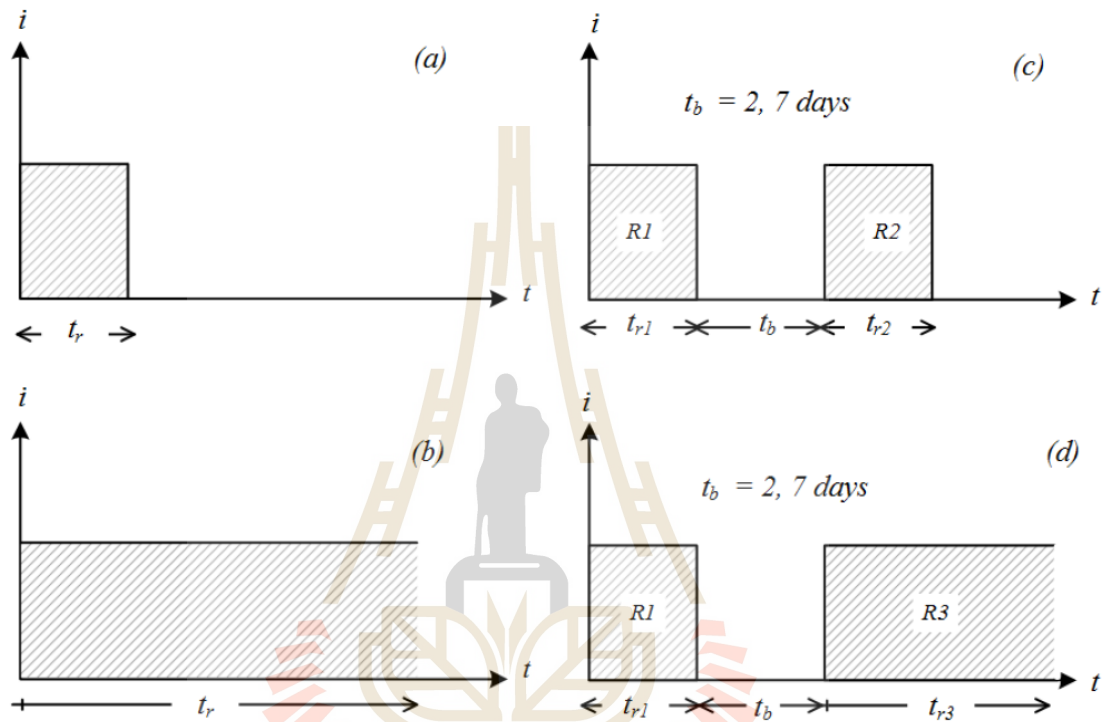
Figure 4.1   Schematic explanation of periodical rainfall assigned in this study (a) single storm with constant duration, (b) single storm with infinite duration, (c) multiple storm under constant duration R1, R2 with 2 and 7 days between storm periods and (d) multiple storm under constant duration R1, infinite duration R3 with 2 and 7 days between storm periods

A series of numerical experiments were conducted under finite element environments. The influence factors consist of the soil type in term of soil saturated permeability, the slope angle and the antecedent rainfall. The analysis was conducted with the shallow slope subjected to four patterns of rainfall conditions as shown in Figure 4.1; (1) a single storm rainfall of a certain intensity for a period of 24 hours, (2) a continuous rainfall of a certain intensity until the arrival of slope failure, (3) a periodical rainfall with a sequential rainfall of a certain intensity for a period of 24 hours, and (4) a periodical rainfall with a sequential rainfall of a certain intensity until the arrival of slope failure. Results from this study might enhance knowledge in the mechanisms of rainfall induced shallow slope failure, and hence improvement of the current warning system for rainfall-induced shallow slope failures.

4.2 Finite element analysis

Finite element PLAXIS code with a fully coupled flow-deformation analysis (Brinkgreve et al. 2010) was used in this study. The application of the code to rainfall infiltration related problems was verified by Hamdhan and Schweiger (2013). Mohr-Coulomb failure criterion is assigned to this study. The shear strength of soil related to unsaturated conditions is obtained by combining Bishop's effective stress concept (Bishop and Blight 1963) and Mohr-Coulomb failure criterion, which can be expressed as:

$$\tau = c' + (\sigma_n - u_a)\tan\varphi' + \chi(u_a - u_w)\tan\varphi' \qquad (4.1)$$

where τ is shear strength of unsaturated soil, σ_n is the normal stress, u_a is the pore air pressure, u_w is the pore-water pressure, $(\sigma_n - u_a)$ is net normal stress, $(u_a - u_w)$ is matric suction c' is the effective soil cohesion, φ' is internal soil friction angle and χ is scalar multiplier which is assumed as effective degree of saturation(θ_e) in this study.

The safety factor (*FS*) is calculated by means of the shear strength reduction technique or $c' - \varphi'$ reduction technique (Ugai 1989; Griffiths and Lane 1999; Brinkgreve et al. 2010). In this technique, the safety factor (*FS*) of a soil slope is defined as the number by which the original shear strength parameters are divided to bring the slope to failure state. If the shear strength parameters at failure are c_r and φ_r, the safety factor can be defined as:

$$FS = \frac{\tan \varphi}{\tan \varphi_r} = \frac{c}{c_r} \qquad (4.2)$$

As for the hydrological process, Richard's equation (Richards, 1931) was used to simulate transient flow through unsaturated soil. At equilibrium, the summation of the change in the rate of flow in *x, y* and *z* directions is equal to the change in the rates of the head with respect to time and can be expressed as:

$$\frac{\partial}{\partial x}\left[k_x(h)\frac{\partial h}{\partial x} \right] + \frac{\partial}{\partial y}\left[k_y(h)\frac{\partial h}{\partial y} \right] + \frac{\partial}{\partial z}\left[k_z(h)\left(\frac{\partial h}{\partial z} + 1 \right) \right] = \left\{ C(h) + S_s \right\}\frac{\partial h}{\partial t} \qquad (4.3)$$

where k_x, k_y, k_z are coefficients of permeability in directions of x, y and z, respectively, $C(h) = (\partial\theta/\partial h)$ is the rate of change in the volumetric water content (θ) with respect to the pressure head (h), and S_s is the specific storage of a porous media or soil.

The permeability in unsaturated soil depends highly on soil-water characteristics (SWC). The SWC is a relationship between water content and pressure head which can be explained by van Genuchten model (van Genuchten 1980) and the permeability function is explained by van Genuchten-Mualem model (Mualem 1976). Equations 4.4 and 4.5 are the van Genuchten and van Genuchten-Mualem models, respectively.

$$\theta_e = \frac{\theta - \theta_{res}}{\theta_w - \theta_{res}} = \left\{\frac{1}{1 + [\alpha(u_a - u_w)]^n}\right\}^{1-\frac{1}{n}} \tag{4.4}$$

$$k(h) = k_{sat}\frac{\left\{1 - [\alpha(u_a - u_w)]^{n-1}\left\langle 1 + [\alpha(u_a - u_w)]^n\right\rangle^{\frac{1}{n}-1}\right\}^2}{\left\{1 + [\alpha(u_a - u_w)]^n\right\}^{\frac{1}{2}-\frac{n}{2}}} \tag{4.5}$$

where θ is volumetric water content, θ_{res} is residual volumetric water content, θ_{sat} is saturated volumetric water content, k_{sat} is saturated permeability of soil and α, n are fitting parameters which represent air-entry value of soil and the rate of water extraction from the soil once the air entry has been exceeded, respectively. These two group of material parameters including shear strength parameters (c', φ') and hydraulic related

parameters (α, n, k_{sat}) are the required parameters to perform an analysis of rainfall-induced slope failures in PLAXIS. In this study, relevant parameters were obtained from previous research works and they will be discussed in the following section.

4.3   Materials and methods

Shallow slope failures are commonly found in many parts of the world. The geological setting in each hazardous area is different depended upon climate conditions, rate of weathering, slope geometry, etc. As such, this study gathered the soil properties reported from the relevant literature in slope failure, including Dahal et al. (2008); Godt and McKenna (2008); Jotisankasa and Vathananukij (2008); Jotisankasa and Mairaing (2010); Vieira et al. (2010); Bordoni et al. (2015) and Oh and Lu (2015) and summarized them in Table 4.1. It is shown that the parameter α is ranged from 0.016 to 0.360 kPa^{-1}, the desaturation parameter n ranges from 1.290 to 2.780, θ_{sat} ranges from 0.286 to 0.480 and θ_{res} ranges from 0.0 to 0.250. Besides, the saturated permeability of soil is ranged from 1.0×10^{-6} to 2.1×10^{-4} m/sec.

Figures 4.2(a) and (b) show the soil-water characteristics and the permeability function plotted from equations (4.4) and (4.5), respectively, with the given magnitude of the above mentioned parameters. As for the shear strength parameters, the cohesion and friction angle of the soils ranged from 0.0 to 17.60 kN/m^2 and from 32° to 38.6°, respectively. Variation of the strength envelopes is shown in Figure 4.2(c). The total unit weight of the soils is found ranging from 14.30 to 19.80 kN/m^3.

Previous literatures (Rahardjo et al. 2007; Xu et al. 2009; Li et al. 2013; Shen et al., 2014; Shen et al. 2015; Wu et al. 2015a) reveal that the saturated permeability plays

a major role on the stability of slope and other hydrologic-mechanical related problems. Hence, the saturated permeability is being focused on this study. While, the other parameters, including c', φ', α and n were kept constant at 6.74 kN/m², 33.6˚, 0.162 kPa^{-1} and 1.564 respectively. The magnitude of these parameters were deducted from the average of the parameters reported in Table 4.1. In this study, variation of the saturated permeability is represented by type of soil, i.e. the soils A, B and C stand for low (k_{sat}=1x10^{-6} m/sec), medium (k_{sat}=1x10^{-5} m/sec) and high (k_{sat}=1x10^{-4} m/sec) drainage ability, respectively. The magnitude of the saturated permeability assigned to the soil A, B, and C was simply deduced from the saturated permeability reported in Table 4.1.

Three series called series I, series II and series III were conducted in this study to evaluate stability and time to failures of the shallow slope under various conditions of the influence factors, including rainfall intensity; slope angle; and antecedent rainfall. As shown in Table 4.2, the numerical experiment includes 156 cases of the simulation run. The simulations include 78 cases of rainfall period of 24 hours and 78 cases of continuous rainfall until the arrival of slope failure.

For series I, 42 cases included 21 cases of rainfall period of 24 hours and 21 cases of continuous rainfall until the arrival of slope failure (21+21) were conducted. For each soil type, a constant rainfall intensity was assigned in a range from 0.36 to 360 mm/hr depending on the saturated permeability of each soil type. In addition, an extreme rainfall condition (EXT) is assigned to every soil types. This condition may occur once the rainfall intensity is much higher than the drainage capacity of soil at saturation ($i \geq k_{sat}$) and the infiltration excess might exist since the start of rainfall. In this study, the extreme rainfall condition is assumed to generate a ponding rain water -

Table 4.1 Summary of soil parameters from previous studies

Data No.	Author/Year	Location/Country	Hydrualic property					Strength property		
			θ_{sat}	θ_{res}	k_{sat} (m/sec)	α $(kPa)^{-1}$	n	γ_{sat} (kN/m^3)	c' (kN/m^2)	φ' (deg
1	Jotisankasa and Vathananukij(2008)& Jotisankasa A. and Mairaing W.(2010)	Tak/ Thailand	0.475	0.200	-	0.360	1.290	-	6.5	37.0
2		Nakhon Nayok/ Thailand	0.470	0.170	2.1×10^{-4}	0.290	1.316	17.61	12.8	33.1
3		Chonburi/ Thailand	0.400	0.250	1.0×10^{-5}	0.265	1.596	-	8.7	38.6
4		Omkoi/ Thailand	0.470	0.230	-	0.066	1.298	-	17.6	28.7
5	Bordoni et al.(2015)	Oltrepò Pavese/ Italy	0.370	0.010	2.0×10^{-5}	0.016	1.300	17.70	0	32.0
6	Dahal et al.(2008)	Shikoku Island/ Japan	-	-	4.9×10^{-5}	-	-	19.80	4.9	31.5
7	Oh H. and Lu N.(2015)	Hadong/ Korea	0.282	0.00	5.6×10^{-6}	0.044	1.370	17.41	0	34.1
8	Vieira et al.(2010)	Sao Paulo/ Brazil	-	-	1.0×10^{-6}	-	-	14.3	6	34
9	Godt JW. and MaKenna JP (2008)	Washington/ USA	0.480	0.066	5.0×10^{-5}	0.096	2.780	-	4.2	33.6
MAX.	-	-	0.480	0.250	2.1×10^{-4}	0.360	2.780	19.80	17.6	38.6
MEAN	-	-	0.421	0.132	4.29×10^{-5}	0.162	1.564	17.36	6.74	33.6
MIN.	-	-	0.286	0	1.0×10^{-6}	0.016	1.290	14.30	0	28.7
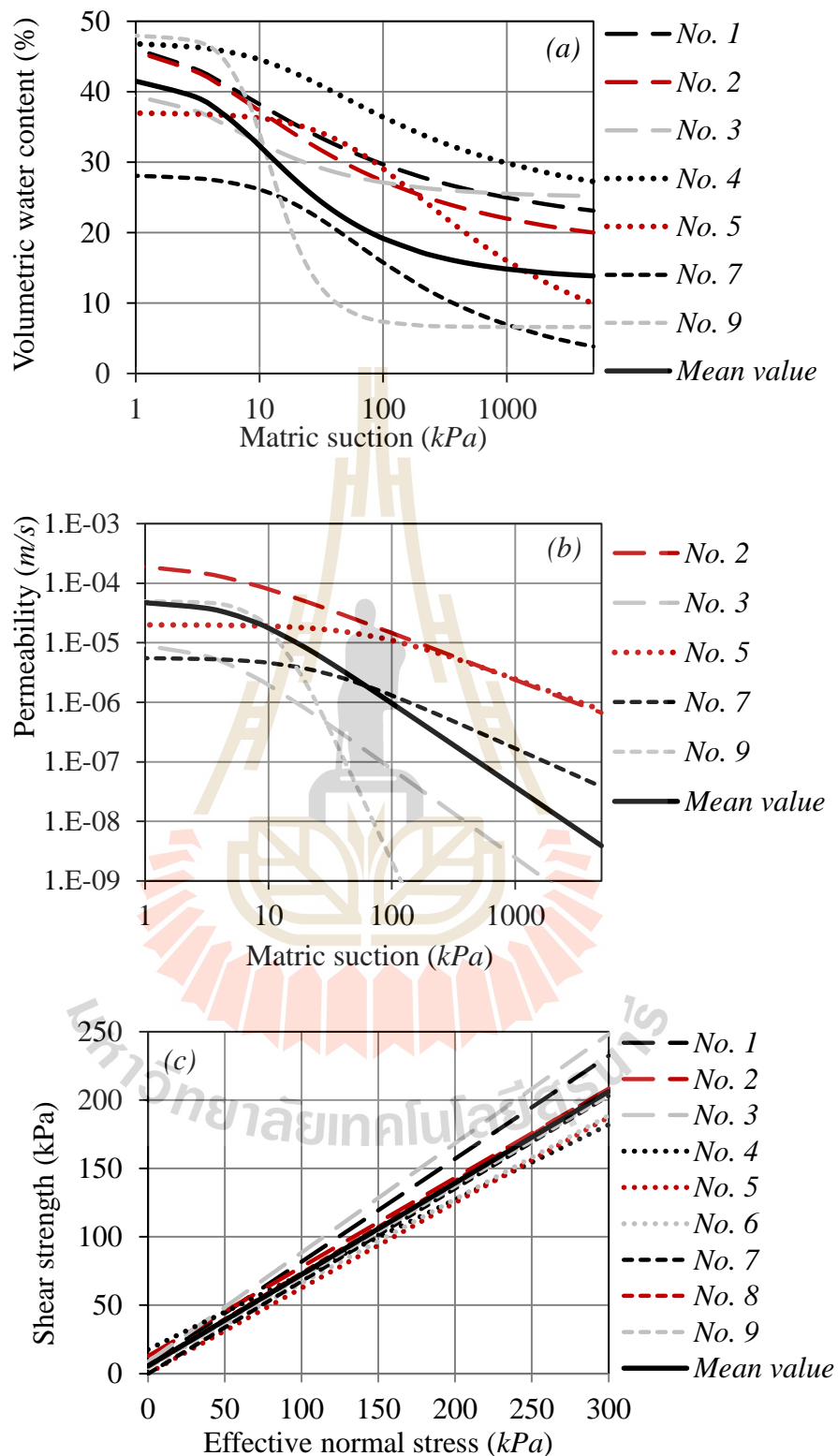
Figure 4.2 Soil properties (a) soil water characteristic curves, (b) computed soil

permeability and (c) soil shear strength

height of 5 cm for a whole period of the simulation. In PLAXIS, this condition can be simulated by a prescribed maximum pressure head (Ψ_{max}) of 5 cm.

The effect of slope angle on the stability and time to failure were evaluated in series II. 78 cases (39+39) of simulation run were conducted by varying the slope angle from 20° to 40°. Three types of soil with three or four rainfall intensities were assigned to each slope angle in this series.

Finally, 36 cases of simulation run were conducted in series III to evaluate the effect of antecedent rainfall. The antecedent rainfall imitates the periodical rainfall in real field. The previous rainfall affects the initial conditions of the soil subjected to the sequential rainfall, and hence the initial stability of the slope. In this study, the rainfall was assigned periodically as shown in Figures 4.1 (c) and 4.1 (d). The simulation started with an antecedence rainfall of certain rainfall intensity for 24 hours (R1). Subsequently, the rainfall was terminated for a certain period (antecedent condition) prior to an arrival of another rainfall event (R2 or R3). These 36 cases include 18 cases of the rainfall R2 (24 hours rainfall) and 18 cases of R3 (continuous rainfall until the arrival of slope failure) (18+18). For each simulation, the same rainfall intensity was prescribed to the rainfall events R1 and R2 or R1 and R3. In series III, two antecedent conditions of rainfall of 48 and 168 hours (2 days and 7 days) were prescribed to the simulations. The magnitudes of rainfall intensity, rainfall duration, and period of the antecedent condition used in this case series are summarized Table 4.2. For sake of simplicity, the effects of evaporation is neglected in this study. The slope instability triggered rainfall is typically taken place during rainfall period having high relative humidity, and hence evaporation is negligible.

Table 4.2.   Summary of case study

Numerical series	Rainfall intensity for soil type A, B, C i, (*mm/hr.*)			Slope angle β, (*deg*)	Rainfall duration (*hr*)	Between storm rainfall period t_b, (*day*)	Number of combinations	
							24-hr rainfall	∞*-hr rainfall
	A	B	C					
I	0.36 0.5 1 3.6 5 7.2 EXT	0.5 1 5 10 20 36 EXT	5 10 20 50 100 360 EXT	30	24,∞*	-	7x3 = 21	7x3 = 21
II	0.36 1 3.6 EXT	1 10 36 EXT	1 10 100 360 EXT	20 30 40	24,∞*	-	(4x3)+(4x3) +(5x3) =39	(4x3)+(4x3) +(5x3) =39
III	0.36 3.6 5	1 5 10	1 5 10	30	24,∞*	2 7	(3x2)+(3x2) =18	(3x2)+(3x2) =18
						SUM	78	78

* is rainfall duration assigned until an initiation of slope failure

4.4   Set up of the experiments

Slope geometry, boundary conditions and fixity used in this study are shown in Figure 4.3. The slope model is divided into two layers. The bedrock is overlaid by a uniform shallow soil layer with thickness of 3 meters(d = 3 m.), which gives the ratio of slope length (L) to soil depth (d) of about 31, 29 and 26 for the slope angle of 20˚, 30˚ and 40˚, respectively. These L/d ratios are greater than 20 which is far enough to avoid boundary effects in calculation of safety factor (Griffiths et al. 2011; Tiwari et al. 2014). Standard fixities were prescribed to allow only vertical movement along the boundary sides, while lateral and vertical movements were fixed at bottom boundary. 15-node triangular finite element mesh is assigned in the problem. The finer elements were generated at the soil layer, and the finest mesh was generated along the soil slope where the failure tends to occur.

A prescribed flux, which relates to the desired intensity of rainfall, was assigned along the slope surface BC. Along the slope surface BC, a range of pore water pressure between -0.05 m and 0.05 m was prescribed. By this maximum pore water pressure of 0.05 m, the ponding water due to the excess of rainfall intensity over the infiltration capacity at soil saturation state could be developed up to 5 cm. over the slope surface. While the minimum pore water pressure of -0.05 m was used to represent a depth of negative flux due to evaporation. The boundaries AB and CD were assigned as no flux boundaries, while the boundaries AHG, DEF and GF were prescribed as impervious boundaries. The initial conditions were prescribed by variation of initial pore water pressure (u_{wi}) ranges from -50 kPa to -80 kPa from soil-bedrock interface to soil surface to represent ground conditions prior to rainfall season. The volumetric water content at field capacity (θ_{fc}) and the residual water content (θ_{res}) were used as references to

Figure 4.3 Slope geometry and boundary conditions

Table 4.3   Soil parameters required for Mohr-Coulomb model

Parameter	Symbol	Soil layer			Bedrock layer	Unit
Material models						
Mechanical model	Model	Mohr-Coulomb			Mohr-Coulomb	-
Type of material behavior	Type	Undrained A			Non-porous	-
Cohesion	c'	6.74			25^{a*}	kPa
Friction angle	φ'	33.62			50^{a*}	deg
Hydraulic model	Model	Van Genuchten			-	-
Soil type	-	A	B	C	-	-
Saturated permeability of soil	$k_{sat,x} = k_{sat,y}$	1×10^{-6}	1×10^{-5}	1×10^{-4}	-	m/sec
n	n	1.564			-	-
α	α	0.162			-	kPa^{-1}
Deformation parameters						
Effective modulus of elasticity	E'^{a*}	50000			100000	kPa
Effective Poisson's ratio	v'^{a*}	0.33			0.2	-
Dry unit weight	γ_{unsat}	17.36			23^{a*}	kN/m^3
Total unit weight	γ_{sat}	17.36			23^{a*}	kN/m^3

a* is assumed values.

prescribe the range of θ_i, and hence u_{wi}. The θ_{fc} is known as the content of water, on a mass or volume basis, remaining in a soil 2 or 3 days after having been wetted with water and after free drainage is negligible (Soil Science Glossary Terms Committee 2008; Meyer and Gee 1999). It corresponds to the pore water pressure of -34 kPa (Dingman 2002) for any soil type. If no addition water added into the soil for 2-3 days after rainfall, the water content might further decrease due to evaporation and plant root uptake. As such, a range of θ_i might possibly be between θ_{fc} and θ_{res}. According to the soil water characteristic assigned to the model (dash line in Figure 4.2a), the variation of pore water pressure range from -80 kPa to -50 kPa is presented by the variation of volumetric water content of 20% to 22% as shown in Figure 4.3.

Table 4.3 summarizes the material properties categorized into three categories; strength parameters, hydraulic related parameters, and deformation parameters. Mohr-Coulomb model was used to explain the mechanical behavior of soil and bedrock layers. Van Genuchten and van Genuchten-Mualem models were used to explain the hydraulic behavior of the soil layer, while the bedrock layer was assumed as an impermeable non-porous material.

4.5   Results and discussions

Results from the numerical experiments are presented in three aspects; 1) The possible failure mechanism related to the response of pore-water pressure, 2) Safety factor characteristics of a slope subjected to a certain rainfall duration, and 3) The rainfall thresholds for the initiation of slope failure presented through the relationship between rainfall intensity and duration (ID).

4.5.1 General mechanism of rainfall-induced shallow slope failures

Simulation results partly deducted from the case series I were used to analyze the shallow slope failure mechanism. They include 6 cases with the continuous rainfall intensity of 5, 10, 36 mm/hr for the soils B and C, respectively. Noted that the rainfall intensities of 36 and 360 mm/hr. are equal to the infiltration capacity at saturation state of the corresponding soils, i.e. the saturated permeability of the soil type B is 10^{-5} m/sec = 10^{-5} m/sec x 10^3 mm/m x 3600 sec./hr. = 36 mm/hr.

Figure 4.4 presents variation of FS against the simulated rainfall duration to failure. For the lowest rainfall intensity (5 mm/hr), the FS of the soils B and C decreases in a similar manner. The FS gradually decreases with increasing rainfall period of no longer than 76 hours. For the slope subjected to the rainfall period of longer than 76 hours, the FS drastically decreases. A similar trend is found for the rainfall intensity of 10 mm/hr. As the FS retains its high magnitude and subsequently drops drastically, the slope failure might takes place immediately after the rainfall period reaches a critical threshold without any sign of physical response. As for the rainfall intensity equal or greater than the infiltration capacity of the corresponding soils at their saturation state, the rapid reduction of FS is found almost immediately after the rainfall start.

Figures 4.5 and 4.6 present pore water pressure profile along the depth of a vertical section located at a mid of the slope (section a-a in Figure 4.3) for the soils B and C, respectively. Figures a, b, and c are for the rainfall intensity of 5 mm/hr, 10 mm/hr, and 36 or 360 mm/hr, respectively. The distribution of pore water pressure can be characterized into two stages; a rainfall infiltration stage, and a rising of water table stage. The stage of rising of water table starts after the rainfall infiltrates to the soil -
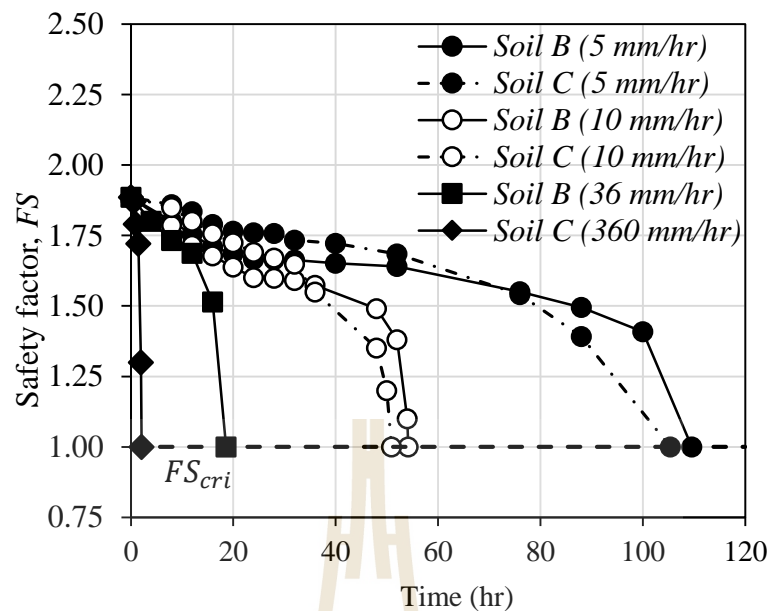
Figure 4.4   Relationship between safety factor and simulated rainfall duration under

four constant rainfall intensities and two types of soil with medium (soil

B) and high (soil C) permeability

bedrock interface. During the infiltration stage, the negative pore water pressure

decreases from the initial stage to reach the single greatest magnitude of pore water

pressure. Hence, at the end of the infiltration stage the magnitude of pore water pressure

at any the depth is equal to this greatest value. Thereafter, the pore water pressure

increases and become positive pore water pressure due to the rising of water table.

Figures 4.5a and 4.6a show that, for the rainfall intensity of 5 mm/hr.,

the end of infiltration stage take place about 76 hr and 52 hr for the soils B and C,

respectively. The figures also show that the magnitudes of pore water pressure at the

end of the infiltration stage are -4 kPa (for the soil B) and -10 kPa (for the soil C). This

constant magnitude of the negative pore water pressure depends upon flux boundary

and hydraulic properties of soil (Lu and Griffiths 2004; Lu and Likos 2006; Lu and -
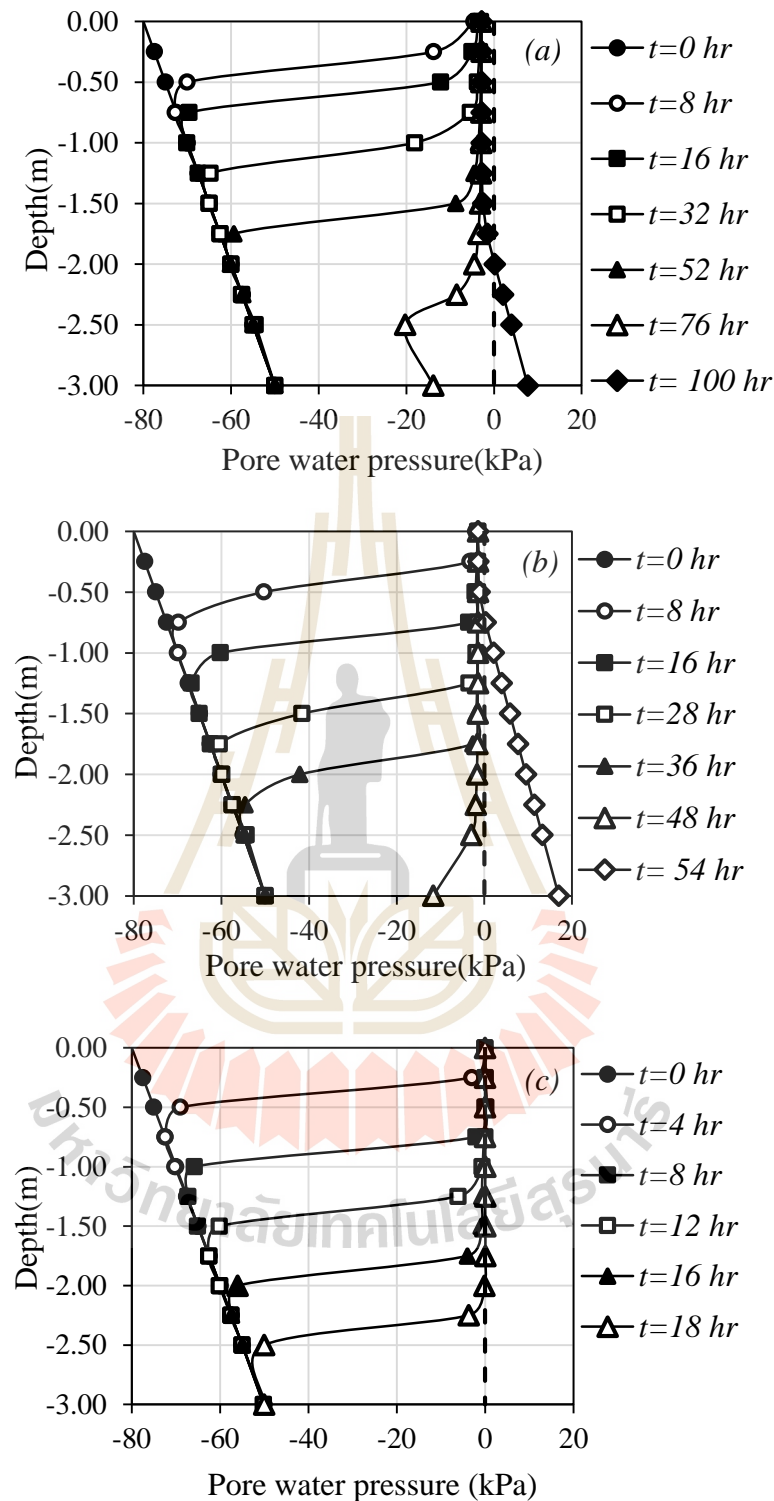
Figure 4.5 Pore water pressure profile with different rainfall intensity duration of

soil B (a) constant rainfall intensity (i) = 5 mm/hr, (b) i=10 mm/hr and

(c) i=36 mm/hr
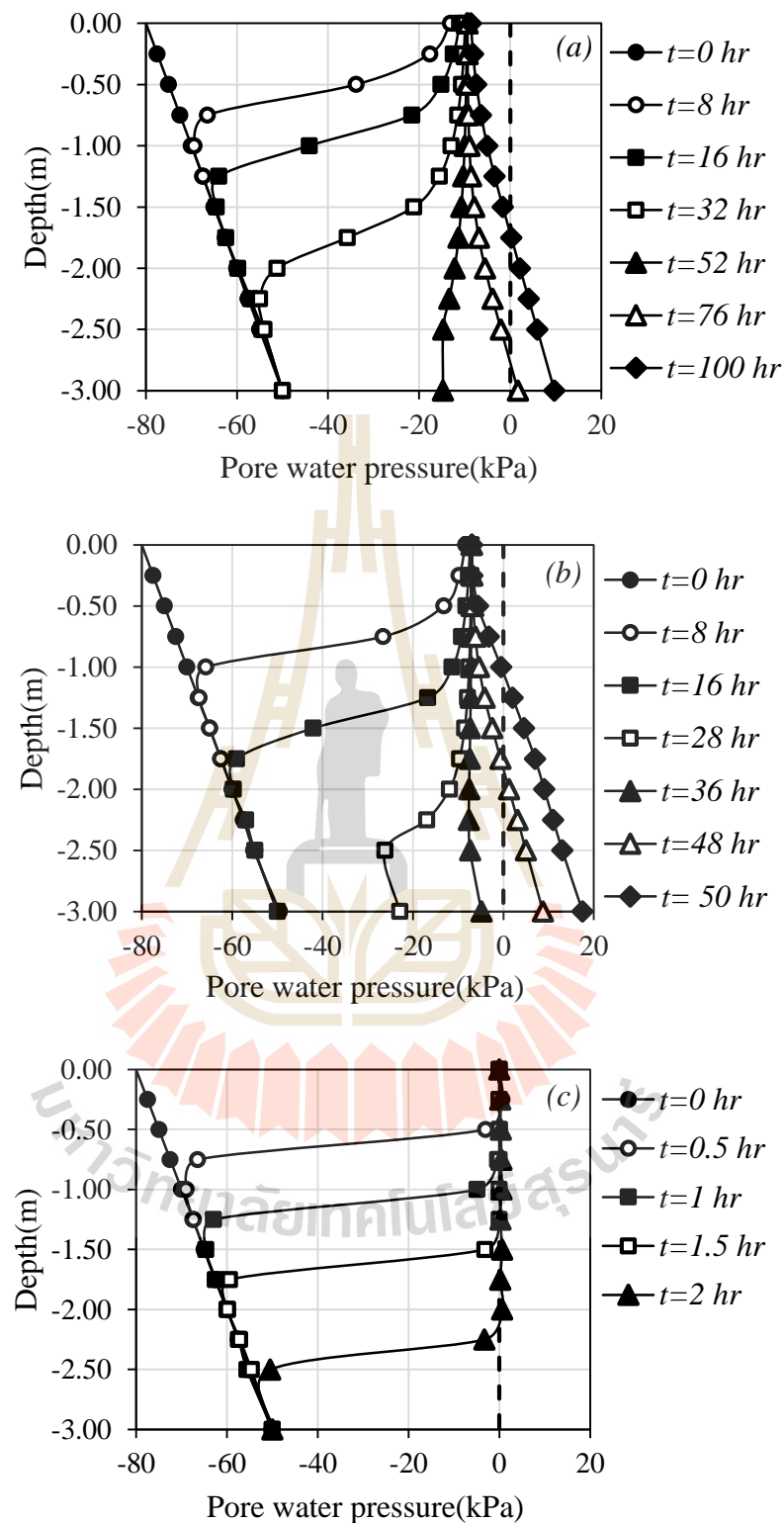
Figure 4.6 Pore water pressure profile with different rainfall intensity duration of soil C (a) constant rainfall intensity (*i*) = 5 mm/hr, (b) *i*=10 mm/hr and (c) *i*=360 mm/hr

Godt 2008; Vahedifard et al. 2016; Chinkulkijniwat et al. 2016), hence the higher magnitude of pore water pressure at the end of infiltration stage for the soil C is due to the higher infiltration capacity of the soil C at saturation state (higher saturated permeability).

Referring to the variation of *FS* shown in Figure 4.4, the *FS* against the shallow slope failure is far greater than 1.0 during the rainfall infiltration stage because of the remaining of negative pore water pressure (suction) both in the soils B and C. In addition, the greater *FS* in the soil C than that in the soil B during the infiltration stage is because the magnitude of negative pore pressure at the end of the rainfall infiltration stage in the soil C is greater than that in the soil B. A similar trend is found in the cases for the rainfall intensity of 10 mm/hr as shown in Figures 4.5b and 4.6b. Noted that the magnitudes of negative pore water pressure at the end of infiltration stage for this rainfall intensity are -2 kPa and -8 kPa for the soils B and C, respectively.

The rising of water table after the end of infiltration stage results in an increasing of positive pore-water pressure, and hence the loss of shear strength specially at the interfacial zone of the soil and the bedrock. At this stage, due to its higher saturated permeability, the drop of the *FS* in the soil C is faster than that in the soil B.

Figures 4.5c and 4.6c are results obtained for the rainfall intensity equals to the infiltration capacity at of the soils at their saturated state. Vanishing of the negative pore water pressure at the shallow depth is taking place since the start of rainfall. As such, the sharp drop of safety factor is encountered since the rainfall start as revealed in Figure 4.4.

4.5.2   Safety factor characteristics of a slope subjected to a certain period of rainfall

In this section, the results obtained from the 78 cases of the numerical experiments with the rainfall period of 24 hour. Figure 4.7 presents the time series of *FS* of the slope subjected to various intensity of 24 hours rainfall duration. Figure 4.7a is for the lowest permeability soil (the soil A). The *FS* successively decrease during the rainfall period. The decrease of *FS* lasts even after the rain had stopped. This reduction of *FS* after the rain had stopped is according to the inertia of rain water infiltration. However, the *FS* gradually increases afterward. The rate of reduction in the *FS* is accelerated by the rainfall intensity. The maximum rate of reduction in *FS* occurs when the rainfall intensity is greater or equal to 3.6 mm/hr which is the infiltration capacity of the soil A at saturation state.

Figures 4.7(b) and (c) present the time series of *FS* for the intermediate (soil B) and the high (soil C) permeability soils, respectively. For light rainfall intensity, the *FS* characteristic of these soil types is similar to that of the soil A. However, for the heavy rainfall intensity, slope failure is encountered during the rainfall period. These results confirms previous studies (Brand 1984; Rahardjo et al. 2007) which reported that the short heavy rainfall intensity might trigger slope failure in intermediate and high permeability soils. It is found again that the maximum rate of reduction in *FS* takes place when the rainfall intensity is greater or equal to the infiltration capacity of the soil at saturation state.

Figure 4.8 presents the variation of *FS* for three slope angles ($\beta = 20^\circ$, 30°, and 40°). As expected, the greater magnitude of slope angle yields the lower value of initial *FS*. Regardless of the magnitude of *FS*, the variations of *FS* of each soil at -
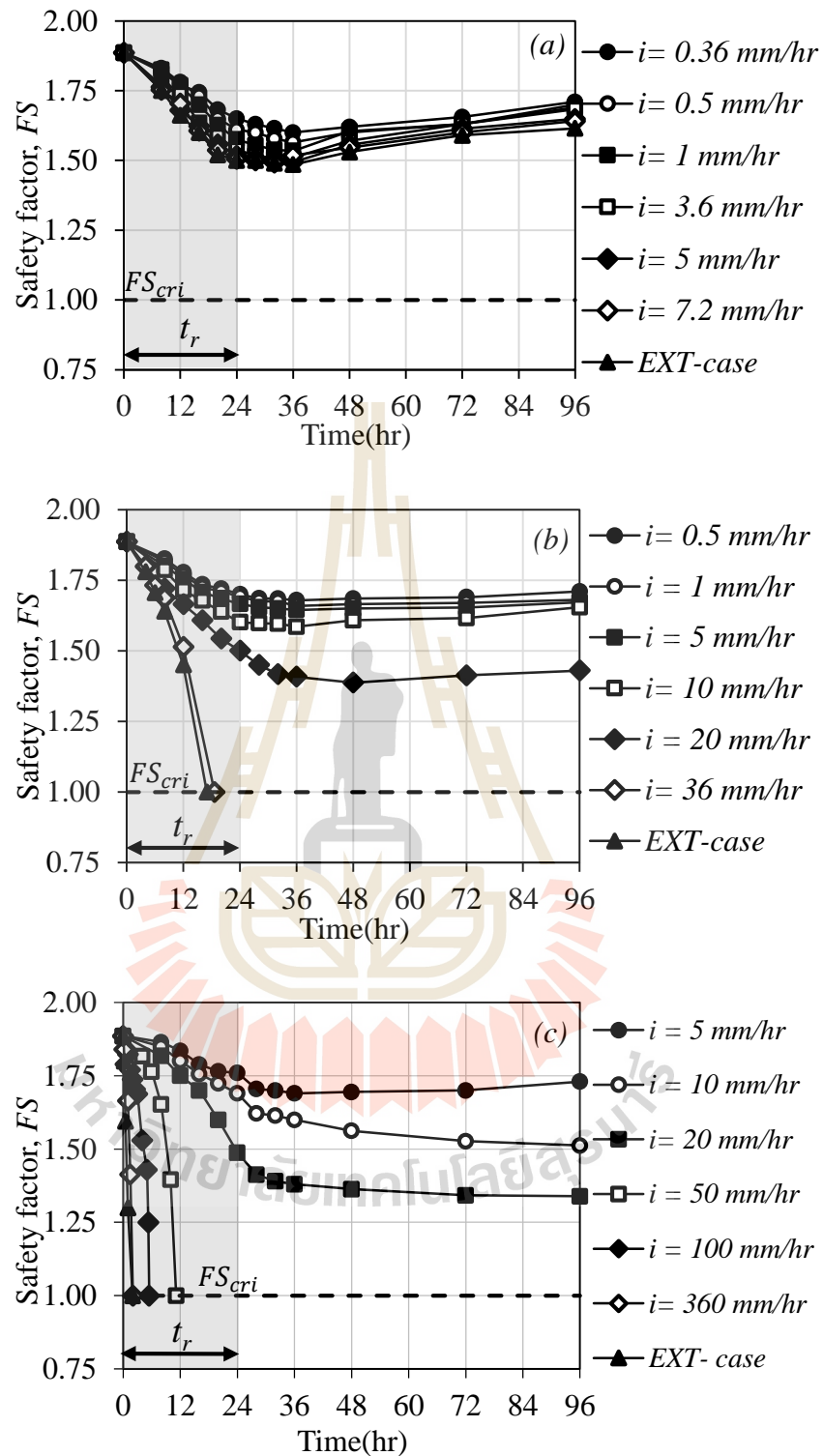
Figure 4.7 Characteristic of safety factor with simulated time under constant rainfall

intensity (a) soil A, (b) soil B and (c) soil C
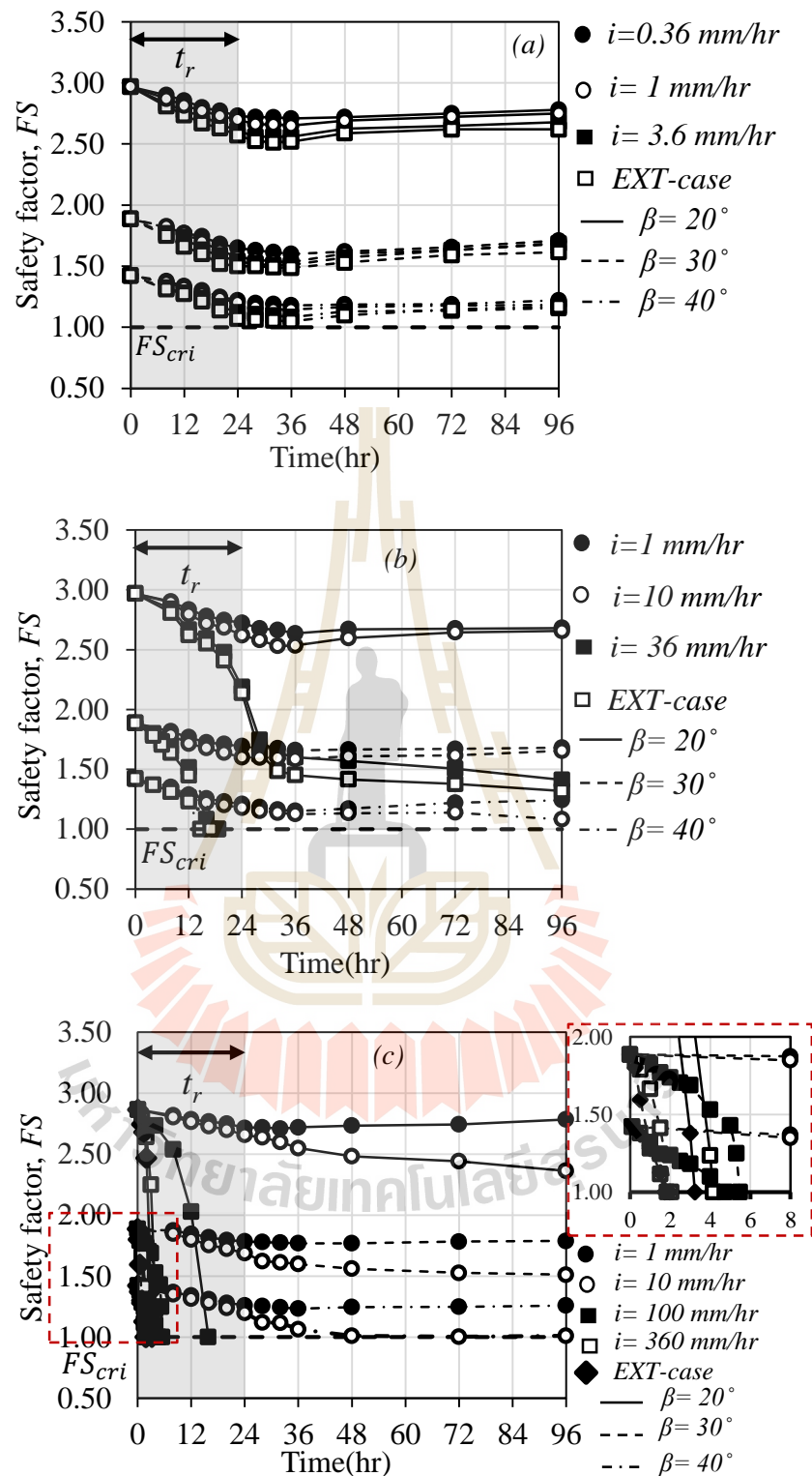
Figure 4.8 Characteristic of safety factor with simulated time under different rainfall intensities (i) and three slope angle (β), (a) soil A, (b) soil B and (c) type C

every slope angles shows a similar trend to each other. For the intermediate

permeability (soil B) and high permeability (soil C) soils, whose *FS* reach the critical

value of 1.0 at the rainfall intensity of greater or equal to the infiltration capacity at their

saturation state, the rate of reduction in *FS* is accelerated by angle of the slope. The

time to the trigger point is hence faster for the steeper slope is according to the lower

initial *FS* and the faster rate of driving force increment which results in faster the rate

reduction in *FS*.

Figure 4.9 present the effect of antecedent rainfall on shallow slope

stability. Results from 18 cases of the cases series III in which the 24 hours period of

rainfall R2 is assigned are shown in Figure 4.9. The maximum rainfall intensity used in

this case series is 10 mm/hr which is significantly lower than 36 mm/hr (the infiltration

capacity at saturated state of the soil B) and/or 360 mm/hr (the infiltration capacity of

saturated state of the soil C). The stability of slope subjected to multiple storm rainfalls

R1 and R2 was monitored. Prior to the rainfall event R2, the antecedent storm rainfall

(t_b) with 2- and 7-day inter-storm period was assigned to this experiment series.

Figures 4.9a, 4.9b, and 4.9c present the variation of *FS* for the cases of

t_b of 2 days in the soils A, B, and C, respectively. As expected, the *FS* in every soil

decreases successively after the rainfall R2 start. In addition, reduction of *FS* after the

end of the rainfall R2 is also observed in every soil, according to the inertia of rain

water. For the intermediated (soil B) and the high (soil C) permeability soils, slope

failure is encountered few hours after the end of rainfall R2 of 10 mm/hr. With this

intermediate rainfall intensity (10 mm/hr), the rain water might infiltrate deeply though

the intermediate and high permeable soils, close to the soil-bedrock interface during the

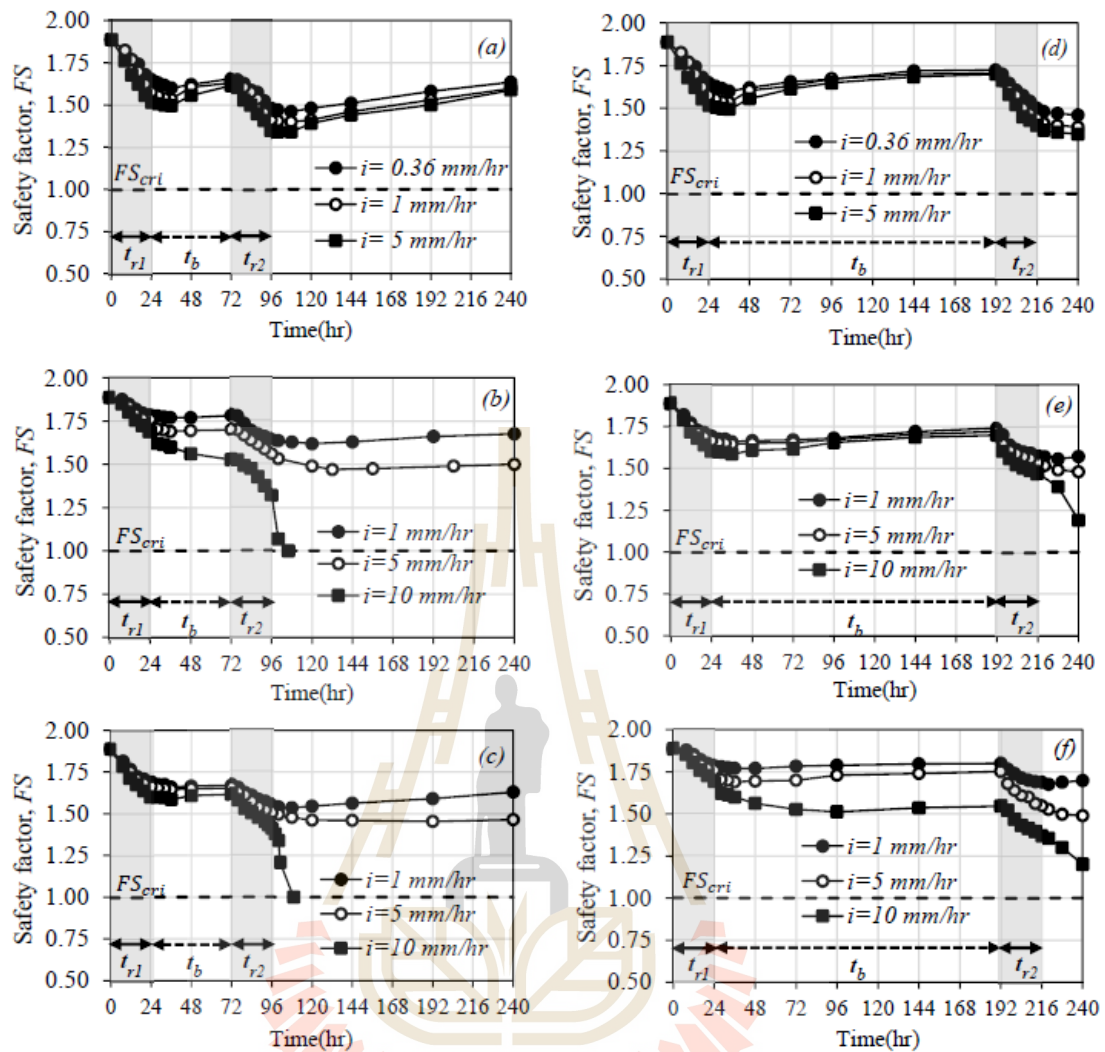period of rainfall. Thereafter, even the rainfall had stopped, the inertia of rain water -

Figure 4.9 Characteristic of safety factor with simulated time under different rainfall intensities (i) and slope angle (β=30°), (a-c) soil A,B,C with 2 storm rainfall (1 day duration) and 2 days inter-storm and (d-f) soil A,B,C with 2 storm rainfall(1 day duration) and 7 days inter-storm

drives the water far enough to reach the soil-bedrock interface, and hence slope failure is triggered. For a given rainfall intensity, the rain water infiltrates through the low permeability soil slower than the rain water does through the high permeability soil. In addition, the driven distance due to the inertia of rain water is shorter in the low

permeable soil than that in the high permeable soil. As such, the *FS* of the low permeable soil (soil A) remains far beyond the critical value of 1.0 throughout the monitored period.

Figures 4.9d, 4.9e, and 4.9f present the variation of *FS* for the case of t_b of 7 days in the soils A, B, and C, respectively. The variation of *FS* is found similar to that of the case of t_b of 2 days. The drop of *FS* after the end of rainfall R2 is still found for the inter-storm period of 7 days. However, slope failure was not encountered within the monitored period. Thus, the shallow slope subjected to the shorter inter-storm period might experience failures soon after the end of the sequential rainfall.

4.5.3 Rainfall intensity-duration thresholds for initiation of shallow slope failure (ID thresholds)

The rainfall intensity-duration thresholds for initiation of slope failure (ID thresholds) which is a relationship between the rainfall intensity (I_f) and rainfall period (T_{rf}) to trigger slope failure is widely used to simply assess the stability of shallow slope (Caine 1980; Calcaterra et al. 2000; Corominas 2000; Crosta and Frattini 2001; Aleotti 2004; Cannon and Gartner 2005; Chien et al. 2005; Guzzetti et al. 2007). Figure 4.10 shows a set of ID thresholds developed from the above mentioned literatures. From these thresholds, a mathematic expression for ID thresholds can be expressed as:

$$I_f = a + cT_{rf}^m \tag{5}$$

where *a*, *c* and *m* are the ID thresholds parameters which represent the curvature, intercept and gradient of ID thresholds, respectively.
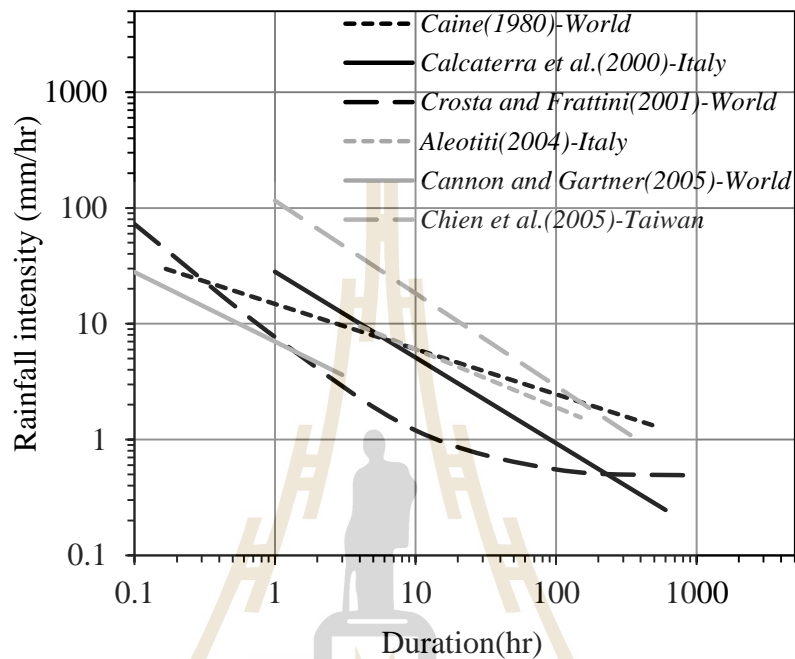
Figure 4.10 ID thresholds for initiation of shallow slope failures proposed by previous researchers

Usually, the magnitude of these model parameters are obtained from regression analysis of the data gathered from previous slope failure events. By this approach, it is not possible to interpret the effect of possible factors triggering rainfall-induced shallow slope failures. This study attempted to examine the influence of the interested factors on the ID thresholds based on physical mechanisms taking place along the rainfall-induced shallow slope failure. All failure cases from 156 cases in the numerical experiment were used to establish the ID thresholds presented in this section.
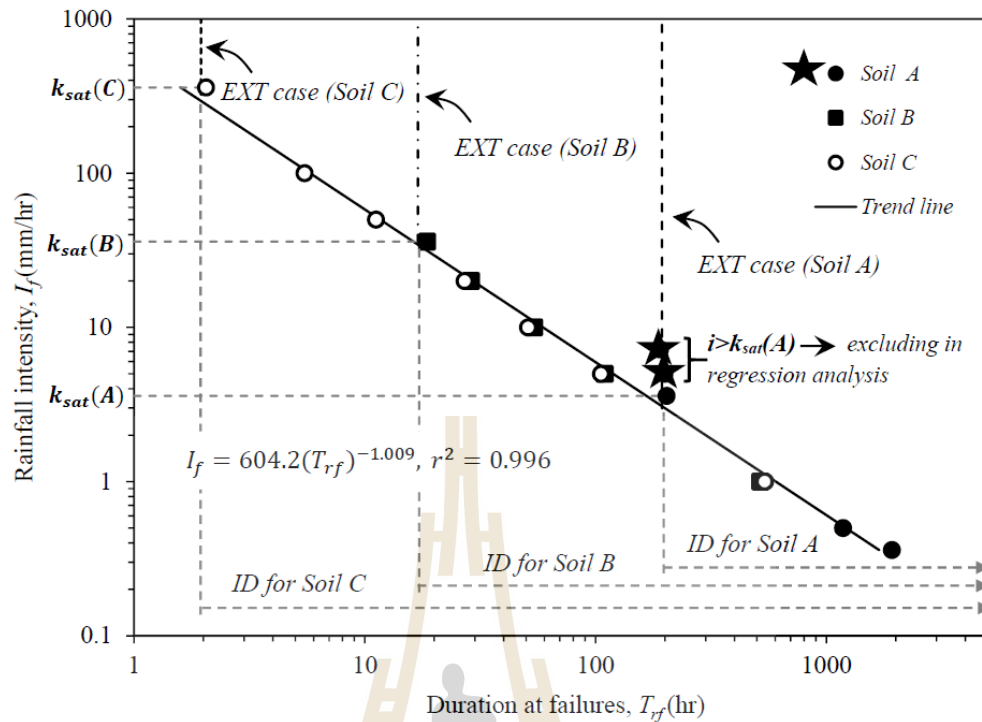
Figure 4.11 ID thresholds based on Soil A, Soil B and Soil C with varying rainfall intensities, β=30°, non-stop rainfall

Figure 4.11 shows the ID thresholds for various type of soils (in term of their saturated permeability) with the slope angle of 30°. The coordinates (I_f, T_{rf}) lay on a single linear line on log-log scale regardless of the magnitude of saturated permeability. The T_{rf} decreases with increasing the rainfall intensity. However, the T_{rf} does not decrease if rainfall intensity increases beyond the infiltration capacity at saturated state of the corresponding soils (shown as black star symbols for the rainfall intensity of greater than the infiltration capacity at soil saturated state and as vertical dashed line for the extreme rainfall condition). According to the Green and Ampt model (Green and Ampt 1911), if rainfall intensity is greater than the infiltration capacity of the soil at saturation, the final rate of infiltrated rainwater is equal to the infiltration

capacity at the soil saturation state. And the infiltration excess of rainwater is formed as the surface runoff. In the other words, the T_{rf} decreases with increasing the rainfall intensity if the rainfall intensity is not greater than the infiltration capacity of the soil at saturation. Therefore, the maximum rainfall intensity, which the relationship between I_f and T_{rf} obeys the ID thresholds, is governed by soil types in term of their saturated permeability.
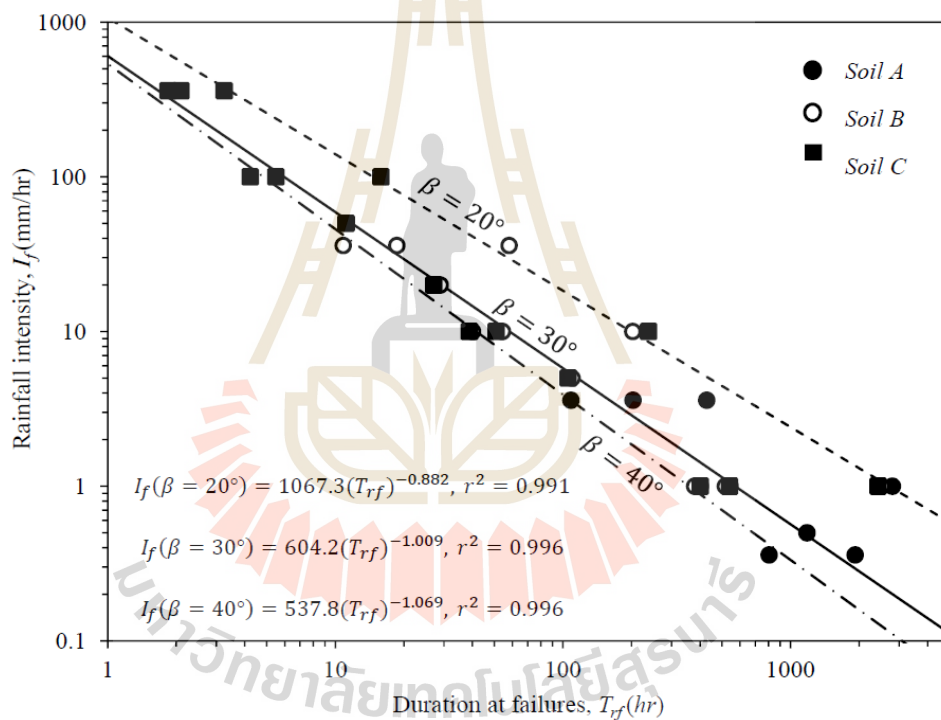
Figure 4.12 ID thresholds based on slope angle 20, 30 and 40° with varying rainfall intensities, Soil A, B and C, non-stop rainfall

Figure 4.12 presents the effect of slope angle on the time-intensity of rainfall at the failures state. The absolute value of ID thresholds parameter *m* slightly increases with increasing slope angle. In the other word, the steepness of the ID thres-
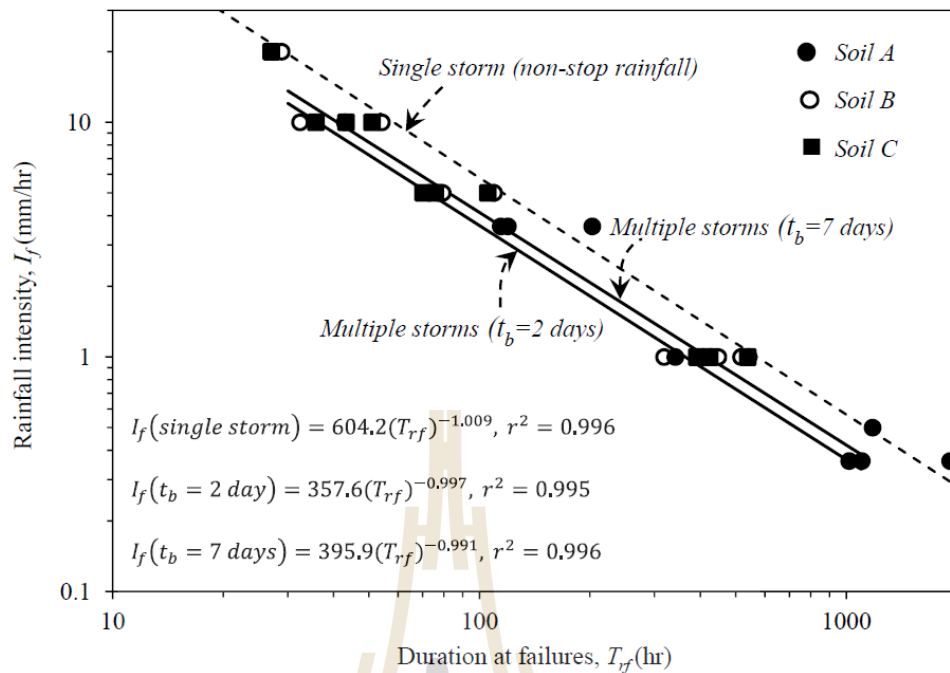
Figure 4.13 ID thresholds based on 2 types of antecedent rainfall (t_b=2 and 7 days)

with varying rainfall intensities, β=30°, Soil A, B and C

holds increases with increasing slope angle. Moreover, the ID threshold parameter, c, which represents the rainfall intensity required to trigger the slope failure at a unit time of rainfall, clearly decreases with increasing slope angle. The drop of the ID threshold parameter c with increasing slope angle is due to the lower initial FS for the greater slope angle. The increment of the ID threshold parameter m with increasing slope angle implies that the time to failure is faster for the steeper slope. Chinkulkijniwat et al. (2016) investigated the depth of failure plane in cohesionless soil slope subjected to continuous rainfall. For the soil slope of greater than the soil frictional angle itself, they found that the greater slope angle results in the shallower depth of failure plane, and hence the faster the time to failure. In total, the time to slope failure is accelerated by

the slope angle. Under a specific rainfall intensity, the higher slope angle results in the shorter T_{rf}.

Figure 4.13 presents the effect of antecedent rainfall on the ID thresholds. Prior to the continuous rainfall R3, the slope is subjected to 24 hours of the rainfall R1 followed by between-storm period t_b of 2 days or 7 days. The ID thresholds parameter m remains almost constant regardless the magnitude of t_b, but the parameter c increases with increasing the magnitude of t_b. The drop of the ID threshold parameter c with decreasing t_b is due to the lower of initial FS for the shorter t_b. As shown in Figure 4.9 that the shorter t_b results in the lower initail FS prior to the subsequent rainfall. Under the same rainfall intensity, the T_{rf} decreases with decreasing t_b from that of 7 days to that of 2 days. In the other word, the faster slope failure is found for the slope subjected to the shorter between-storm period t_b.

4.6   Conclusions

A series of parametric studies were performed through a fully coupled flow-deformation analysis using a finite element analysis. The numerical experiment was conducted under two different conditions: 1) the slope was subjected to a certain rainfall intensity for a specified period and 2) the slope was subjected to a certain rainfall intensity continuously until the initiation of slope failure. The following conclusions can be made on this research study:

1)   Under a certain slope geometry, shallow slope failure can be triggered either under the rainfall infiltration or under the rising of water table

modes depending on the soil saturated permeability and rainfall intensity. The soil saturated permeability is one of the critical factors controlling the range of rainfall intensity on which the mode of water flow at the slope failure depending on. For the rainfall intensity of lower than the infiltration capacity at saturated state, the slope is possibly stable during infiltration stage because of the remaining matric suction, hence the slope failure is possible found during the rising of water table. For rainfall intensity of equal or greater than the infiltration capacity at saturated state, matric suction will completely disappear during infiltration stage, and hence the slope failure is possibly found during the infiltration state.

2) The magnitude of the soil saturated permeability plays an important role on a characteristic of the shallow slope stability. The rate of reduction in *FS* increases with increasing rainfall intensity and reaches the maximum rate at the rainfall intensity equal to the infiltration capacity at saturated state of the soil. Moreover, for the high permeable soil, the slope failure might be triggered by the high intensity and short duration rainfall.

3) The steepness of slope and antecedent rainfall also affect stability of shallow slope. The initial *FS* is governed by the slope angle and the antecedent rainfall. The steeper slope opposes the smaller magnitude of the initial *FS* and the subsequent failure might be triggered more easily. The initial *FS* decreases with decreasing inter-storm period, and causes the lower initial *FS* and an easier arrival of the failure.

4)   As the slope angle and the antecedent rainfall affect the initial stability of the shallow slope, both factors directly affect ID thresholds parameter *c* which indicate the intensity of rainfall to trigger the slope failure at a unit time of rainfall. In addition, the time to slope failure is accelerated by the slope angle. This fact reflects the ID thresholds parameter *m* as its absolute value increases with increasing the slope angle.

5)   The maximum rainfall intensity, which the relationship between I_f and T_{rf} obeys the ID thresholds, is governed by soil types in term of their saturated permeability. In addition, the soil saturated permeability can be used to categorize the modes of disaster. The high permeability soil subjected to high rainfall intensity might lead to rapid slope failure. While, this magnitude of rainfall intensity might result in an infiltration excess rainwater (formed as the surface runoff) and a sequential slope failure in the low saturated permeability soil.

4.7   References

Aleotti P. 2004. **A warning system for rainfall-induced shallow failures.** Engineering Geology 73(3-4):247-265.

Bishop AW, and Blight GE. 1963. **Some aspects of effective stress in saturated and partly saturated soils.** Géotechnique 13(2):177-197.

Bordoni M, Meisina C, Valentino R, Bittelli M, and Chersich, S. 2015. **Site-specific to local-scale shallow landslides triggering zones assessment using TRIGRS.** Natural Hazards Earth System Sciences 15(5):1025-1050.

Brand EW. 1984. **State-of-the-art report of landslides in Southeast Asian.** 4th Int. Symp. on Landslides, Toronto, Canada, 1, 377-384.

Brinkgreve RBJ, Swolf WM, and Engin E. 2010. **Plaxis: Users manual**. Plaxis bv, Delft, Netherlands.

Cai F, and Ugai K. 2004. **Numerical analysis of rainfall effect on slope stability. International Journal of Geomechanics** 4(2):69-78.

Caine N. 1980. **The rainfall intensity-duration control of shallow landslides and debris flows.** Geografiska Annaler Series A-physical Geography:62:23-27.

Calcaterra D, Parise M, Palma B, and Pelella L. 2000. **The influence of meteoric events in triggering shallow landslides in pyroclastic deposits of Campania.** Proc. 8th Int. Symp. on Landslides, (Bromhead E, Dixon N, Ibsen ML, eds) Cardiff: AA Balkema 1:209-214.

Cannon SH, and Gartner JE. 2005. **Wildfire-related debris flow from a hazards perspective.** In: Debris flow Hazards and Related Phenomena (Jakob M, Hungr O, eds). Springer Berlin Heidelberg, 363-385.

Chien YC, Tien CC, Fan CY, Wen CY, and Chun CT. 2005. **Rainfall duration and debrisflow initiated studies for real-time monitoring.** Environmental Geology:47, 715-724.

Chinkulkijniwat A, Yubonchit S, Horpibulsuk S, Jothityangkoon C, Jeebtaku C, and Arulrajah A. 2016. **Hydrological responses and stability analysis of shallow slopes with cohesionless soil subjected to continuous rainfall.** Canadian Geotechnical Journal, http://dx.doi.org/10.1139/cgj-2016-0143.

Corominas J. 2000. **Landslides and climate.** Keynote lecture- In: Proc. 8th Int. Symp. on Landslides, (Bromhead E, Dixon N, Ibsen ML, eds) Cardiff: AA Balkema, 4:1-33.

Crosta GB, and Frattini P. 2001. **Rainfall thresholds for triggering soil slips and debris flow.** In: Proc. 2nd EGS Plinius Conference on Mediterranean Storms (Mugnai A, Guzzetti F, Roth G, eds) Siena, 463–487.

Dahal RK, Hasegawa S, Nonomura A, Yamanaka M, Masuda T, and Nishino K. 2008. **Failure characteristics of rainfall-induced shallow landslides in granitic terrains of Shikoku Island of Japan.** Environmental Geology 56(7):1295-1310.

Dingman SL. 2002. **Physical Hydrology.** Prentice Hall, NJ, USA.

Godt JW, and McKenna JP. 2008. **Numerical modeling of rainfall thresholds for shallow landsliding in the Seattle, Washington, area.** Review in Engineering Geology 20:121-136.

Green WH, and Ampt CA. 1911. **Studies on soil physics: flow of air and water through soils.** Journal of Agricultural Sciences, 4, 1-24.

Griffiths DV, Huang J, and de Wolfe GF. 2011. **Numerical and analytical observations on long and infinite slopes.** International Journal for Numerical and Analytical Methods in Geomechanics 35:569–585.

Griffiths DV, and Lane PA. 1999. **Slope stability analysis by finite elements.** Geotechnique 49(3):387-403.

Griffiths, D. V., and Lu, N. (2005). **Unsaturated slope stability analysis with steady infiltration or evaporation using elasto-plastic finite elements.** International Journal for Numerical and Analytical Methods in Geomechanics 29(3):249-267.

Guzzetti F, Peruccacci S, Rossi M, and Stark CP. 2007. **Rainfall thresholds for the initiation of landslides in central and southern Europe.** Meteorology and Atmospheric Physics 98: 239-267.

Hamdhan IN, and Schweiger HF. 2013. **Finite Element Method–Based Analysis of an Unsaturated Soil Slope Subjected to Rainfall Infiltration.** International Journal Geomechanics 13(5):653-658.

Jotisankasa A, and Vathananukij H. 2008. **Investigation of soil moisture characteristics of landslide-prone slopes in Thailand.** Proc. of Int. Conf. on Management of Landslide Hazard in the Asia-Pacific Region, Sendai Japan, 1-12.

Jotisankasa A, and Mairaing W. 2010. **Suction-Monitored Direct Shear Testing of Residual Soils from Landslide-Prone Areas.** Journal of Geotechnical and Geoenvironmental Engineering 136(3): 533-537.

Keefer DK, Wilson RC, Mark RK, Brabb EE, Brown WM-I, Ellen SD, Harp EL, Wieczorek GF, Alger CS, and Zatkin R. S. 1987. **Real-time landslide warning during heavy rainfall.** Science 238:921-925.

Khalilnejad A, Ali F, Hashim R, and Osman N. 2013. **Finite-element simulation for contribution of matric suction and friction angle to stress distribution during pulling-out process.** International Journal Geomechanics DOI:10.1061/(ASCE)GM.1943-5622.0000243:527-532.

Li WC, Lee LM, Cai H, Li HJ, Dai FC, and Wang ML. 2013. **Combined roles of saturated permeability and rainfall characteristics on surficial failure of homogeneous soil slope.** Engineering Geology 153:105-113.

Lu N, and Griffiths DV. 2004. **Profiles of Steady-State Suction Stress in Unsaturated Soils.** Journal of Geotechnical and Geoenvironmental Engineering 130(10):1063-1076.

Lu N, and Likos WJ. 2006. **Suction Stress Characteristic Curve for Unsaturated Soil.** Journal of Geotechnical and Geoenvironmental Engineering 132(2):131-142.

Lu N, and Godt J. 2008. **Infinite slope stability under steady unsaturated seepage conditions.** Water Resources Research 44(11):1-13.

Meyer PD, and Gee GW. 1999. **Flux-based estimation of field capacity.** Journal of Geotechnical and Geoenvironmental Engineering 125(7):595-599.

Mualem Y. 1976. **A new model predicting the hydraulic conductivity of unsaturated porous media.** Water Resources Research 12:513-522.

Ng CWW, and Shi Q. 1998. **Influence of rainfall intensity and duration on slope stability in unsaturated soils.** Quarterly Journal of Engineering Geology and Hydrogeology 31(2):105-113.

Oh S, and Lu N. 2015. **Slope stability analysis under unsaturated conditions: Case studies of rainfall-induced failure of cut slopes.** Engineering Geology 184:96-103.

Rahardjo H, Ong TH, Rezaur RB, and Leong EC. 2007. **Factors controlling instability of homogeneous soil slopes under rainfall.** Geotechnical and Geoenvironmental Engineering 133(12):1532-1543.

Rahardjo H, Nio AS, Leong EC, and Song NY. 2010. **Effects of Groundwater Table Position and Soil Properties on Stability of Slope during Rainfall.** Journal of Geotechnical and Geoenvironmental Engineering 136(11):1555-1564.

Rahimi A, Rahardjo H, and Leong EC. 2010. **Effect of hydraulic properties of soil on rainfall-induced slope failure.** Engineering Geology 114(3-4):135-143.

Richards LA. 1931. **Capillary conduction of liquids through porous mediums.** Physics 1(5):318-333.

Shen S–L, Wang J–P, Wu H–N, Xu Y–S, Ye G–L, and Yin Z-Y. 2015. **Evaluation of hydraulic conductivity for both marine and deltaic deposits based on piezocone testing.** Ocean Engineering 110:174-182.

Shen S–L, Wu H–N, Cui Y–J., and Yin Z-Y. 2014. **Long-term settlement behaviour of metro tunnels in the soft deposits of Shanghai.** Tunnelling and Underground Space Technology 40:309-323.

Shen S–L, and XuY-S. 2011. **Numerical evaluation of land subsidence induced by groundwater pumping in Shanghai.** Canadian Geotechnical Journal 48(9):1378-1392.

Sirangelo B, and Braca G. 2004. **Identification of hazard conditions for mudflow occurrence by hydrological model. Application of FLaIR model to Sarno warning system.** Engineering Geology 73:267-276.

Soil Science Glossary Terms Committee. 2008. **Glossary of Soil Science Terms 2008.** Madison: SSSA, pp. 92.

Tiwari RC, Bhandary NP, and Yatabe R. 2014. **Spectral element analysis to evaluate the stability of long and steep slopes.** Acta Geotechnica 9:753–770.

Ugai K. 1989. **A method of calculation of total factor of safety of slopes by elasto-plastic FEM.** Soils and Foundations 29(2):190-195.

Vahedifard F, Leshchinsky D, Mortezaei K, and Lu N. 2016. **Effective stress-based limit-Equilibrium analysis for homogeneous unsaturated slopes.** International Journal of Geomechanics D4016003 http://dx.doi.org/10.1061/ (ASCE)GM.19435622.0000554.

Van Genuchten MT. 1980. **A closed-form equation for predicting the hydraulic conductivity of unsaturated soil.** Soil Science Society of America Journal 44:615–628.

Vieira BC, Fernandes NF, and Filho OA. 2010. **Shallow landslide prediction in the Serra do Mar, São Paulo, Brazil.** Natural Hazards and Earth System Sciences 10(9):1829-1837.

Wilson RC, Mark RK., and Barbato G. 1993. **Operation of a real-time warning system for debris flows in the San Francisco Bay area, California.** Int. Conf. Hydraulics Division, ASCE 2, 1908-1913.

Wu Y–X, Shen S–L, Xu Y–S, and Yin Z-Y. 2015a. **Characteristics of groundwater seepage with cut-off wall in gravel aquifer. I: Field observations1.** Canadian Geotechnical Journal 52(10):1526-1538.

Wu Y–X, Shen S–L, Yin Z–Y, and Xu Y-S. 2015b. **Characteristics of groundwater seepage with cut-off wall in gravel aquifer. II: Numerical analysis1.** Canadian Geotechnical Journal 52(10):1539-1549.

Xu Y–S, Ma L, Shen S–L, and Sun W-J. 2012. **Evaluation of land subsidence by considering underground structures that penetrate the aquifers of Shanghai, China.** Hydrogeology Journal 20(8):1623-1634.

Xu Y–S, Shen S–L, and Du Y-J. 2009. **Geological and hydrogeological environment in Shanghai with geohazards to construction and maintenance of infrastructures.** Engineering Geolology 109(3-4):241-2.

CHAPTER V

CONCLUSIONS AND RECOMMENDATIONS

5.1 Summary and conclusions

This thesis consists of two main parts. First part is to obtain comprehensive understanding of hydro-mechanical responses within shallow soil slope leading to primary framwork for quantifying critical locations, which is useful for early warning system based on monitoring device installations. A series of experiments were undertaken in this part to evaluate the hydrological responses of shallow soil slopes of varying steepness and when subjected to varying intensities, periods, and inter-storm periods of rainfall. An analysis of infinite slopes were also undertaken to develop a fundamental understanding of rainfall-induced shallow landslide characteristics. Second objective of this thesis is to exemine factors influencing rainfall-induced shallow landslides and the critical rainfall thresholds (ID thresholds) used for early warning system. A sets of parametric study performed via finite element modeling to investigate the effect of saturated permeability of soil, slope angle and antecedent rainfall on instability of a shallow slope.

5.5.1 Hydrological Responses and Failure Characteristics of Shallow Soil Slope Subjected to Rainfall

The experimental results showed that the hydrological and physical responses within shallow soil slope subjected to rainfall were characterized in the

infiltration and saturation phases. During the infiltration phase, the maximum magnitude of water content was found behind the wetting front, termed as the water content behind the wetting front (θ_{wb}). For a certain soil type, the magnitude of θ_{wb} was found to be dependent on the magnitude of rainfall intensity, regardless of the slope gradient and initial water content. Based on the relative depth of the failure plane, the failure can be categorized by three prime modes: 1) along the impervious layer mode, 2) shallow depth mode, and 3) transitional mode. These modes can be characterized by the magnitude of a stability index termed as $\tan\varphi'/\tan\beta$ ratio. An infiltration index, termed as i/k_s ratio, was found to play a role in the depth of failure plane only for the transitional mode.

5.5.2 Factors Influencing Rainfall-Induced Shallow Slope Failures

Factors influencing rainfall-induced shallow landslides and the critical rainfall thresholds (ID thresholds) were examined via finite element method. The numerical results showed that the rate of reduction in safety factor (*FS*) increases with an increasing the intensity of rainfall, only in a range of lower than the infiltration capacity at soil saturated state. As such the saturated permeability of the soil, which is equal to the infiltration capacity at soil saturated state, plays an important role in the shallow slope failure. The saturated permeability was found also to govern a range of applicability of ID thresholds. If the rainfall intensity is not greater than the infiltration capacity at soil saturated state, the rainfall duration to failure (T_{rf}) can be read from the ID thresholds. Slope angle and antecedent rainfall were found to play significant roles on instability of shallow slopes, as they control the initial stability of slope, which results in the different

linear relationship of ID thresholds. In addition, the slope angle might accelerate the rate of rain water infiltration, and hence it reflects the slope of the ID thresholds.

5.2   Limitations and recommendations for future works

- Sandy soil was only used for conducting laboratory experiments, difference of soil properties in term of their hydrological properties might affect hydrological responses and instability of shallow soil slope subjected to rainfall.

- Slope stability analysis based on infinite slope concept was focused on cohesionless soil, the analysis on cohesion soil must be taken into account in further study.

- Another environment factors especially for plant root system must be considered on both laboratory investigation and slope stability analysis, to get comprehensive thresholds for early warning system based on monitoring device installations.

- The ID thresholds proposed in this thesis only used to study influence factors on initiation of rainfall-induced shallow slope failures. For using as an early warning system, variations of soil properties, slope geometries, rainfall conditions and vegetation covers in concerned areas must be considered in numerical analysis.

- In this study, the failure planes (in Chapter III) and ID thresholds (in Chapter IV) were assessed via the analytical and numerical slope stability analyses in which the failure states were only defined by the safety factor of 1.0. Therefore, soil mass movements in natural shallow soil slopes after the failure states have not been examined in this study yet. Different types of the mass movements, depending on other relevant factors, such as creep (slow movement), sliding, slump, avalanches, mudflows and debris flows might affect the waning time to people living nearby hazardous areas, which need to be examined in future works.

APPENDIX A
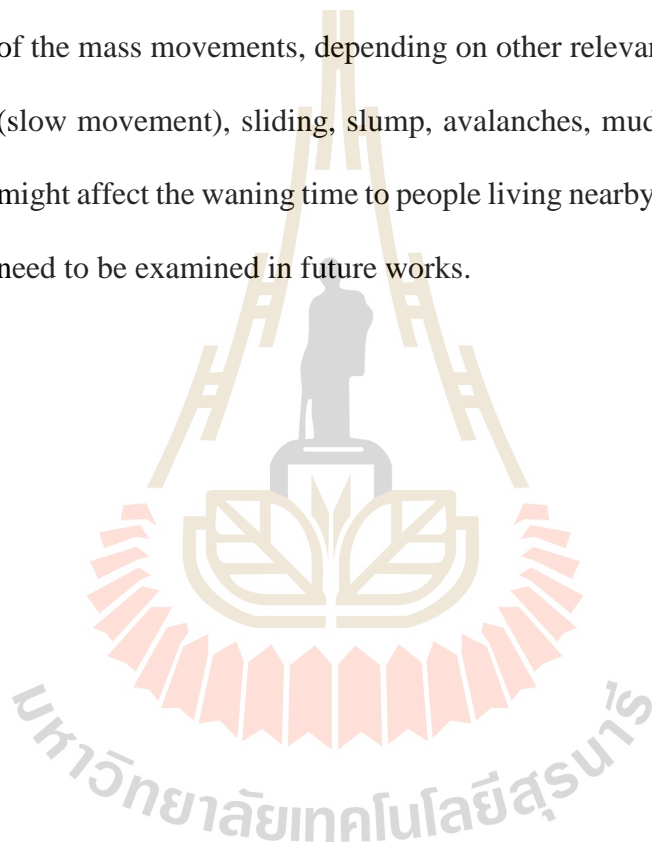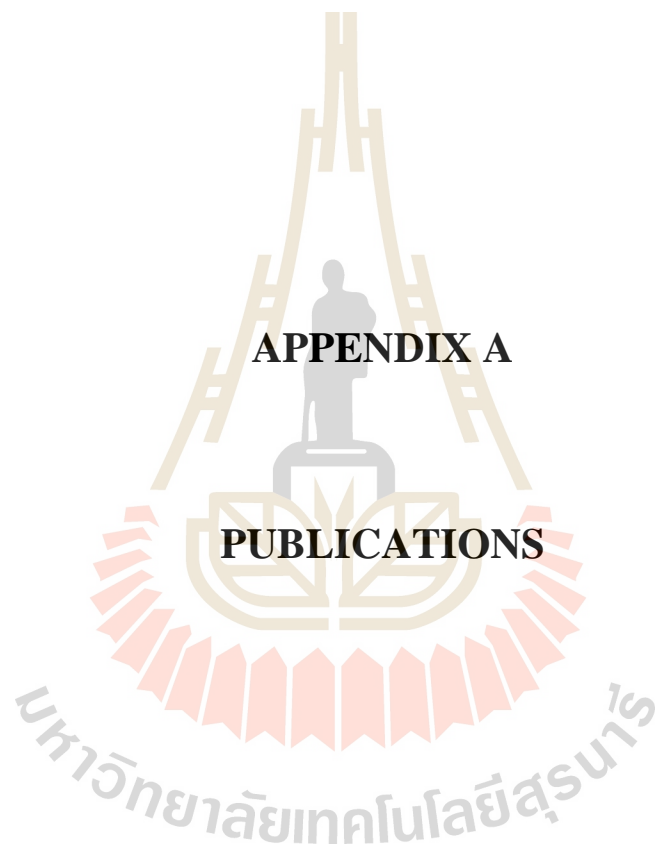
PUBLICATIONS

List of Publications

INTERNATIONAL JOURNAL PAPERS

Chinkulkijniwat A., Yubonchit S., Horpibulsuk S., Jothityangkoon C., Jeeptaku C., and Arulrajah A. **Hydrological responses and stability analysis of shallow slopes with cohesionless soil subjected to continuous rainfall**. Canadian Geotechnical Journal, 53(12):2001-2013.

Yubonchit S., Chinkulkijniwat A., Horpibulsuk S., Jothityangkoon C., Arulrajah A., Suddeepong A. **Influence factors involving rainfall-induced shallow slope failure: numerical study**. International Journal of Geomechanics, doi:10.1061/(ASCE)GM.1943-5622.0000865, accepted on 20 October 2016.

INTERNATIONAL CONFERENCES

Jeeptaku C., Chinkulkijniwat A., and Yubonchit S. **Effect of rainfall intensity on internal moisture content in shallow slope with high permeable soil.** International Conference on Advances in Civil Engineering for Sustainable Development, Nakhon Ratchasima, Thailand, 27-29 August 2014.

Chinkulkijniwat A., and Yubonchit S. **Influence of periodical rainfall on shallow slope failures based on finite element analysis.** 12th International Symposium on Landslides, Napoli, Italy, 12-19 June 2016.

Chinkulkijniwat A., Yubonchit S., Goodary R., and Bui DV. **Effect of periodical rainfall on shallow slope failures: Finite element analysis.** GEOMATE, Bangkok, Thailand, 14-16 November 2016.

ARTICLE

Hydrological responses and stability analysis of shallow slopes with cohesionless soil subjected to continuous rainfall

Avirut Chinkulkijniwat, Somjai Yubonchit, Suksun Horpibulsuk, Chatchai Jothityangkoon, Cholticha Jeeptaku, and Arul Arulrajah

Abstract: Understanding the hydrological and physical responses of shallow slopes subject to rainfall events is vital for the efficiency of a warning system setup. In this research, a series of experiments were undertaken to evaluate the hydrological responses of shallow slopes of varying steepness and when subjected to varying intensities, periods, and inter-storm periods of rainfall. An analysis of infinite slopes was also undertaken to develop a fundamental understanding of rainfall-induced shallow slope failure characteristics. The hydrological and physical responses were characterized in the infiltration and saturation phases. During the infiltration phase, the maximum magnitude of water content was found behind the wetting front, termed as the water content behind the wetting front (θ_{wb}). For a certain soil type, the magnitude of θ_{wb} was found to be dependent on the magnitude of rainfall intensity, regardless of the slope gradient and initial water content. Based on the relative depth of the failure plane, the failure can be categorized by three prime modes: (i) along the impervious layer mode, (ii) shallow depth mode, and (iii) transitional mode. These modes can be characterized by the magnitude of a stability index termed as $\tan\varphi'/\tan\beta$ ratio. An infiltration index, termed as i/k_s ratio, was found to play a role in the depth of the failure plane only for the transitional mode.

Key words: rainfall infiltration, stability analysis, infinite slope, stability index, infiltration index.

Résumé : Comprendre les réponses hydrologiques et physiques des pentes douces sous réserve des épisodes de pluviosité est vital pour l'efficacité d'un programme d'installation de système d'alerte. Dans cette recherche, une série d'expérimentations ont été réalisées pour évaluer les réponses hydrologiques des pentes douces à cambrure variant et lorsqu'ils sont soumis à des précipitations à des intensités, périodes variables et à des périodes d'intertempêtes variables. Une analyse de pentes infinies a également été entreprise pour développer une compréhension fondamentale des caractéristiques de défaillance de pente douce induites par des précipitations. Les réponses hydrologiques et physiques ont été caractérisées dans les phases d'infiltration et de saturation. Pendant la phase d'infiltration, l'amplitude maximale de la teneur en eau se trouve derrière le front d'humectation, appelée la teneur en eau derrière le front d'humectation (θ_{wb}). Pour un certain type de sol, l'amplitude de θ_{wb} a été trouvée à être dépendante de l'amplitude de l'intensité des précipitations, quel que soit le gradient de la pente et la teneur en eau initiale. Sur la base de la profondeur relative du plan d'échec, l'échec peut être classé par trois modes principaux : (i) le long du mode de la couche imperméable, (ii) le mode de faible profondeur, et (iii) le mode de transition. Ces modes peuvent être caractérisés par la valeur d'un indice de stabilité désignée par le rapport $\tan\varphi'/\tan\beta$. Un indice d'infiltration, désignée par le rapport i/k_s, a été trouvé à jouer un rôle dans la profondeur du plan de défaillance uniquement pour le mode de transition. [Traduit par la Rédaction]

Mots-clés : infiltration des précipitations, analyse de stabilité, pente infinie, indice de stabilité, indice d'infiltration.

Introduction

Early warning systems are a widely used tool to manage rainfall-induced disasters, including landslides, floods, and debris flows. In general, current early warning systems evaluate the level of disaster risks based on real-time data observations. Common real-time data observations include measurements of the period and intensity of rainfall and comparisons of rainfall intensity with corresponding risk thresholds. The risk thresholds related to rainfall-induced shallow landslides have been proposed by researchers such as Caine (1980), Calcaterra et al. (2000), Corominas (2000), Crosta and Frattini (2001), Aleotti (2004), Cannon and Gartner (2005), Chen et al. (2005), and Guzzetti et al. (2007). These risk thresholds are mostly represented as a relationship between rainfall intensity and the time to failure, named as intensity duration thresholds (ID thresholds). Due to its simplicity and ease of usage, ID thresholds are currently implemented as a part of early warning systems worldwide. However, the ID thresholds approach is empirical based and neglects several critical factors that govern true landslide characteristics, thus making this system not applicable outside the area where the ID thresholds were established. The critical factors currently neglected in the ID thresholds approach are soil hydraulic properties (Pradel and Raad 1993; Rahimi et al. 2010; Ma et al. 2011; Santoso et al. 2011), slope geometries (Cho and Lee 2002; Rahardjo et al. 2007; Cho 2009; Xu et al. 2009; Ali et al. 2014a; Shen

A. Chinkulkijniwat and C. Jothityangkoon. Center of Excellence in Civil Engineering, School of Civil Engineering, Suranaree University of Technology, 111 University Avenue, Muang District, Nakhon Ratchasima 30000, Thailand.
S. Yubonchit. School of Civil Engineering, Suranaree University of Technology, 111 University Avenue, Muang District, Nakhon Ratchasima 30000, Thailand.
S. Horpibulsuk. Center of Excellence in Innovation for Sustainable Infrastructure Development and Chair, School of Civil Engineering, Suranaree University of Technology, 111 University Avenue, Muang District, Nakhon Ratchasima 30000, Thailand.
C. Jeeptaku. CHC Engineering Office, 65/148 Rama 9 Road, Huaykwang, Bangkok 10310, Thailand.
A. Arulrajah. Department of Civil and Construction Engineering, Swinburne University of Technology, Melbourne, Australia.
Corresponding author: Avirut Chinkulkijniwat (email: avirut@sut.ac.th).

et al. 2015), and antecedent rainfall conditions (Rahardjo et al. 2001; Rahimi et al. 2011; Cuomo and Della Sala 2013; Zhan et al. 2013).

An interesting early warning system is the physically based method (Tohari et al. 2007; Greco et al. 2010; Eichenberger et al. 2013). In this method, the warning levels are evaluated via the real-time hydraulic responses read from a set of monitoring devices. The common monitoring devices are moisture sensors, piezometers, and tensiometers. Location of instrumentation is vital for early warning systems to be effective. Few attempts have been made to date on the study of suitable instrumentation locations for effective early warning systems. Tohari et al. (2007) conducted a series of large-scale tests on homogeneous slopes to understand the triggered mechanism of rainfall-induced slope failures and reported that most of the failure planes took place near the slope surface and were triggered by the rise in water table. Consequently, Tohari et al. (2007) suggested that the monitoring devices should be installed close to the slope surface and suggested two levels of warning phases, termed as early warning and final warning. The early warning is initiated when the wetting front moves through the sensor, and the final warning is initiated soon after the wetting front reaches the impervious layer and the water table starts to rise. However, this recommendation is based on a homogeneous soil slope, where the dominant failure mode is a shallow noncircular sliding failure. However, for shallow slopes, where the thickness of the soil slope is thin compared with the length of the slope, the dominant mode of failure is translational sliding failure, which is different from the failure mechanisms reported by Tohari et al. (2007).

Insight into the development of seepage responses on shallow slopes during rainfall period will further enhance the efficiency of physical warning systems. Pradel and Raad (1993), Lee et al. (2009), Li et al. (2013), and Ali et al. (2014b) reported that the increment of pore pressure depends on an infiltration index, termed as a ratio of rainfall intensity (i) to the saturated permeability of the soil (k_s). The higher the infiltration index, the more likely the failure occurs during the period of downward advance of wetting front termed the infiltration phase, and hence the shallower the depth of failure, and vice versa. Though works have been undertaken to study the hydrological responses in shallow slopes due to rainfall, few of the previous attempts have incorporated the angle of slope into consideration. Lee et al. (2011) conducted a set of laboratory experiments on one-dimensional soil columns on an 18° tilted slope model to investigate the hydrological response of four soil types subjected to two magnitudes of rainfall intensity (3.35×10^{-6} and 1.85×10^{-5} m/s) and rainfall period (1 and 24 h). Li et al. (2013) conducted numerical experiments with two computational cases: (i) one-dimensional flow, and (ii) two-dimensional flow with a single slope angle. Although these researchers included the slope angle in their investigations, comparisons were carried out only on the hydrological responses between one-dimensional and two-dimensional flows with single slope angle. There are no known studies to date involving a series of laboratory experiments to evaluate the hydrological responses due to rainfall on shallow slopes, whereby the slope angle is conclusively taken into consideration.

In landslides, there is an interaction between the slope angle and the soil frictional angle (Ma et al. 2011; Eichenberger et al. 2013; Li et al. 2013; Ali et al. 2014b). Li et al. (2013) derived a closed-form solution and presented the interaction between the slope angle and the soil frictional angle on failure mechanisms including the depth of the failure plane. They showed that the slope might fail through either the advance of wetting front or the rise of water table, depending on the magnitudes of soil frictional angle and the slope angle. These varying failure mechanisms might lead to different depths of the failure plane. Though it is realized that knowledge of the location of the failure plane is vital for enhancing the efficiency of the early warning system, no attempt has been devoted to explain the effect of the relevant factors (such as rainfall intensity, slope angle, soil frictional angle, etc.) on the location of the failure plane.

Fig. 1. Analysis of infinite slope subjected to rainfall event.
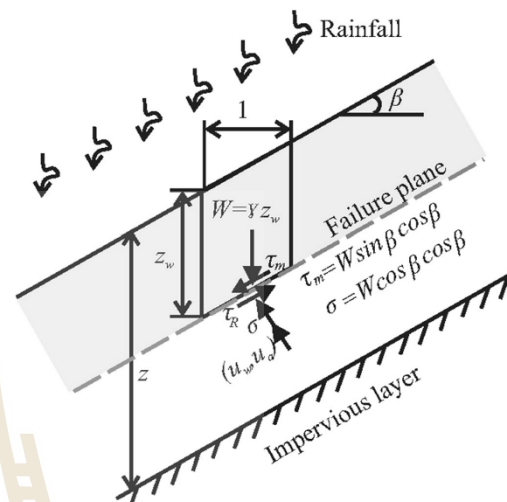
This paper is systematically divided into two parts: (i) laboratory experiments and (ii) stability analysis of the slope. A physical slope model was constructed to evaluate the hydrological responses of soil slopes of varying steepness when subjected to various rainfall intensities and periods. Subsequently, a series of infinite slope analyses was conducted to develop a fundamental understanding of the characteristics of failure planes in shallow slopes when subjected to varying rainfall conditions.

Theoretical background

A limit-equilibrium approach (Skempton and DeLory 1957) is a most common method to assess the stability of infinite slopes when subjected to varying rainfall conditions (Cho and Lee 2002; Tsai et al. 2008; Lu and Godt 2008; Cho 2009; Lee et al. 2009; Ma et al. 2011; Li et al. 2013; Zhan et al. 2013; Zhang et al. 2013; Ali et al. 2014a, 2014b). Figure 1 shows a typical section of infinite slope under rainfall condition. The failure plane is assumed to be parallel to the slope surface. The safety factor (FS) representing slope stability is defined by a term of shear strength (τ_R) over mobilized shear force (τ_M). As natural soil is always not fully saturated, the unsaturated shear strength can be computed based on the Mohr–Coulomb failure criteria for unsaturated soil (Fredlund and Morgenstern 1976; Fredlund et al. 1978; Fredlund and Rahardjo 1993; Vanapalli et al. 1996). In this study, the failure criteria proposed by Lu and Griffiths (2004) and Lu and Likos (2006) was used as

$$(1) \qquad \tau_R = c' + \left[(\sigma - u_a) - \sigma^s \right] \tan\varphi'$$

where c' is effective cohesion, φ' is effective frictional angle, σ is total normal stress, u_a is pore-air pressure, and σ^s is suction stress defined as

$$(2) \qquad \sigma^s = -\frac{\theta_w - \theta_r}{\theta_{sat} - \theta_r}(u_a - u_w) = -S_e(u_a - u_w)$$

where θ_w is volumetric water content; θ_r is residual volumetric water content; θ_{sat} is saturated volumetric water content; a soil suction that is equal to the difference between pore-water pressure and pore-air pressure is expressed as $(u_a - u_w)$; and S_e is the

Fig. 2. Schematic diagram of physical slope model.
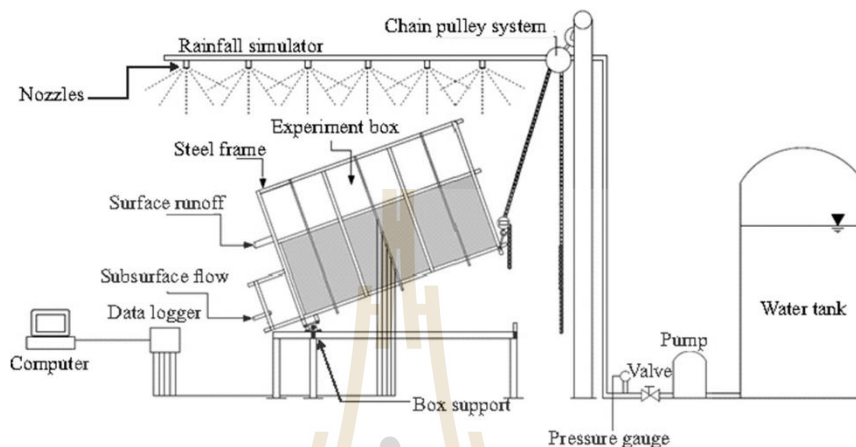
effective degree of saturation. As such, FS of the infinite slope shown in Fig. 1 can be expressed as

$$(3) \quad \text{FS} = \frac{\tau_R}{\tau_M} = \frac{c' + \left[(\sigma - u_a) - \sigma^s\right]\tan\varphi'}{W\sin\beta\cos\beta}$$

where β is the slope angle, and W is the weight of the soil slice. Because $W = \gamma Z_w$, $\sigma = \gamma Z_w \cos^2\beta$, and $u_a = 0$ for atmospheric pressure, eq. (3) can be rewritten as

$$(4) \quad \text{FS} = \frac{c' + \left(\gamma Z_w \cos^2\beta - \sigma^s\right)\tan\varphi'}{\gamma Z_w \sin\beta\cos\beta}$$
$$= \frac{c' - \sigma^s\tan\varphi'}{\gamma Z_w \sin\beta\cos\beta} + \frac{\tan\varphi'}{\tan\beta}$$

where γ is unit weight of soil, Z_w is vertical depth at failure plane.

Equation (4) is used to assess the stability of shallow soil slopes under either saturated or unsaturated soil conditions. However, the hydrological responses due to flow in unsaturated soil subjected to rainfall should be better understood. As such, a series of laboratory experiments to investigate the hydrological responses on shallow slopes subjected to rainfall conditions was carried out in this research.

Materials and methods

Physical model

A schematic diagram and photograph of the physical model are shown in Figs. 2 and 3, respectively. The model consists of four components, including the rainfall simulator, the experiment box, the box supports, and the chain pulley system. The box supports are pin and roller type supports such that the experiment box can be raised one side to a prescribed inclined angle by the chain pulley.

Figure 4 shows details of the experiment box. The dimensions of this box are 1550 mm in length, 1000 mm in height, and 200 mm in width. The sides and bottom base of the box were made from impervious acrylic plates of 15 mm thick. Five of 5 mm diameter holes were vertically drilled at mid of the side boundary to insert the moisture sensor probes (Decagon 5TE, Decagon Devices Inc. (2007–2010)). Three of 9 mm diameter holes were

Fig. 3. Photograph of physical slope model. [Colour online.]

drilled at the bottom of the experiment box at distances of 375 mm (downslope), 750 mm (middle slope), and 1125 mm (upslope). These holes were used to insert the piezometers. To reduce entrapped air that might affect the measurement of the volumetric water content (θ_w), three other holes were drilled nearby the piezometer holes to install the opening valves. At downslope, permeable porous concrete overlaid by geotextile was placed to allow free water outflow at nearly saturated state, and to prevent the clogged soil in porous concrete.

Fig. 4. Details of experiment box: (*a*) side view; (*b*) top view.
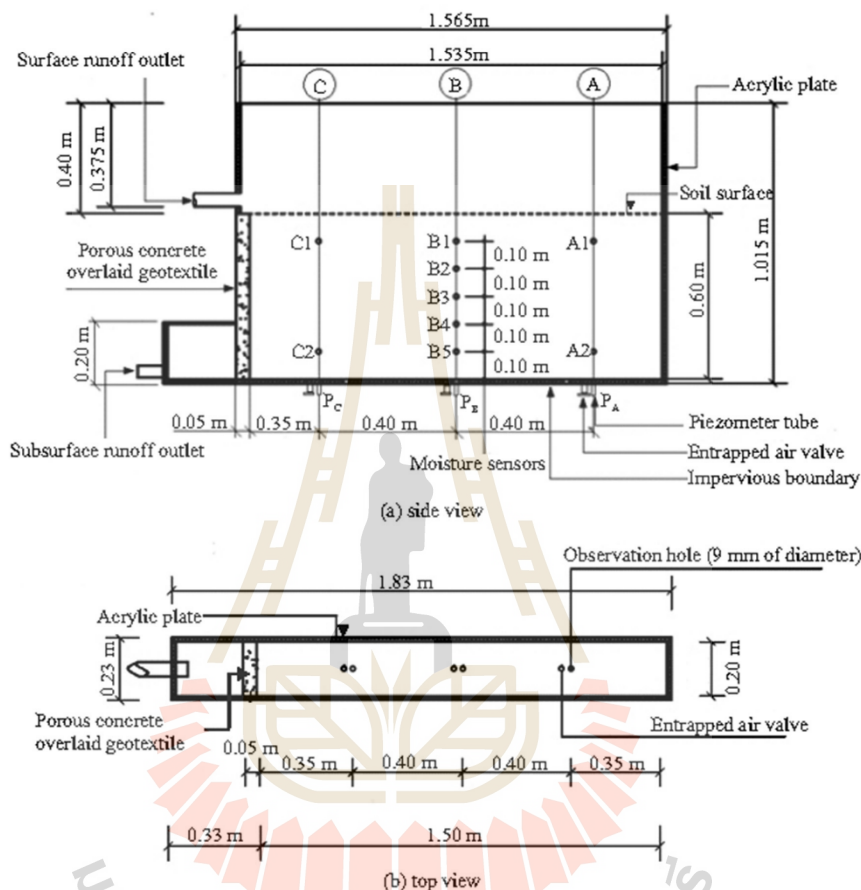
(a) side view

(b) top view

A rainfall simulator was installed above the experiment box. The simulator consists of a water tank, a constant-pressure pump, a pressure gauge, a set of plastic pipes, a set of small opening nozzles, and a set of control valves. The nozzles were placed in four plastic pipes, each with spaces of 300, 450, 600, and 900 mm to reproduce various rainfall intensity. The desired rainfall intensities were assigned to the slope model through the rainfall simulator calibrated with the uniformity coefficients (CU) (Hall et al. (1989)) of greater than 90%.

The calibration was conducted by measuring the volume of water sprayed from the nozzles for 30 min. Thirty-five cups were placed above the slope surface to collect the nozzled water. For each rainfall intensity, CU was determined to verify the uniformity of rainfall distribution. The expression of CU is written as shown in eq. (5).

$$(5) \qquad CU = 1 - \frac{\sum\limits_{i=1}^{n} I_i - I_m}{\sum\limits_{i=1}^{n} I_i}$$

where I_i is measured rainfall intensity for the ith cup, I_m is average rainfall intensity for all cups, and n is total number of cups ($n = 30$).

Materials

A local sandy soil was used in this study to prepare the homogeneous soil slope. This soil is classified as poorly graded sand (SP) according to Unified Soil Classification System (USCS) (ASTM D2487 (ASTM 1991*b*)). Figure 5*a* presents grain-size distribution of the soil. Other soil properties such as the specific gravity of the soil (G_s), the saturated permeability (k_s), the strength parameters (φ', c') are presented in Table 1. The soil-water characteristic (SWC) determined by the pressure plate (ASTM D6836-02 (ASTM 2003)) is shown in Fig. 5*b*. Nonlinear regression was performed to validate the tested data with eq. (6) (van Genuchten 1980). The validated parameters for van Genuchten's model are shown in Table 1.

$$(6) \qquad S_e = \frac{\theta_w - \theta_r}{\theta_{sat} - \theta_r} = \left\{ \frac{1}{1 + [\alpha(u_a - u_w)]^n} \right\}^{1-1/n}$$

Fig. 5. Properties of sandy soil: (*a*) grain-size distribution; (*b*) soil-water characteristic (SWC). r^2, coefficient of determination.
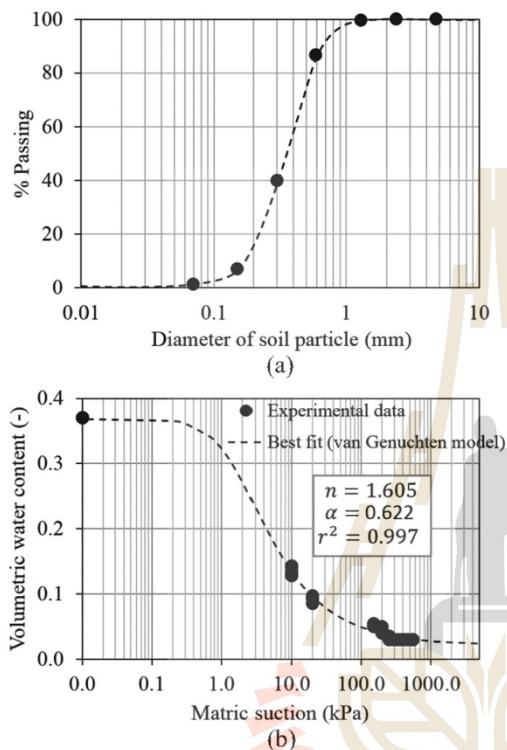

(a)

(b)

Table 1. Summary of soil properties.

Soil property	Value
Soil type (USCS classification)	SP
Dry unit weight, γ_d (kN/m³)	16.9
Specific gravity, G_s	2.69
Soil hydrologic parameters	
Saturated permeability, k_s (m/s)	1.54×10^{-4}
Saturated volumetric water content, θ_{sat}	0.371
Residual volumetric water content, θ_r	0.021
Fitting parameter, α (kPa⁻¹)	0.662
Fitting parameter, n	1.605
Soil strength parameters	
Internal friction angle, φ' (°)	38
Cohesion, c' (kPa)	0

where α and n are fitting parameters relating to the inverse of air-entry pressure and pore-size distribution, respectively.

Prior to placement of the soil, the soil was air dried and turned over every day for 14 days. The soil was then carefully placed into the box to get homogenous soil slopes. Ten layers of 60 mm thick were compacted with a certain weight of dry soil to achieve the dry unit weight and void ratio (*e*) of 16.9 kN/m³ and 0.59, respectively. This unit weight of 16.9 kN/m³ was acquired from the dry soil sample compacted at a standard effort of 600 kJ/m³ (ASTM D698 (ASTM 1991*a*)). The moisture sensors and piezometers were installed during this process.

Table 2. Experimental programs conducted in this study.

Series	Rainfall intensity, i (mm/h)	Slope angle, β (°)	Rainfall sequence	Inter-storm rainfall period, t_b (day)
I	45	20		—
	70	20		—
	100	20		—
	130	20		—
	160	20		—
II	100	5		—
		10		—
		20		—
		30		—
III	100	20		4
				7
				14
				—

Experimental program

Three sets of laboratory experiments were conducted as shown in Table 2. In total, 13 tests were carried out. In each test, rainfall was continuously applied until the arrival of the steady state, which is indicated when the rate of water outflow at slope toe is equal to the rainfall intensity. The magnitudes of rainfall intensity assigned to each test were lower than the soil's saturated permeability ($k_s = 1.54 \times 10^{-4}$ m/s = 554.4 mm/h). Monitored data were recorded during the test until the steady state (end of each test) was achieved.

The variation of rainfall intensity was conducted in test series I. The rainfall intensities of 45, 70, 100, 130, 160 mm/h were applied to the model at slope angle (β) of 20°. The variation of slope angle was conducted in the test series II. The slope angles (β) of 5°, 10°, 20°, and 30° were assigned to the model subjected to rainfall intensity of 100 mm/h. The inter-storm rainfall period was assigned to the model in the test series III. This test is to study the effect of antecedent water content from the previous rainfall, which might affect the hydrological responses. The two rainfall events of 100 mm/h each were applied to the model at slope angle (β) of 20° with the inter-storm periods of 4, 7, and 14 days.

Test results

The volumetric water contents (θ_w) read from the moisture sensors B1, B2, B3, B4, and B5, located at a vertical distance from the impervious surface of 100, 200, 300, 400, and 500 mm, respectively (see Fig. 4*a*).

Figures 6–8 present development of the θ_w profile in the soil subjected to rainfall experiment series I, II, and III, respectively. The developments of the θ_w profile of all experimental series look similar to each other. The general characters of θ_w profile development were determined as follows:

(1) The development of the θ_w profile begins when the rainwater starts infiltrating into the soil. During the rainwater infiltration process, termed as the infiltration phase, the volumetric water content increases from its initial value (θ_{wi}) to a volumetric water content of θ_{wb}, named the volumetric water content behind the wetting front. The θ_{wb} presents a possible maximum magnitude of θ_w taking place during the infiltration phase.

Fig. 6. Volumetric water content profiles for test series I: (a) i/k_s = 0.081; (b) i/k_s = 0.126; (c) i/k_s = 0.180; (d) i/k_s = 0.234; (e) i/k_s = 0.289. [Colour online.]
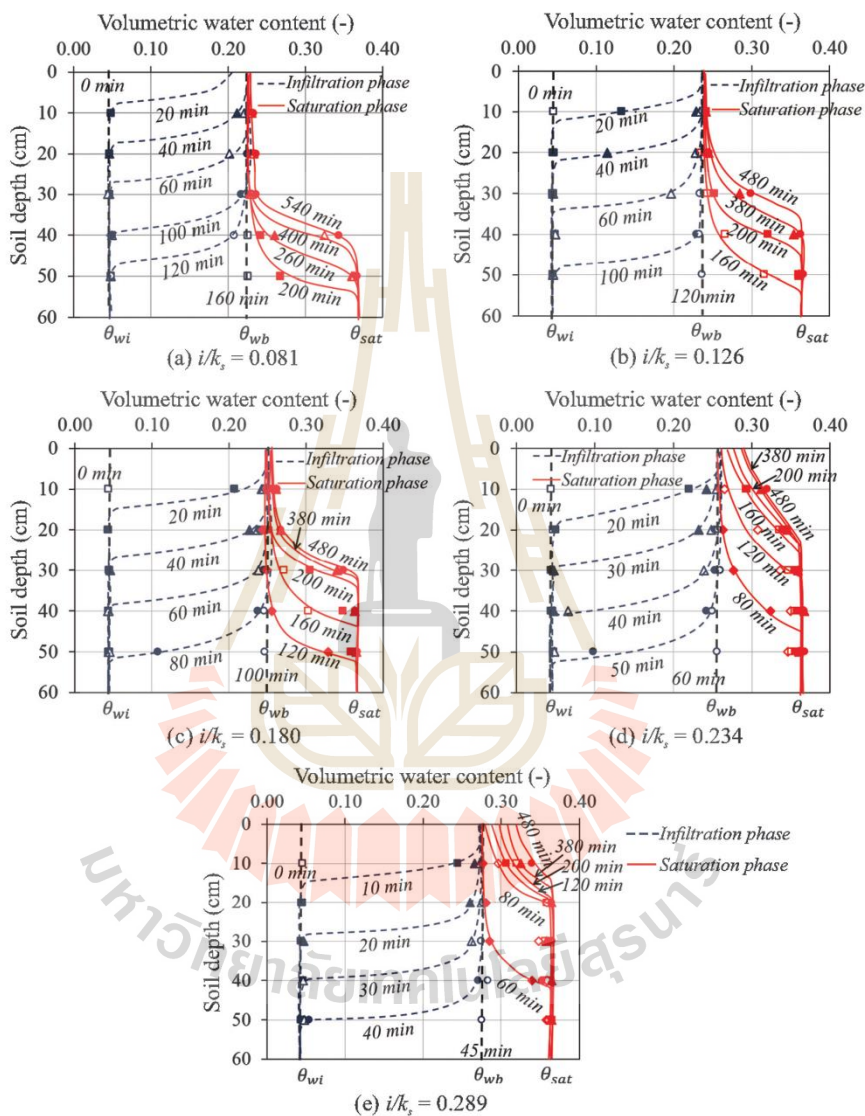

(2) After reaching the impervious boundary of the wetting front, an upward movement of the water table begins. This process is called the saturation phase. At this phase, θ_w increases from θ_{wb} to the magnitude of θ_w that is closest to θ_{sat}.

The characters of the summarized θ_w development are in accordance with those reported by previous studies (Tohari et al. 2007; Huang et al. 2008; Huang and Yuin 2010; Sharma and Nakagawa 2010; Phi et al. 2013).

Figures 6a–6e present the variation of volumetric water content in shallow slope of the experimental series I for rainfall intensities of 45, 70, 100, 130, and 160 mm/h, respectively. The results show that the θ_w profile development in the infiltration phase clearly depends on the magnitudes of rainfall intensity. The higher rainfall intensity results in the faster move of wetting front, and hence the deeper development of a wetting front. In addition, the results show that the magnitude of θ_{wb} increases with the magnitude of rainfall intensity. These findings are similar to those reported by Lee et al. (2011).

Fig. 7. Volumetric water content profiles for test series II: (a) β = 5°; (b) β = 10°; (c) β = 20°; (d) β = 30°. [Colour online.]
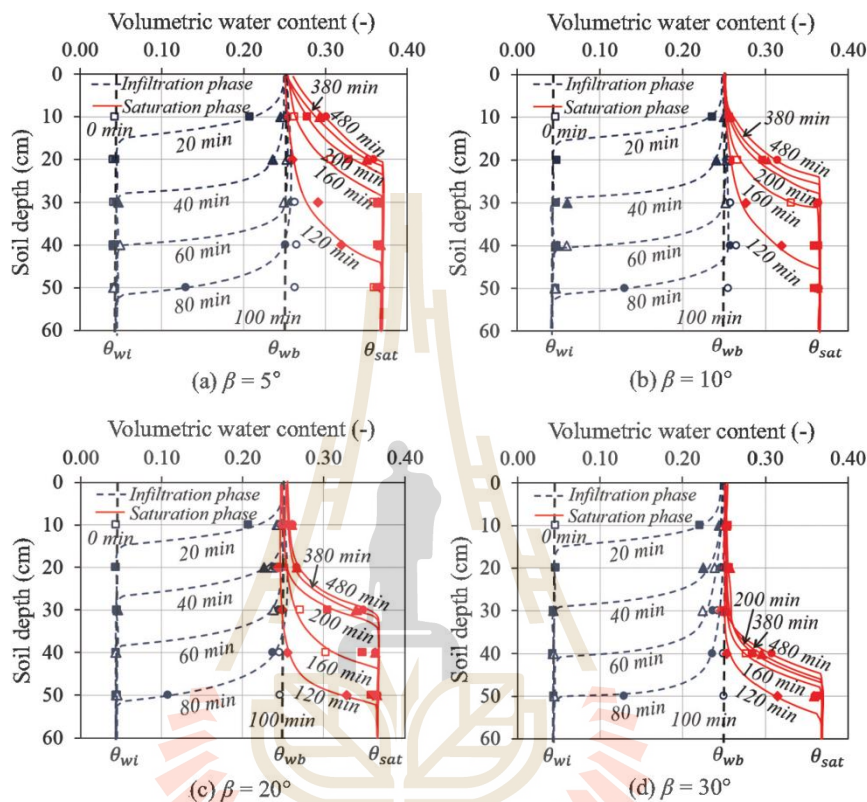
The rainfall intensity also affects the θ_w profile development in the saturation phase. In the plots, the rise of the water table is indicated at the magnitude where θ_w reaches θ_{sat}. The level of the water table is indicated by the point where the θ_w profile in the saturation phase deviates from θ_{sat}. It is found that the greater rainfall intensity causes the faster rise of the water table. In addition, the final level of the water table at steady state also depends on the rainfall intensity, and the greater rainfall intensity yields the higher level of the water table at steady state.

Figures 7a–7d present variation of volumetric water content in shallow slope of the experimental series II for the slope angle (β) of 5°, 10°, 20°, and 30°, respectively. The θ_w development and the magnitude of θ_{wb} in the infiltration phase are not dependent on the slope angle. In other words, within the β range conducted in this study, the magnitude of slope angle β does not affect the hydrological response. It is due to the vertical seepage flow, which plays an important role in the hydrological responses in isotropic shallow slope soil during the rainwater infiltration process. This finding is similar to that found by Lee et al. (2011) who conducted two sets of laboratory seepage flow tests: one-dimensional soil column and 18° tilted slope model.

The slope angle, however, affects the θ_w profile development in the saturation phase. Figures 7a–7d clearly show that the rise of the water table depends on the slope angle; the faster water table development is found at a mild slope angle. This result may naturally be attributed to a dominant role of lateral flow along the

impervious layer at the soil saturated state. The higher slope angle provides the higher hydraulic gradient and the faster lateral flow, and thus the less accumulated rain water at the impervious boundary.

Figure 8 presents variation of volumetric water content in shallow slope of the experimental series III for a continuous storm, and for the different inter-storm periods (t_b) of 4, 7, 14 days, respectively. The θ_w development in the infiltration phase depends on the magnitude of t_b, as it affects the magnitude of an initial θ_w of the subsequent rainfall (θ_{wi}); the shorter t_b results in the higher magnitude of θ_{wi}. The speed of the wetting front advancement is more rapid for the shorter t_b. Although the variation of t_b significantly affects the wetting front development, it does not affect the magnitude of the volumetric water content behind the wetting front (θ_{wb}). In other words, the magnitude of θ_{wb} is independent of the magnitude of t_b.

Analytical approach for hydrological responses

The influence factors involving the hydrological responses in shallow slope soil subjected to rainfall events are discussed in the former section. When the rainfall intensity (i) is less than the soil's saturated permeability (k_s), the development of θ_w is divided into two phases: the infiltration and saturation phases. Both phases are characterized by a so-called "steady infiltration profile" in which its magnitude is equal to θ_{wb}.

Published by NRC Research Press

178

Fig. 8. Volumetric water content profiles for test series III: (a) t_b = 4 days; (b) t_b = 7 days; (c) t_b = 14 days; (d) continuous storm t_b = 0 days. [Colour online.]
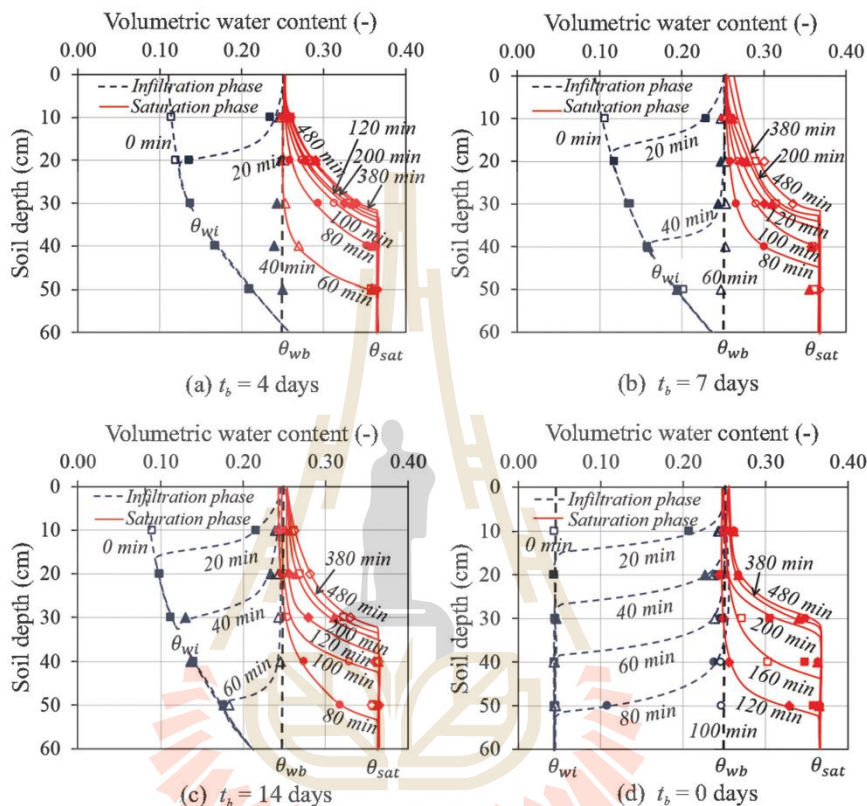

(a) t_b = 4 days

(b) t_b = 7 days

(c) t_b = 14 days

(d) t_b = 0 days

Figure 9 presents a relationship between the measured water content behind the wetting front (θ_{wb}) and the rainfall intensity (*i*) assigned to the slope model. The permeability function (Gardner 1958) of the studied soil was plotted in this figure. The point of coincidence between the θ_{wb}–*i* and permeability function plots indicates that the state at water content of θ_{wb} is a steady infiltration state at which infiltration rate is equal to the rainfall intensity. In addition, the plot shows that the magnitude of θ_{wb} clearly depends on the rainfall intensity, regardless of the variation in slope angle and the inter-storm period.

Based on the relationship between θ_{wb} and *i* shown in Fig. 9, development of the steady infiltration profile can be explained. At first, the permeability of the soil layer ($k(\theta_{wi})$) is lower than the magnitude of rainfall intensity (*i*). Consider a thin surface layer of soil, where $k(\theta_{wi})$ is lower than *i*. Soon after initiation of the infiltration phase, the infiltrated rainwater is stored in this layer, subsequently leaving and resulting in an increase of its water content, hence an increase in the permeability of this layer. As long as the flux out of the layer is lower than the magnitude of *i*, the water content continues to increase. When the water content in this layer reaches the magnitude at which $k(\theta_w)$ = *i*, the rate of water outflow is equal to the rate of water inflow, and there is no further change in water content as long as the rainfall event is continuously applied to the slope. This process takes place successively in each layer as water input continues, producing a descending wetting front at which water decreases more or less abruptly. The water content equals θ_{wb} behind the front and θ_{wi} below it.

Figure 9 also presents the other important water content, at a steady infiltration state called the "field capacity" (θ_{fc}), defined as the content of water, on a mass or volume basis, remaining in a soil 2 or 3 days after having been wetted with water and after free drainage is negligible (Soil Science Glossary Terms Committee 2008). Meyer and Gee (1999) suggested that field capacity (θ_{fc}) occurred when the permeability decreases to between 10^{-9} and 10^{-11} m/s, depending on soil type.

Figure 10 presents a conceptual idea of the FS profile plotted at any time during the infiltration and saturation phases. At a specific time t_1 during the infiltration phase, the variation of θ_w along a vertical depth will vary between its initial and the steady infiltration profiles. The water content value at the initial infiltration profile is potentially the water content at field capacity (θ_{fc}), while the water content value at the steady infiltration profile is the water content behind the wetting front (θ_{wb}). The variation of FS along a vertical depth will vary between two FS lines corresponding to the initial θ_w profile and the steady infiltration profile. The minimum magnitude of FS possibly occurs along the wetting front profile. Figure 10d presents the FS profile development with wetting front advance. The depth of the failure plane, which is

Fig. 9. Relationship between measure volumetric water content behind wetting front (θ_{wb}) and rainfall intensity (i). [Colour online.]
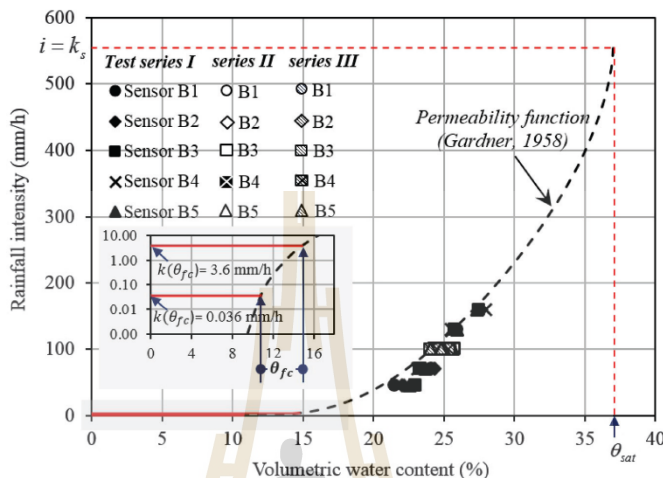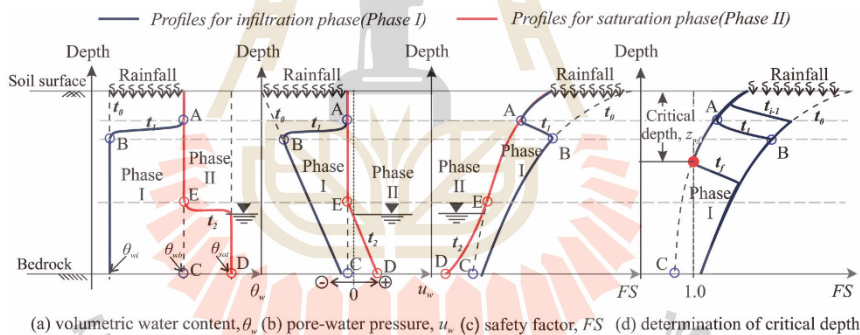

Fig. 10. Safety factor characteristics based on hydraulic responses during rainfall event: (a) water content profile; (b) pore-water pressure profile; (c) safety factor profile; (d) determination of critical depth. [Colour online.]

(a) volumetric water content, θ_w (b) pore-water pressure, u_w (c) safety factor, FS (d) determination of critical depth

later called a critical depth, is located where the magnitude of FS reaches 1.0.

At a specific time t_2 during the saturation phase, the magnitude of FS decreases with increasing depth, and the minimum magnitude of FS is found at the interface between the soil and the impervious layer. The FS profile idealization presented in Fig. 10 is similar to those reported by previous studies (Santoso et al. 2011; Ali et al. 2014a, 2014b).

As the minimum FS possibly occurs along the wetting front, it is vital to take the hydrologic states at steady infiltration profile into consideration for the critical depth calculation. Considering the permeability function proposed by Gardner (1958),

$$(7a) \qquad k(\theta) = k_s \exp[-\alpha(u_a - u_w)]$$

which can be rewritten in terms of $\alpha(u_a - u_w)$ as

$$(7b) \qquad \alpha(u_a - u_w) = -\ln\left[\frac{k(\theta)}{k_s}\right]$$

Replacing eq. (7b) into eq. (6) yields

$$(8) \qquad S_e = \frac{\theta_w - \theta_r}{\theta_{sat} - \theta_r} = \left\langle \frac{1}{1 + \{-\ln[k(\theta)/k_s]\}^n} \right\rangle^{1-1/n}$$

At $\theta_w = \theta_{wb}$, $k(\theta_{wb}) = i$. Hence, eq. (8) is

$$(9a) \qquad S_{eb} = \frac{\theta_{wb} - \theta_r}{\theta_{sat} - \theta_r} = \left\langle \frac{1}{1 + \{-\ln[k(\theta_{wb})/k_s]\}^n} \right\rangle^{1-1/n}$$
$$= \left\{ \frac{1}{1 + [-\ln(i/k_s)]^n} \right\}^{1-1/n}$$

and the magnitude of suction at $\theta_w = \theta_{wb}$ is

$$(9b) \qquad (u_a - u_w)_b = -\frac{1}{\alpha}\ln\left(\frac{i}{k_s}\right)$$

where S_{eb} and $(u_a - u_w)_b$ are the effective saturation and suction behind the wetting front, respectively. Equations (9a) and (9b) are the same as the analytical solutions proposed by Lu and Griffiths

(2004) and Lu and Likos (2006) to describe the hydrological responses at steady state for one-dimensional seepage flow where the groundwater table does not exist. The experimental results from the former section show that the volumetric water content at steady (θ_{wb}) is not dependent on the slope angle. As such, the proposed equations are applicable to rainfall infiltration on unsaturated soil slope. Furthermore, the variations of the S_e and u_w of a certain soil depend only on the magnitude of rainfall intensity.

Assessment of stability under rainfall infiltration

Stability prediction of a shallow slope subjected to rainfall infiltration is demonstrated in this section. Properties of the tested soil are reported in this demonstration as summarized in Table 1. The soil is 3 m thick and overlaid by an impervious layer. Prior to rainfall event, the groundwater table is assumed not to exist. The calculation procedure is as follows:

Step 1: Calculate the suction stress ($\sigma^s = S_e(u_a - u_w)$) for a specific rainfall intensity (i). The initial groundwater table was assumed to not exist prior to a rainfall event, hence the magnitudes of S_e and $(u_a - u_w)$ at steady state were calculated from eq. (9a) and eq. (9b), respectively.

Step 2: Use eq. (4) to perform the slope stability analysis. In the infiltration phase, the magnitude of FS was calculated at a line that coincides with the wetting front. This calculation was done at various depths of the wetting front advance. When the wetting front reaches the impervious layer, slope stability analysis for the saturation phase has taken place. The magnitude of FS was calculated along the interface between the soil and the impervious layer. This calculation was done at various heights of water table development.

To investigate the effect of rainfall intensity (i) and the slope angle (β) on FS of the shallow slope subjected to rainfall event, the preceding procedures were repeated for various magnitudes of i and β. Figure 11a presents the variation of FS according to the wetting front advance Z_w for a 40° inclined slope subjected to various magnitudes of i. Figure 11b presents the variation of FS according to the wetting front advance Z_w for a various angles of the inclined slope subjected to various magnitudes of i. According to Lu and Griffiths (2004) and Lu and Likos (2006), the hydrological states at steady condition are a function of the infiltration index (i/k_s). Hence, the effect of i on the variation of FS is presented in terms of the infiltration index. The magnitude of FS successively decreases with an increasing Z_w for every magnitude of the infiltration index lower than 1.0. As the suction stress σ^s decreases to zero immediately after the initiation of the infiltration phase for the infiltration index of 1.0, the magnitude of FS reduces to its lowest value soon after the initiation of the infiltration phase.

For the infiltration index of lower than 1.0, the magnitude of FS decreases drastically with small increments of the wetting front advance Z_w. The faster loss of FS is found at the greater magnitude of the infiltration index. As the wetting front infiltrates deep enough, the magnitude of FS gradually decreases with the increment of Z_w. Figure 11b shows that the depth where FS gradually decreases with Z_w depends solely on the magnitude of the infiltration index regardless of the magnitude of slope angle β, which is in accordance with the hydrological responses during the infiltration phase found in the former session.

At the end of the infiltration phase ($Z_w = Z_t$), the volumetric water content in soil is equal to θ_{wb}, which is lower than that at the saturated state. However, immediately after the rainwater starts accumulating along the impervious boundary, i.e., the saturation phase begins, the state of the soil at the impervious boundary changes from unsaturated to saturated states. It results in the drop of FS from points B, C, and D (the i/k_s of 0.0019, 0.19, and 0.67, respectively) to point A because of the decrease in σ^s.

Fig. 11. Variation of safety factor with depth: (*a*) various *i* values with $\beta = 40°$; (*b*) various values of *i* and β. [Colour online.]
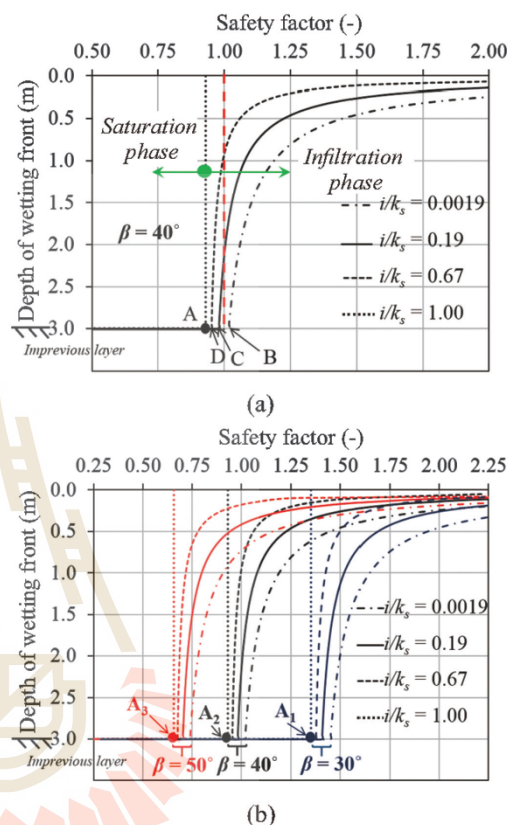
With the rising of the water table, the FS drops continuously due to the increasing of u_w.

Regarding the calculation of FS written in eq. (4), there are three components that contribute to the shear strength of a soil: soil cohesion, suction stress, and the soil frictional components. According to Lu and Griffiths (2004) and Lu and Godt (2008), the suction stress is negative for the soil at the unsaturated state and is equal to the magnitude of positive pore water when the state of the soil becomes saturated. Thus, for a cohesionless soil ($c' = 0$ kN/m²), the slope failure might take place during either the infiltration or saturation phases, depending on the magnitude of the slope angle compared with the soil frictional angle. The failure state of a steep shallow slope defined by $\beta > \varphi'$ might take place during the infiltration phase. However, the failure state of a mild slope ($\beta \leq \varphi'$) might occur during the saturation phase.

Location where the failure plane takes place is vital for assessment of the slope failure. For the shallow slope failure taken place during the saturation phase, the failure plane always occurs at the interfacial between the soil and the impervious layer. However, the location of the failure plane taken place during the infiltration phase might vary from depth to depth, depending on many factors. Figure 12 presents the relationships between the normalized critical depth (Z_{wf}/Z_t) and the infiltration index (i/k_s) for various magnitudes of stability index ($\tan\varphi'/\tan\beta$) for this demonstrated
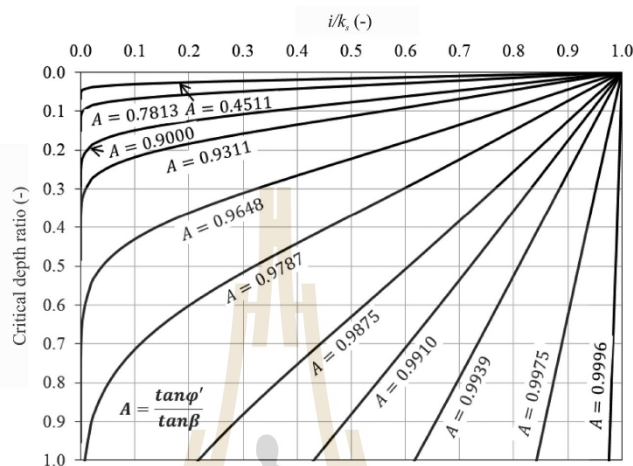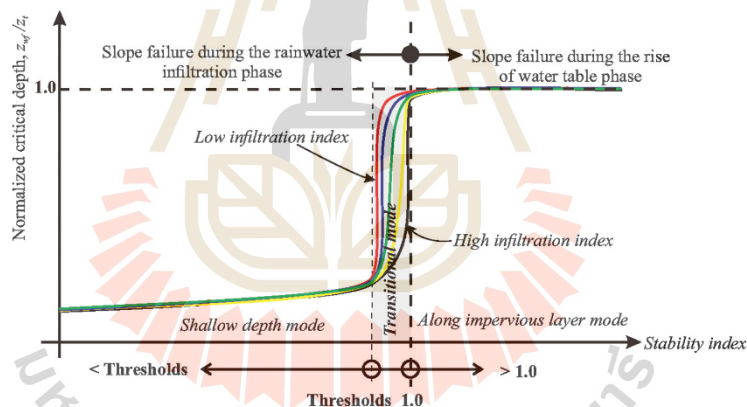
Fig. 12. Critical depth chart.

Fig. 13. Modes of failure in shallow slope classified by stability number. [Colour online.]

case. The vertical distance measured from the slope surface to the failure plane is called the critical depth (Z_{wf}), while the thickness of the shallow slope is denoted as Z_t. For a certain soil, the critical depth decreases with an increasing rainfall intensity. In other words, the shallower depth of the failure plane is encountered in the slope subjected to the greater magnitude of rainfall intensity.

Figure 12 shows that the depth of the failure plane is very sensitive to the change of rainfall intensity for the stability index ranged from 0.9 to 1.0. The depth of the failure plane can occur at any depth, depending on the magnitudes of the infiltration and stability indices. However, the depth of the failure plane is inert with the change of rainfall intensity for the stability index lower than 0.9. In addition, in this case, the depth of the failure plane might take place at very shallow depth ($Z_{wf}/Z_t < 0.2$).

Categorization of slope failures

Once the critical depth chart is available, the threshold value can be assigned to the slope based on personal judgment. The threshold is the stability number at which the critical depth is slightly sensitive to rainfall intensity, i.e., the threshold value

used in the illustrated case is 0.9, which is the stability index at which an infiltration index (i/k) to a normalized critical depth (Z_{wf}/Z_t) ratio is no greater than 0.2.

Based on the relative depth of the failure plane, possible modes of slope failure are as follows: (i) along the impervious layer mode; (ii) shallow depth mode, which occurs very close to the slope surface; and (iii) transitional mode, which occurs at any depth from the impervious layer to the slope surface. These modes are governed by the stability index ($\tan\varphi'/\tan\beta$) as depicted in Fig. 13 and summarized as follows:

(1) For the mild slope ($\tan\varphi'/\tan\beta \geq 1.0$), the failure mode is along the impervious layer mode, which is triggered by an increment of positive pore-water pressure taking place during the saturation phase.

(2) For the steep slope ($\tan\varphi'/\tan\beta < 1.0$), the failure is triggered by the loss of matric suction during the infiltration phase. With the assistance of the critical depth chart, the failure mode is characterized according to the magnitude of $\tan\varphi'/\tan\beta$ ratio.

(2.1) If the slope's stability number ($\tan\varphi'/\tan\beta$) is lower than the threshold (for the illustrated case, the $\tan\varphi'/\tan\beta$ ratio is lower than 0.9), the failure mode is the shallow depth mode that occurs close to the slope surface.

(2.2) If the slope angle is within a small range between the soil frictional angle and an angle slightly greater than the soil frictional angle (for the illustrated case shown in the study, the $\tan\varphi'/\tan\beta$ ratio ranges from 0.90 to 1.0), the failure mode is the transitional model. The depth of the failure plane can occur at any depth in the soil layer, depending on the magnitude of the infiltration index. A greater $\tan\varphi'/\tan\beta$ ratio results in a more sensitive depth of the failure plane relative to the infiltration index.

According to the failure modes shown in Fig. 13, instrumentations on a specific slope can be characterized by its stability index. In the mild slope ($\tan\varphi'/\tan\beta \geq 1.0$), slope failure will be triggered during the saturation phase. The end of the infiltration phase, which is notified by the arrival of θ_{wb} near the interface layer, may be set as the first warning point. For the very steep slope ($\tan\varphi'/\tan\beta \leq$ threshold), the mode of failure is a shallow depth slope failure. Time to reach the failure might occur shortly after a rainfall event. Warning systems might not be suitable for this type of slope. The area and the vicinities should be classified as a sensitive area, in which human activities are prohibited. For an intermediate steep slope ($1.0 > \tan\varphi'/\tan\beta >$ threshold), the failure plane can occur at various depths, depending on the stability and infiltration indices. Intensive instrumentation to monitor the rainfall intensity and the development of wetting front must be assigned to this area.

Conclusions

The physical model was conducted in this study to investigate the effect of rainfall intensity, slope angle, and inter-storm period on hydrological responses taking place in the soil shallow slope with cohesionless soil, with no water table. The rainfall characteristics used in this study were continuously applied until steady-state condition was achieved (end of the test). The magnitudes of rainfall intensity assigned to every test were lower than the soil's saturated permeability ($k_s = 1.54 \times 10^{-4}$ m/s = 554.4 mm/h). The comprehensive understanding of the hydraulic responses gained led to simplicity analysis of a shallow slope with cohesionless soil subjected to a continuous rainfall of $i < k_s$ and could be concluded that

(1) The hydrological response is characterized by infiltration and saturation phases. During the infiltration phase, the magnitude of volumetric water content increases from its initial value to the final volumetric water content called "volumetric water content behind the wetting front: θ_{wb}". Further increment of the magnitude of volumetric water content takes place again when the saturation phase begins. At the saturation phase, the magnitude of water content increases from θ_{wb} to the saturated volumetric water content (θ_s).

(2) The magnitude of rainfall intensity (i) affects the volumetric water content on both phases. The higher magnitude of rainfall intensity induces faster movement of the wetting front and rise of water table. In addition, the magnitude of θ_{wb} increases with increasing the magnitude of rainfall intensity.

(3) The slope angle (β) does not affect the variation of volumetric water content during the infiltration phase. In addition, the magnitude of θ_{wb} does not depend on the magnitude of β. However, the slope angle affects the variation of volumetric water content during the saturation phase. The flatter slope coincides with the faster rise of the water table.

(4) The inter-storm period affects both stages of θ_w in terms of temporal variation. The shorter inter-storm period (t_b) induces the faster movement of wetting front and faster rising

in water table, whereas the magnitude of θ_{wb} is independent with inter-storm period.

(5) The failure state of a steep shallow slope with cohesionless soil of $\beta > \varphi'$ might take place during the infiltration phase, whereas the failure state of a mild slope of $\beta \leq \varphi'$ might occur during the saturation phase.

(6) For the steep slope ($\beta > \varphi'$), the location of the failure plane can occur at any depth varied from the impervious layer to the slope surface, depending on the stability and infiltration indices.

(7) The "threshold", which is the stability number at which the critical depth is slightly sensitive to rainfall intensity, is vital to categorize a steep slope as a very steep slope. Proper disaster prevention approaches can be implemented based on the threshold and the slope's stability number.

Acknowledgements

References

Aleotti, P. 2004. A warning system for rainfall-induced shallow failures. Engineering Geology, 73: 247–265. doi:10.1016/j.enggeo.2004.01.007.

Ali, A., Huang, J., Lyamin, A.V., Sloan, S.W., and Cassidy, M.J. 2014a. Boundary effects of rainfall-induced landslides. Computers and Geotechnics, 61: 341–354. doi:10.1016/j.compgeo.2014.05.019.

Ali, A., Huang, J., Lyamin, A.V., Sloan, S.W., Griffiths, D.V., Cassidy, M.J., and Li, J.H. 2014b. Simplified quantitative risk assessment of rainfall-induced landslides modelled by infinite slopes. Engineering Geology, 179: 102–116. doi:10.1016/j.enggeo.2014.06.024.

ASTM. 1991a. Test Method for Laboratory Compaction Characteristics of Soil Using Standard Effort (12,400 ft-lbf/ft³ (600 kN-m/m³)). ASTM standard D698. ASTM International, Philadelphia, PA, USA.

ASTM. 1991b. Standard Classification of Soils for Engineering Purpose (Unified Soil Classification System). ASTM standard D2487. ASTM International, West Conshohocken, PA, USA.

ASTM. 2003. Test methods for determination of the soil water characteristic curve for desorption using a hanging column, pressure extractor, chilled mirror hygrometer, and/or centrifuge. ASTM standard D6836-02. ASTM International, West Conshohocken, PA, USA.

Caine, N. 1980. The rainfall intensity: duration control of shallow landslides and debris flows. Geografiska Annaler Series A, Physical Geography, 62: 23–27. doi:10.2307/520449.

Calcaterra, D., Parise, M., Palma, B., and Pelella, L. 2000. The influence of meteoric events in triggering shallow landslides in pyroclastic deposits of Campania. In Proceedings of the 8th International Symposium on Landslides, AA Balkema, Cardiff. Edited by E. Bromhead, N. Dixon, and M.L. Ibsen. Vol. 1, pp. 209–214.

Cannon, S.H., and Gartner, J.E. 2005. Wildfire-related debris flow from a hazards perspective. In Debris-flow hazards and related phenomena. Edited by M. Jakob and O. Hungr. Springer Berlin Heidelberg, pp. 363–385.

Chen, C.-Y., Chen, T.-C., Yu, F.-C., Yu, W.-H., and Tseng, C.-C. 2005. Rainfall duration and debris-flow initiated studies for real-time monitoring. Environmental Geology, 47: 715–724. doi:10.1007/s00254-004-1203-0.

Cho, S.E. 2009. Infiltration analysis to evaluate the surficial stability of two-layered slopes considering rainfall characteristics. Engineering Geology, 105(1–2): 32–43. doi:10.1016/j.enggeo.2008.12.007.

Cho, S.E., and Lee, S.R. 2002. Evaluation of surficial stability for homogeneous slopes considering rainfall characteristics. Journal of Geotechnical and Geoenvironmental Engineering, 128: 756–763. doi:10.1061/(ASCE)1090-0241(2002)128:9(756).

Corominas, J. 2000. Landslides and climate. Keynote lecture. In Proceedings of the 8th International Symposium on Landslides, AA Balkema, Cardiff. Edited by E. Bromhead, N. Dixon, and M.L. Ibsen, Vol. 4, pp. 1–33.

Crosta, G.B., and Frattini, P. 2001. Rainfall thresholds for triggering soil slips and debris flow. In Proceedings of the 2nd EGS Plinius Conference on Mediterranean Storms, Siena, Italy. Edited by A. Mugnai, F. Guzzetti, and G. Roth, pp. 463–487.

Cuomo, S., and Della Sala, M. 2013. Rainfall-induced infiltration, runoff and failure in steep unsaturated shallow soil deposits. Engineering Geology, 162: 118–127. doi:10.1016/j.enggeo.2013.05.010.

Decagon Devices Inc. 2007–2010. Operator's manual. Version 6. 2365 NE Hopkins Court, Pullman WA 99163, USA.

Eichenberger, J., Ferrari, A., and Laloui, L. 2013. Early warning thresholds for partially saturated slopes in volcanic ashes. Computers and Geotechnics, 49: 79–89. doi:10.1016/j.compgeo.2012.11.002.

Fredlund, D.G., and Morgenstern, N.R. 1976. Constitutive relations for volume change in unsaturated soils. Canadian Geotechnical Journal, 13(3): 261–276. doi:10.1139/t76-029.

Fredlund, D.G., and Rahardjo, H. 1993. Soil mechanics for unsaturated soils. Wiley, New York.

Fredlund, D.G., Morgenstern, N.R., and Widger, R.A. 1978. The shear strength of unsaturated soils. Canadian Geotechnical Journal, 15(3): 313–321. doi:10.1139/t78-029.

Gardner, W. 1958. Some steady-state solutions of the unsaturated moisture flow equation with application to evaporation from a water table. Soil Science, 85: 228–232. doi:10.1097/00010694-195804000-00006.

Greco, R., Guida, A., Damiano, E., and Olivares, L. 2010. Soil water content and suction monitoring in model slopes for shallow flowslides early warning applications. Physics and Chemistry of the Earth, Parts A/B/C, 35(3–5): 127–136. doi:10.1016/j.pce.2009.12.003.

Guzzetti, F., Peruccacci, S., Rossi, M., and Stark, C.P. 2007. Rainfall thresholds for the initiation of landslides in central and southern Europe. Meteorology and Atmospheric Physics, 98: 239–267. doi:10.1007/s00703-007-0262-7.

Hall, M.J., Johnston, P.M., and Wheather, H.S. 1989. Evaluation of overland flow models using laboratory catchment data. I. An apparatus for laboratory catchment studies. Hydrological Sciences Journal, 34: 277–288. doi:10.1080/02626668909491335.

Huang, C.-C., and Yuin, S.-C. 2010. Experimental investigation of rainfall criteria for shallow slope failures. Geomorphology, 120(3–4): 326–338. doi:10.1016/j.geomorph.2010.04.006.

Huang, C.-C., Lo, C.-L., Jang, J.-S., and Hwu, L.-K. 2008. Internal soil moisture response to rainfall-induced slope failures and debris discharge. Engineering Geology, 101(3–4): 134–145. doi:10.1016/j.enggeo.2008.04.009.

Lee, L.M., Gofar, N., and Rahardjo, H. 2009. A simple model for preliminary evaluation of rainfall-induced slope instability. Engineering Geology, 108(3–4): 272–285. doi:10.1016/j.enggeo.2009.06.011.

Lee, L.M., Kassim, A., and Gofar, N. 2011. Performances of two instrumented laboratory models for the study of rainfall infiltration into unsaturated soils. Engineering Geology, 117(1–2): 78–89. doi:10.1016/j.enggeo.2010.10.007.

Li, W.C., Lee, L.M., Cai, H., Li, H.J., Dai, F.C., and Wang, M.L. 2013. Combined roles of saturated permeability and rainfall characteristics on surficial failure of homogeneous soil slope. Engineering Geology, 153: 105–113. doi:10.1016/j.enggeo.2012.11.017.

Lu, N., and Godt, J. 2008. Infinite slope stability under steady unsaturated seepage conditions. Water Resources Research, 44(11): 1–13. doi:10.1029/2008WR006976.

Lu, N., and Griffiths, D.V. 2004. Profiles of steady-state suction stress in unsaturated soils. Journal of Geotechnical and Geoenvironmental Engineering, 130(10): 1063–1076. doi:10.1061/(ASCE)1090-0241(2004)130:10(1063).

Lu, N., and Likos, W.J. 2006. Suction stress characteristic curve for unsaturated soil. Journal of Geotechnical and Geoenvironmental Engineering, 132(2): 131–142. doi:10.1061/(ASCE)1090-0241(2006)132:2(131).

Ma, K.-C., Tan, Y.-C., and Chen, C.-H. 2011. The influence of water retention curve hysteresis on the stability of unsaturated soil slopes. Hydrological Processes, 25(23): 3563–3574. doi:10.1002/hyp.8081.

Meyer, P.D., and Gee, G.W. 1999. Flux-based estimation of field capacity. Journal of Geotechnical and Geoenvironmental Engineering, 125(7): 595–599. doi:10.1061/(ASCE)1090-0241(1999)125:7(595).

Phi, S., Clarke, W., and Li, L. 2013. Laboratory and numerical investigations of hillslope soil saturation development and runoff generation over rainfall events. Journal of Hydrology, 493: 1–15. doi:10.1016/j.jhydrol.2013.04.009.

Pradel, D., and Raad, G. 1993. Effect of permeability on surficial stability of homogeneous slopes. Journal of Geotechnical Engineering, 119(2): 315–332. doi:10.1061/(ASCE)0733-9410(1993)119:2(315).

Rahardjo, H., Li, X.W., Toll, D.G., and Leong, E.C. 2001. The effect of antecedent rainfall on slope stability. Geotechnical and Geological Engineering, 19: 371–399. doi:10.1023/A:1013129725263.

Rahardjo, H., Ong, T.H., Rezaur, R.B., and Leong, E.C. 2007. Factors controlling instability of homogeneous soil slopes under rainfall. Journal of Geotechnical and Geoenvironmental Engineering, 133(12): 1532–1543. doi:10.1061/(ASCE)1090-0241(2007)133:12(1532).

Rahimi, A., Rahardjo, H., and Leong, E.-C. 2010. Effect of hydraulic properties of soil on rainfall-induced slope failure. Engineering Geology, 114(3–4): 135–143. doi:10.1016/j.enggeo.2010.04.010.

Rahimi, A., Rahardjo, H., and Leong, E.-C. 2011. Effect of antecedent rainfall patterns on rainfall-induced slope failure. Journal of Geotechnical and Geoenvironmental Engineering, 137(5): 483–491. doi:10.1061/(ASCE)GT.1943-5606.0000451.

Santoso, A.M., Phoon, K.-K., and Quek, S.-T. 2011. Effects of soil spatial variability on rainfall-induced landslides. Computers & Structures, 89(11–12): 893–900. doi:10.1016/j.compstruc.2011.02.016.

Sharma, R.H., and Nakagawa, H. 2010. Numerical model and flume experiments of single- and two-layered hillslope flow related to slope failure. Landslides, 7(4): 425–432. doi:10.1007/s10346-010-0205-0.

Shen, S.-L., Wang, J.-P., Wu, H.-N., Xu, Y.-S., Ye, G.-L., and Yin, Z.-Y. 2015. Evaluation of hydraulic conductivity for both marine and deltaic deposits based on piezocone testing. Ocean Engineering, 110: 174–182. doi:10.1016/j.oceaneng.2015.10.011.

Skempton, A., and DeLory, F. 1957. Stability of natural slopes in London Clay. In Proceedings of the 4th International Conference on Soil Mechanics and Foundation Engineering, Butterworths Scientific Publications, London, Vol. 2, pp. 378–381.

Soil Science Glossary Terms Committee. 2008. Glossary of Soil Science Terms 2008. SSSA, Madison, Wisc., p. 92.

Tohari, A., Nishigaki, M., and Komatsu, M. 2007. Laboratory rainfall-induced slope failure with moisture content measurement. Journal of Geotechnical and Geoenvironmental Engineering, 133(5): 575–587. doi:10.1061/(ASCE)1090-0241(2007)133:5(575).

Tsai, T.-L., Chen, H.-E., and Yang, J.-C. 2008. Numerical modeling of rainstorm-induced shallow landslides in saturated and unsaturated soils. Environmental Geology, 55(6): 1269–1277. doi:10.1007/s00254-007-1075-1.

van Genuchten, M.T. 1980. A closed-form equation for predicting the hydraulic conductivity of unsaturated soil. Soil Science Society of America Journal, 44: 892–898. doi:10.2136/sssaj1980.03615995004400050002x.

Vanapalli, S.K., Fredlund, D.G., Pufahl, D.E., and Clifton, A.W. 1996. Model for the prediction of shear strength with respect to soil suction. Canadian Geotechnical Journal, 33(3): 379–392. doi:10.1139/t96-060.

Xu, Y.-S., Shen, S.-L., and Du, Y.-J. 2009. Geological and hydrogeological environment in Shanghai with geohazards to construction and maintenance of infrastructures. Engineering Geology, 109(3–4): 241–254. doi:10.1016/j.enggeo.2009.08.009.

Zhan, T.L.T., Jia, G.W., Chen, Y.M., Fredlund, D.G., and Li, H. 2013. An analytical solution for rainfall infiltration into an unsaturated infinite slope and its application to slope stability analysis. International Journal for Numerical and Analytical Methods in Geomechanics, 37(12): 1737–1760. doi:10.1002/nag.2106.

Zhang, L.L., Zuo, Z.B., Ye, G.L., Jeng, D.S., and Wang, J.H. 2013. Probabilistic parameter estimation and predictive uncertainty based on field measurements for unsaturated soil slope. Computers and Geotechnics, 48: 72–81. doi:10.1016/j.compgeo.2012.09.011.

184

BIOGRAPHY

Mr. Somjai Yubonchit was born in December 1986 in Roi-Et Province, Thailand. He obtained his Bachelor's degree and Master's degree in Civil Engineering from the School of Civil Engineering, Suranaree University of Technology in 2008 and 2011, respectively. Then, he has been awarded an OROG Scholarship from the Thailand Research Fund (TRF) in 2011 for his Ph.D. study in the School of Civil Engineering, Suranaree University of Technology. During his Ph.D. study (2011-2016), he has worked as a teaching assistant for Surveying Laboratory, Soil Mechanics Laboratory and Applied Mechanics Laboratory. He has been also awarded an Ernst Mach Grant–worldwide scholarship (OeAD scholarship) from Austria government to visit Institute for Soil Mechanics and Foundation Engineering, Graz University of Technology, Graz, Austria for his oversea research under the supervision of Prof. Dr. Helmut F. Schweiger from March 1, 2015 to August 26, 2016. He has published 2 international ISI journal papers and 3 international conferences during his Ph.D. study.